Addis Ababa University
Addis Ababa Institute of Technology
School of Mechanical and Industrial Engineering

Investigation on the Intralaminar Fracture Toughness of Woven Sisal/Epoxy Composite: Effect of Glass Fiber Hybridization

A thesis submitted to the School of Mechanical and Industrial Engineering in partial fulfillment of the Degree of Master of Science in Mechanical Engineering (Mechanical Design)

By: Biruk Hussen

Advisor: Dr. Mulugeta H.

Addis Ababa, Ethiopia

March 2024

Addis Ababa University

Addis Ababa Institute of Technology

School of Mechanical and Industrial Engineering

Investigation on the Intralaminar Fracture Toughness of Woven Sisal/Epoxy Composite: Effect of Glass Fiber Hybridization

By

Biruk Hussen

Approved by the Board of Examiners:

Dr. Mulugeta Habtemariam Advisor	_____ Signature	_____ Date
Dr. Hairedin Ismael Internal Examiner	_____ Signature	_____ Date
Dr. Araya Abera External Examiner	_____ Signature	_____ Date
Dr. Araya Abera School Dean	_____ Signature	_____ Date
Dr. Sosina Mengistu Associate Director for PG Program	_____ Signature	_____ Date

Declaration

I hereby declare that the work which is being presented in this thesis entitled “Investigation on the Intralaminar Fracture Toughness of Woven Sisal/Epoxy Composite: Effect of Glass Fiber Hybridization” is original work of my own, has not been presented for a degree of any other university and all the resource of materials used for this thesis have been duly acknowledged.

_____	_____
Biruk Hussen	Date

This is to certify that the above declaration made by the candidate is correct to the best of my knowledge.

_____	_____
Dr. Mulugeta Habtemariam (Advisor)	Date

Acknowledgement

First and foremost, I would like to praise and thank The Almighty God and The Holy Theotokos Saint Mary. My deepest gratitude goes to my thesis advisor Dr. Mulugeta Habtemariam for recommending the research topic, providing continual guidance and support, unreserved sharing of experience and constructive comments and timely feedbacks since the beginning of the research. Thank you for your fatherly encouragement. My special thanks also goes to Dr. Haileleoul Sahle, Dr. Araya Abera, Dr. Hairedin Ismael and Mr. Behailu Mamo for their invaluable comments. Your comments helped me so much in directing the thesis in the right direction. I am truly thankful to the School of Mechanical and Industrial Engineering at Addis Ababa Institute of Technology and the workshop manager Dr. Hairedin Ismael for providing workshop facilities and kind cooperation, and the workshop staffs Mr. Esrael and Mr. Anteneh for providing technical assistance through preparing test specimens. I am also deeply grateful to the Central Laboratory at Addis Ababa Science and Technology University for providing material testing laboratory facilities and Mr. Yemanebirhan Emiru, research assistant and manager of the Laboratory, for giving indispensable support through the testing procedure. Without your technical support it would have been difficult to realize the experimentation. I would like to express my appreciation to my colleagues and classmates Mr. Gezahegn Gebeyehu, Mr. Kerod Sisay and Mr. Temkin Abdulkader for sharing their valuable ideas. My heartfelt gratefulness is also extended to Mr. Assefa Ayele, Mr. Tefera Ayele, Mr. Tesfaneh Ayele, Mr. Biruk Tsegaye and Ms. Biruktawit Tessema for their imperative support and encouragement during my research work. Last but not least, my sincere thanks goes to my beloved family for their unconditional love, motivation and support.

Abstract

A robust and safe design of composite structures for load bearing applications requires the knowledge of their damage tolerance and crack resistance capabilities. To study the effect of glass fiber hybridization on the intralaminar fracture toughness of woven sisal/epoxy composite, tensile mode-I intralaminar fracture toughness experimental tests were carried out on doubly-tapered compact tension (2TCT) specimens prepared from pure sisal, two hybrids of sisal and glass, and pure glass fiber reinforced epoxy composites under displacement control. A data reduction technique recommended for composite laminates based on the finite element analysis (FEA) was utilized. Load-displacement responses were obtained, fracture toughness values based on critical energy release rate (G_{IC}) were evaluated, and resistance curves (R-curves) were plotted for each group of composite laminates and compared to examine the hybridization effect. The fractography was also discussed. The results showed that interply hybridization of woven sisal fibers with woven glass fibers in an epoxy matrix resulted in a considerable improvement of intralaminar fracture toughness values. The hybrid laminates showed an intermediate fracture behavior among their monolithic counterparts. The critical energy release rate (G_{IC}) values of the pure sisal, two hybrids of sisal and glass, and pure glass fiber reinforced epoxy composites were found to be 16.32, 25.06, 27.64, and 39.62 kJ/m^2, respectively. The results of the research provide an experimental data, which can be used for the safe designing of energy absorbing and other low to medium load bearing structural components.

Keywords: Intralaminar; doubly-tapered compact tension; resistance curve; critical energy release rate; fractography; interply hybridization

Table of Contents

Acknowledgement iii
Abstract iv
List of Tables vii
List of Figures viii
List of Abbreviations x
Nomenclature xi
Chapter 1 1
Introduction 1
1.1. Background 1
1.2. Statement of the Problem 7
1.3. Objectives 8
1.3.1. General Objective 8
1.3.2. Specific Objectives 8
1.4. Methodology 8
1.5. Significance of the Study 9
1.6. Scope of the Study 9
1.7. Organization of the Thesis 9
Chapter 2 11
Literature Review 11
2.1. The Sisal Fiber and its Composite 11
2.1.1. The Sisal Fiber 11
2.1.2. Mechanical Properties of Sisal Fibers 13
2.1.3. Composite Fabrication Methods 13
2.1.4. Mechanical Properties of Sisal/Epoxy Composite 14
2.1.5. Effect of Fiber Treatment 15
2.1.6. Other Factors Affecting Mechanical Properties of Sisal/Epoxy Composite 17
2.2. Hybridization 18
2.2.1. Hybrid Composites 18
2.2.2. Natural/Synthetic Hybrid Composites 18
2.2.3. Mechanical Properties of Sisal/Glass Hybrid Composite 19
2.3. Fracture Toughness 21
2.3.1. Failure Modes of FRCs 22
2.3.2. Types and Modes of Fracture. 22

2.3.3. Fracture Toughness Test Standards 23
2.3.4. Factors Affecting Fracture Toughness of Natural Fiber Composites 25
2.3.5. Intralaminar Fracture Toughness of Natural Fiber Composites 27
2.4. Concluding Points and Research Gaps 29
Chapter 3 31
Materials and Methods 31
3.1. Materials 31
3.1.1. Fiber 31
3.1.2. Matrix 32
3.1.3. Other Chemicals 32
3.2. Experimental Methods 33
3.2.1. Fiber Processing 33
3.2.2. Specimen Preparation 35
3.2.3. Test Procedure and Setups 42
3.3. Computational Methods 43
3.3.1. Data Reduction Technique 43
3.3.2. The FEA Procedure 45
3.3.3. Convergence Test 46
Chapter 4 49
Results and Discussion 49
4.1. Polynomial Coefficients 49
4.2. Load-Displacement Curves 51
4.3. Critical Energy Release Rate Values 52
4.4. Resistance Curves (R-Curves) 55
4.5. Fractography 58
Chapter 5 61
Conclusion and Recommendation 61
5.1. Conclusion 61
5.2. Recommendation 62
5.3. Future Works 62
References 63
Appendix 73

List of Tables

Table 1 Typical properties of cured epoxy [95] 32
Table 2 Relative percentage of constituents in the composite laminates 36
Table 3 Elastic properties of the composite laminae [53], [95], [98] 46
Table 4 Elastic properties of the composite laminates 46
Table 5 Mesh convergence analysis data 47
Table 6 Values of polynomial coefficients for the four composite laminates 50
Table 7 Results of critical energy release rate (G_{IC}) values 53
Table 8 Comparison of critical energy release rate values obtained using data reduction formula of Eq. (1) and ASTM D5045 standard 54
Table 9 Intralaminar fracture toughness of related polymer matrix composites in the literature . 54
Table 10 Results of average critical energy release rate for crack propagation ($G_{IC,\,Pro}$) values .. 57

List of Figures

Figure 1 Percentage of composite materials used in the aerospace industry 1
Figure 2 Sisal fibers [17] 3
Figure 3 Fracture mechanisms in fiber reinforced composite laminates [44] 6
Figure 4 (a) Sisal plant (b) Sisal leaf (c) Optical microscopy of sisal leaf cross-section [47] 12
Figure 5 Sisal fiber types (a) Structural fiber (b) Arch fiber [47] 12
Figure 6 The hand lay-up method 13
Figure 7 Common modes of fracture [44] 21
Figure 8 Fracture modes in laminated composites [69] 22
Figure 9 Doubly-tapered compact tension (2TCT) specimen geometry [43] 24
Figure 10 Fibers used for the study (a) Plain-woven sisal fiber (b) Plain-woven E-glass fiber ... 31
Figure 11 (a) Distilled Water (b) Sodium Hydroxide (NaOH) Pellet (c) Mold Releasing Agent 32
Figure 12 The fiber extraction process (a) Sisal leaves (b) Extracting sisal fibers (c) Washing and drying in the sun (d) Dried sisal fibers 33
Figure 13 The hand weaving process 34
Figure 14 The fiber treatment (with 2% NaOH solution for 4hrs) 35
Figure 15 Schematic representation of the four laminate designs (Brown: Sisal fabric layers and Grey: Glass fabric layers) 36
Figure 16 Steel mold 37
Figure 17 Spike roller 37
Figure 18 The hand layup and compression molding process 38
Figure 19 The fabricated four composite panels 39
Figure 20 2TCT specimen configuration (all dimensions in mm) 40
Figure 21 Specimen marking, drilling, cutting and measuring process 40
Figure 22 Morphology of the initial crack and magnified view of the crack tip 41
Figure 23 Specimens ready for testing (five specimens for each group) 42
Figure 24 Loading fixture 42
Figure 25 (a) Universal testing machine (b) Loading and camera set up 43
Figure 26 Determination of critical load P_c for crack initiation 44
Figure 27 2TCT FE half crack model in Abaqus (the red spot represents the crack tip position) 45
Figure 28 2TCT FE model mesh refinements 46

Figure 29 Mesh convergence plot 47
Figure 30 Chosen mesh refinement (Level 6) (the red spot represents the crack tip position) 48
Figure 31 von Mises stress distribution of 2TCT specimen 49
Figure 32 In-plane principal stress distribution of 2TCT specimen 49
Figure 33 Load-displacement curves for the four laminates (S: Sisal, H: Hybrid, and G: Glass) 51
Figure 34 Results of critical energy release rate values (S: Sisal, H: Hybrid, and G: Glass)..... 53
Figure 35 R-curves for the four laminates (S: Sisal, H: Hybrid, and G: Glass) 56
Figure 36 Results of average critical energy release rate for crack propagation values (S: Sisal, H: Hybrid, and G: Glass) 57
Figure 37 Close-up view of the front faces of the fractured specimens 59
Figure 38 Image of fracture surface (top image: upper surface; bottom image: lower surface) .. 60

List of Abbreviations

ASTM	American Society for Testing and Materials
CT	Compact Tension
DCB	Double Cantilever Beam
DIC	Digital Image Correlation
ECT	Extended Compact Tension
EMS	Epoxy Methyl Soyate
ESO	Epoxidized Soyabean Oil
FE	Finite Element
FEA	Finite Element Analysis
FEM	Finite Element Method
FRC	Fiber Reinforced Composite
FRPC	Fiber Reinforced Polymer Composite
GFRP	Glass Fiber Reinforced Polymer
ILSS	Intralaminar Shear Strength
LEFM	Linear Elastic Fracture Mechanics
NFC	Natural Fiber Composites
PLA	Polylactic Acid
RTM	Resin Transfer Mold
RVE	Representative Volume Element
SENB	Single-edge Notch Bend
SFC	Sisal Fiber Composites
TCT	Tapered Compact Tension
2TCT	Doubly-Tapered Compact Tension
UTM	Universal Testing Machine
UV	Ultraviolet
WCT	Widened Compact Tension
X-FEM	Extended Finite Element Method

Nomenclature

K_{IC}	Critical Stress Intensity Factor
G_{IC}	Critical Energy Release Rate
$G_{IC,Pro}$	Average Critical Energy Release Rate for Crack Propagation
V_f	Fiber Volume Fraction
$wt\%$	Weight Percentage
E_1	Longitudinal Young's Modulus
E_2	Transverse Uoung's Modulus
ν_{12}	Major Poisso's Ratio
G_{12}	In-Plane Shear Modulus
G_{13}	Out-of-Plane Shear Modulus of 13 Plane
G_{23}	Out-of-Plane Shear Modulus of 23 Plane
J	J-integral
C	Compliance
P_c	Experimental load
P_{max}	Maximum load
SD	Standard deviation

Chapter 1

Introduction

1.1. Background

Composite materials have been and continue to be widely used in structural and non-structural applications. They can offer high specific strength, high specific stiffness, weight reduction capability, high impact strength, enhanced fatigue and corrosion resistance, and design flexibility compared to most of the conventional materials [1]–[3]. In addition, by using composite materials, structures can be made with reduced number of parts, hence reducing the possibility of failure of the structure. Contemporary advances in the aerospace, automobile, marine, agricultural and biomedical industries are results of rapid decisive steps taking place in the field of composite materials [4]. Large percentage of the conventional materials such as metals and polymers used in these industries are being replaced by composite materials [5]. For example, a large percentage (~50% by mass) of metal components that were traditionally used in the aerospace structures have been replaced by fiber reinforced polymer composites (FRPCs) (Figure 1).

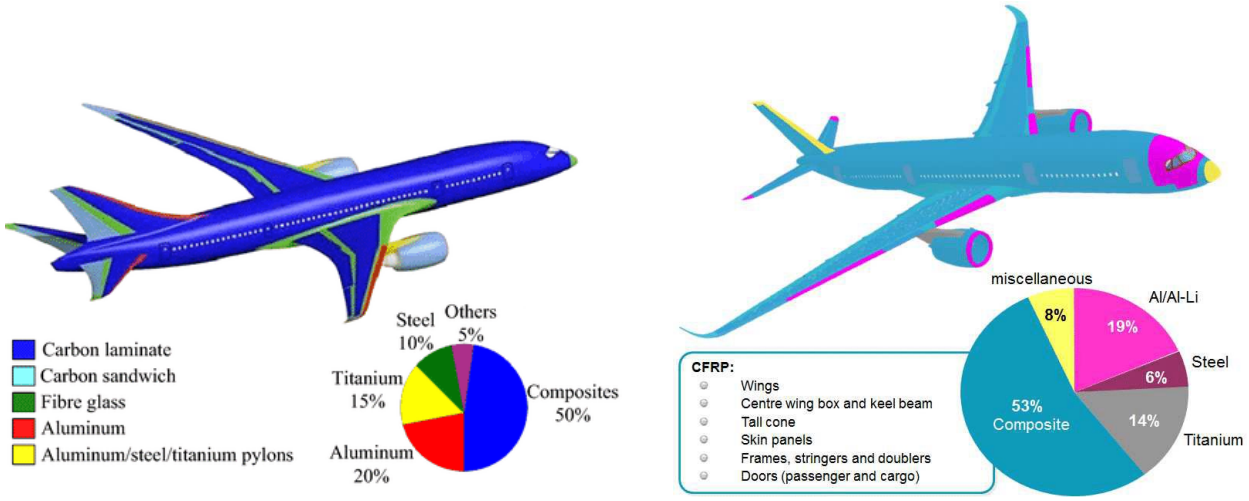

(a) Boeing 787 [5] (b) Airbus A350 [6]

Figure 1 Percentage of composite materials used in the aerospace industry

Fiber reinforced composites (FRCs) are composed of two components: fiber and matrix. Fiber could be synthetic or natural. FRCs which are employed in high performance application areas are mostly synthetic fibers, such as glass, carbon and aramid fibers [7]. Even though synthetic fibers have admirable mechanical properties and are less prone to environmental aging, they have

adverse impact on human health and the environment [8]. Shortcomings of synthetic fibers owing to their non-biodegradability implicates disposal and recycling issues leading to vast pollution to the ecosystem. In addition, health concerns of employees throughout handling and manufacturing processes, and the abrasion effect they impose into processing machines set limitation to their application [7], [9].

Accordingly, there comes a demand for biodegradable materials, like natural fibers. Depending on the technical requirements (such as strength and toughness) in specific application areas of the FRCs, the utilization of synthetic fibers has to be replaced partly or entirely by natural fibers in structural and non-structural applications. As of their high strength to weight ratio, excellent specific stiffness and high fracture toughness, natural fibers are attractive alternatives for application in lightweight mechanical and structural components [7], [8]. Compared with synthetic fibers, natural fibers offer numerous advantages, for instance, low density, low cost, eco-friendly, abundance, biodegradability, renewability, good acoustic property, relative non-abrasiveness and minimal health hazards [3], [10]–[12]. For components made from natural fibers it is possible to use disposal techniques such as composting and incineration, because natural fibers are renewable and biodegradable. However, these techniques are not possible to use for most synthetic fibers [10].

Though natural fibers have several advantages, they also come with shortcomings. The major limitations of natural fibers include low strength, low stiffness, lack of good interfacial adhesion and undesirable moisture absorption property [3]. Heterogeneity of fiber dimension, variation of fiber quality and degradation of fiber quality by mechanical and thermal effects are also other shortcomings of natural fibers that can render them unappealing in some applications. In fact, the significant challenge for producers and suppliers in using natural fibers is the large inconsistency of their properties. Their properties mainly depend on the origin and variety of the plant, and also influenced by weather and soil conditions. Concerns in natural fibers regarding strength, stiffness, interfacial adhesion and moisture absorption can be alleviated by certain strategies such as application of fiber treatment process using appropriate chemicals, and utilization of hybridization technique [9]. Majority of natural fibers have low degradation temperatures, that makes them unattractive for processing them with thermoplastic polymers with processing temperatures more than 200℃ [13].

Based on their origin, natural fibers are categorized into plant, mineral and animal fibers. Plant fibers are the most commonly used fibers. Based on the parts they are obtained, plant fibers are categorized as leaf fibers (sisal, banana and abaca), bast fibers (hemp, flax, jute, ramie and kenaf), seed fibers (cotton, palm, kapok and coir), straw fibers (corn, wheat and rice), grass fibers (bagasse and bamboo) and wood fibers (softwood and hardwood) [14].

Sisal fiber (Figure 2) is one of the strongest natural fibers that is suitable to be use as a reinforcement in composite materials for different engineering applications [15]. It is obtained from the sisal plant (*Agave sisalana*). Its abundance, low density, enhanced specific strength, inexpensive processing, better impregnation and favorable interfacial interaction with thermosets make it a prevalent alternative to be used as a reinforcement in thermoset polymer composites [7], [16]. High cellulose percentage ($66 - 78\%$) and high microfibrillar angle ($10° - 22°$) are unique characteristics of sisal fiber among other natural fibers. In natural fibers, enhancement of tensile properties is attributed to better cellulosic interaction, whereas, improvement of impact properties is related with higher micro microfibrillar angle. Besides, the lesser cells, larger cellulose aspect ratio and larger lumen size of sisal fibers contribute to its higher strength. These sole characteristics made sisal fiber feasible to be used as reinforcement for thermoset matrix composites in many industrial applications [11].

Figure 2 Sisal fibers [17]

Natural fiber composites (NFCs) have generally lower mechanical properties and are susceptible to mechanical property degradation compared to advanced composites such as glass fiber composites. For many of the general-purpose applications, the most widely used synthetic fibers

such as glass and carbon fiber, and more advanced synthetic fibers such as Kevlar and aramid fibers provide properties that are mostly beyond the requirements. The high-level manufacturing technologies associated with these synthetic fibers make their realization costly. This further encourages the incorporation of NFCs in a variety of applications, as evidenced by their implementation in the transport sector [4]. These days, owing to their abundance and affordability, natural fibers are substituting synthetic fibers in some applications [18].

NFCs such as the sisal fiber composite (SFC) and their hybrids are attractive alternatives for industrial applications. Some of their application area include: automotive industry (energy absorbing parts, structural and non-structural interior components like door panels, seat backs, interior fittings, and ceiling panels) [6], renewable energy components (rotor blades of wind turbine), infrastructural and construction parts (roof panels, beams, tanks, and pipes), cargo transportation (cellulose based composites for noise attenuator in cargo floor tray) and other consumer items (luggage, housewares, furniture products and electronic appliances) [19].

Natural fibers generally have low densities and excellent specific properties. These make NFCs suitable alternative in the transportation industry, especially in the automotive sector. The first use of NFCs in the automotive industry goes back in time to the nineties. During this period, Mercedes-Benz used jute fibers to make door panels. Flax and hemp fibers have been the first and second most significant natural fibers in the German automotive sector. These days, NFCs are incorporated into both external and internal components of the latest vehicle models of all the major automakers [20]. German car manufacturers, Volkswagen and Mercedes use NFCs in different car components. For instance, Mercedes used sisal/epoxy composites as door panels and coconut fibers composites for seats. Ford also employed kenaf/polypropylene composite material for door panels in its Mondeo models. Toyota and Volvo also utilized NFCs to make interior parts [21].

Despite their numerous advantages, the use of NFCs for major load carrying structural components is limited. The hydrophilic (water-loving) characteristic of natural fibers is major shortcoming in this regard, which results in poor fiber-matrix interfacial bonding and undesirable moisture absorption behavior of NFCs, which both consequently have adverse effect on mechanical properties of these biocomposites [22]. The use of fiber treatments and hybridization techniques are the two major steps suggested in the literature to counteract the shortcomings of NFCs [3],

[23], [24]. Yet another challenge in the industrial use of NFCs is the lack of reliable material property experimental data for design purpose. This can be attributed to the inconsistency of their properties, as characteristics of natural fibers can depend on the origin and variety of the specific plant they are obtained [9].

Hybridization technique can overcome many of the limitations of natural fibers and extend their use to structural components. Hybrid composites formed by combining natural and synthetic fibers in a polymer matrix system shows synergistic effect, that could not be attained by the individual fibers. With hybridization technique, properties of composite materials can be improved to fulfill certain design requirements. With this technique, it is possible to attain a new class of material, which can expectantly mitigate the shortcomings and preserve the merits of the constituent materials. The other benefit of this technique is the overall cost minimization of the resulting composite, as some of the constituents are less costly than the others [3]. Hybridization reduces the moisture absorption behavior of NFCs. It is also important to obtain well-adjusted mechanical and thermal properties, and enhances the durability of NFCs [3], [7], [21]. In such a hybrid composite, a balance of strength, weight and cost can be achieved for specific required application.

Natural/synthetic fiber hybrid composites have recently become an interesting area of research and development. For example, sisal/glass/epoxy hybrid composite was developed and found to be suitable for orthopedic bone fracture plate application [25], and automotive mono leaf spring application [26]. Glass/jute/epoxy hybrid composite was developed and found to be a viable alternative to the existing industrial safety helmet, as the hybrid composite had better mechanical properties, including better impact behavior, and was light in weight [27].

To successfully implement SFC or its hybrid in the aforementioned engineering applications, it is essential to experimentally conduct tests on these materials and avail reliable mechanical properties (strength, stiffness, fracture properties, etc.) and functional properties (flammability, acoustic and damping properties, etc.), and study ways in which its performance can be improved. Majority of the researches on the mechanical property characterization of sisal fiber reinforced epoxy composites and its hybrids focus on tensile [28]–[38], flexural [29], [31], [33]–[35], [37]–[41], impact [4], [24], [29], [34]–[37], [39] and compressive properties [4], [17], [31], [37], [38]. Research papers addressing the fracture toughness [11], [12], [42], fatigue [25] and in-plane shear properties [31] of these composites are limited.

Before the ultimate failure of FRC structures, various damage mechanisms take place which involve crack initiation and propagation. The detail assessment of damage onset, crack propagation mechanisms, and the corresponding fracture toughness values are crucial factors to take into account for the effective, safe and durable design of FRC structures. Fracture in fiber reinforced composite (FRC) laminates can occur either between two adjacent laminas (interlaminar fracture or delamination) or within a lamina (intralaminar or translaminar fracture) (Figure 3). In the first scenario, two neighboring plies separate, and the crack propagates primarily due to matrix failure or matrix-to-fiber debonding. Besides, fiber failure bridging the delamination could happen as well. In the second scenario, the lamina crack would have either a matrix crack running parallel to the fibers or an angled matrix crack with fiber failure [43].

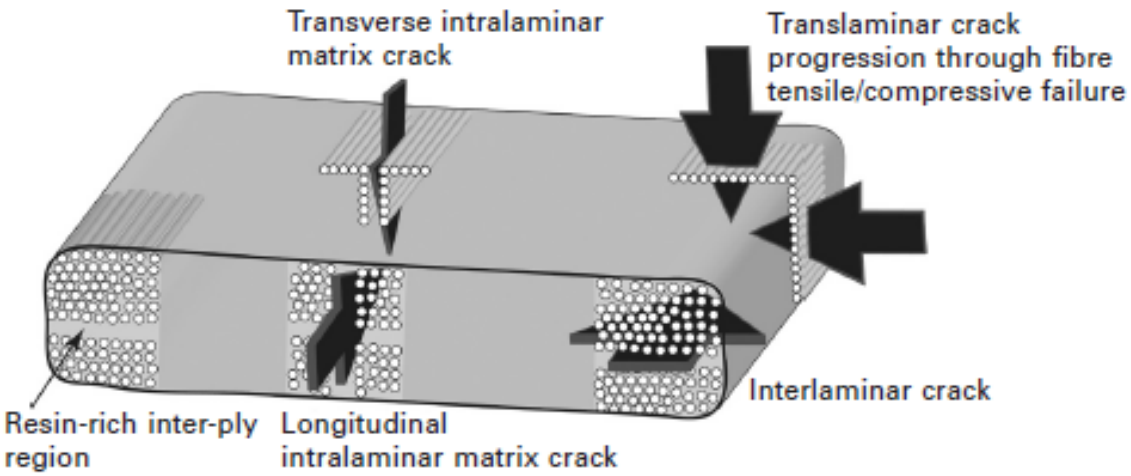

Figure 3 Fracture mechanisms in fiber reinforced composite laminates [44]

FRC failure mechanisms fall into three categories: fiber failure, matrix failure and fiber-matrix debonding. Fiber failure in composites can be classified into two modes of failure: tensile (fiber pullout, fiber fracture and debonding) and compressive fiber failure (fiber micro buckling and kinking). Matrix failure can be categorized as intra-ply matrix failure (inter-fiber fracture) and inter-ply matrix failure (delamination) [45]. All three types of fractures (matrix fracture, matrix-to-fiber debonding, and fiber fracture) should be experimentally characterized for accurate numerical modeling of composite laminates, even though delamination is the most common failure mode in laminated FRCs and fiber fracture typically consumes a much larger amount of energy than the other two [21]. Cohesive elements, smeared crack models, or X-FEM can be used to numerically model the propagation of damage. Experimental determination of the fracture

toughness value corresponding to the particular failure mode that these numerical models are modeling is necessary for each of these models [44].

FRCs intended for structural or semi-structural application should successfully sustain the applied loads and exhibit ideal performance in a range of operating conditions. Prior to the final failure of FRC structures, various damage mechanisms occur involving fracture initiation and propagation. Surface cracks (such as caused by impacted foreign objects) may propagate to the inner layer of the composite upon extended usage and/or internal damages (such as inevitable voids and matrix cracks) may propagate when they are subjected to bending loads. The propagation rate must not exceed the permissible limits to guarantee its safe operation and avoid premature catastrophic failure [46]. NFCs and their hybrids are drawing recognition in structural and semi-structural industrial applications [21]. In this regard, in addition to other physical and mechanical properties, the study of the damage onset, crack propagation mechanisms, and corresponding fracture toughness values are vital steps in the realization of SFC (or its hybrids) in structural or semi-structural applications for the understanding of their damage tolerance and crack resistance capabilities.

1.2. Statement of the Problem

Owing to their good mechanical performance, low density, low cost, biodegradability and abundance of the fiber, sisal fiber reinforced composites are one of the most promising natural fiber composites that could be used in many engineering applications. Nevertheless, one of the reasons for their limited practical use in structural and semi-structural applications is the inadequate knowledge of their fracture toughness properties. A good knowledge of their fracture toughness is essential in designing damage tolerant structures, assessing residual strength and structural integrity of structures. In the literature, very limited data is available about the intralaminar fracture characterization of sisal fiber reinforced epoxy composite and up to the knowledge of the author, the study of the effect of glass fiber hybridization on the intralaminar fracture toughness of woven sisal/epoxy composite has not been adequately addressed yet. In this research, the intralaminar fracture toughness of woven sisal/epoxy composite and the effect of glass fiber hybridization on its intralaminar fracture toughness will be studied following the most recommended method for woven composite laminates.

1.3. Objectives

1.3.1. General Objective

The main objective of this research is to study the effect of glass fiber hybridization on the intralaminar fracture toughness of woven sisal/epoxy composite.

1.3.2. Specific Objectives

The specific objectives of this research are:

- to determine polynomial coefficients using FEA (Abaqus/CAE 2017).
- to generate load-displacement curves experimentally.
- to determine critical energy release rate (G_{IC}) values.
- to plot resistance curves (R-curves) (G_{IC} vs. a).
- to qualitatively discuss the fractography.

1.4. Methodology

To achieve the objectives of the research, experimental based methodology was employed as follows.

- **Literature Survey:** Published articles, conference proceedings, MSc thesis papers, commercial report papers and books were reviewed in the areas of natural fiber composites, their mechanical characterization and application.
- **Fiber Processing:** Sisal fibers were extracted from leaves of sisal plant using manual methods and treated with appropriate chemical to enhance surface adhesion properties and reduce undesirable moisture absorption property. The fibers were then dried in the sun. After that, using hand weaving process, woven sisal fiber fabrics were prepared. Woven glass fibers were purchased from local suppliers.
- **Specimen Preparation:** Epoxy resin, mixed with hardener in the appropriate stochiometric ratio, was reinforced with woven sisal fiber fabrics in a specific fiber volume fraction using the hand layup technique to prepare composite laminates. To study the hybridization effect, a pure sisal, two hybrids of sisal and glass, and pure glass fiber reinforced epoxy composite laminates were prepared. Test specimens were cut from the prepared laminates as recommended for intralaminar fracture test of composite materials.

- **Experimental Investigation:** To evaluate the fracture toughness parameters, tensile mode-I intralaminar fracture toughness tests were performed on doubly-tapered compact tension specimen under displacement control at an appropriate crosshead speed using universal testing machine at room temperature.
- **Computational Analysis:** The FEA using Abaqus/CAE is employed to determine polynomial coefficients, which are useful in the determination of G_{IC} values.
- **Data Analysis:** Data from the tests were compiled, resistance curves (R-curves) were plotted and critical energy release rate (G_{IC}) values were determined for each material system using the recommended data reduction method.

1.5. Significance of the Study

Concerns about environmental pollution due to excessive consumption of fossil fuels have initiated the use of environmentally friendly materials. In this regard, natural fiber composites offer most invaluable alternative to non-biodegradable synthetic fiber composites. The study investigates woven sisal/epoxy composite and its hybrids as a suitable alternative for full synthetic fiber composites in structural and semi-structural applications. Studying the intralaminar fracture toughness provides information about the damage tolerance and crack resistance capabilities of these composite so that components can be designed to avoid catastrophic failure and ensure safety. The study provides an experimental data for the accurate numerical modelling of these composites. It can also be used as a reference for further investigation in this topic area.

1.6. Scope of the Study

In this research, the intralaminar fracture toughness of woven sisal/epoxy composite and the effect of glass fiber hybridization is studied experimentally. Composite specimens are loaded in tension to characterize their mode I intralaminar fracture toughness. The load-displacement responses and resistance curves (R-curves) are plotted, and critical energy release rate (G_{IC}) values are determined for pure sisal, hybrids of sisal and glass, and pure glass fiber reinforced epoxy composites, and the observed fracture behavior of the composites are discussed. Property variation of sisal fiber due to its origin is considered insignificant and is not the scope of the study.

1.7. Organization of the Thesis

The thesis is organized into five chapters. The first chapter provides a general background of the study along with the objectives to be achieved, methodologies to be followed, significance and

scope of the study. In the second chapter, an organized comprehensive review of relevant research papers for the study is provided. The third chapter provides information about the materials, methods and conditions employed in the study. Chapter 4 is dedicated for reporting results, analyzing results and discussing outcomes of the study. In the last chapter, conclusion is drawn, recommendations are provided and future study directions are suggested.

Chapter 2

Literature Review

As a result of the escalating environmental concerns and excessive utilization of fossil fuels, there is a need for eco-friendly materials. Even though synthetic fiber composites have high mechanical properties and durability, they pose problem to the environment and the ecosystem due to their non-biodegradability. In this regard, natural fiber composites are a promising replacement for synthetic fiber composites due to their eco-friendly advantages. Their popularity is rising in engineering, especially within the automotive sector. Car manufacturers are utilizing these composites for various car components. Natural fiber composites not only benefit the environment by being biodegradable and recyclable, but also contribute for the wight reduction of vehicles, which translates to better gas mileage and reduced air pollution. One of the strongest natural fibers that can be used as a reinforcement in composites in a variety of applications is the sisal fiber [15].

2.1. The Sisal Fiber and its Composite

2.1.1. The Sisal Fiber

Sisal fiber is a strong plant fiber obtained from sisal plant (*Agave sisalana*) leaves. While it is originally from tropical parts of North and South America, sisal is now extensively cultivated in tropical regions of Africa, Southeast Asia and Caribbean [7], [22]. Typically, a sisal plant produces $200 - 250$ leaves before flowering. A matured leaf constituents 4% fiber, 0.75% cuticle, 8% dry matter and 87.25% water and contains about $1000 - 1200$ fiber bundles which has a length of $1 - 1.5m$ and a diameter of $100 - 300\mu m$. Sisal fiber has an average density of $1450\ kg/m^3$, which is about 40% lower than that of glass fiber [22].

In the leaf of the sisal plant, there are three types of fibers, namely, structural, arch, and xylem fibers. Structural fibers (also called mechanical or technical fibers) are found in the periphery of the leaf (Figure 4(c)) which gives its stiffness. The cross-section of these fibers is rarely circular and usually have a horseshoe shape (Figure 5(a)). These fibers are commercially valuable since they almost never break during extraction process. Whereas, arch fibers (also called ribbon fibers) appear as part of the conducting tissues (Figure 5(b)) and are normally scattered at the central part of the leaf cross-section (Figure 4(c)). They extend all the way from base to the tip of the leaf and possess excellent strength. In contrary, Xylem fibers run in the opposite direction to that of the ribbon fibers. They are joined to the ribbon fibers within the conducting tissues. Xylem fibers are

frequently damaged and lost in the course of the extraction process since they are made up of thin-walled cells [47].

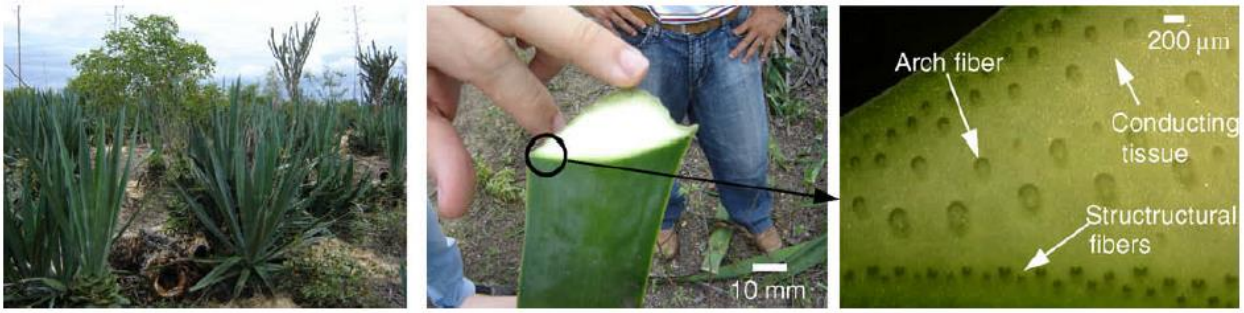

(a) (b) (c)

Figure 4 (a) Sisal plant (b) Sisal leaf (c) Optical microscopy of sisal leaf cross-section [47]

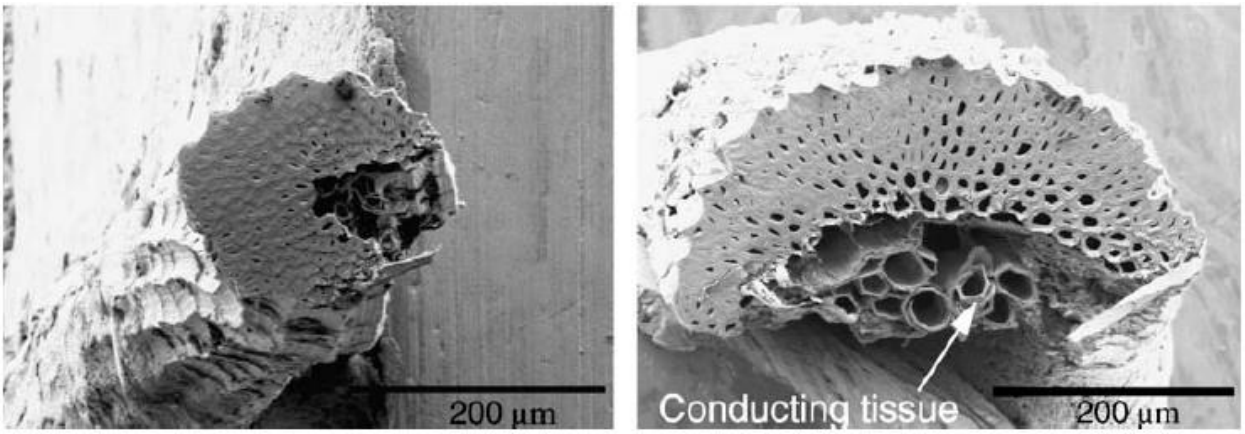

(a) (b)

Figure 5 Sisal fiber types (a) Structural fiber (b) Arch fiber [47]

Extraction of sisal fibers from the plant can be done in two main ways: (1) through soaking and scraping process (retting method), or (2) using specialized machines known as decorticators (mechanical method). While mechanical methods produce smaller amount of high-quality fibers, the retting method yields a larger quantity of fibers having lower quality. Once extracted, the sisal fibers get a thorough washing with clean water to remove any leftover plant material like leaf juices, sticky residue, and chlorophyll. Finally, they get dried in the sun or by other drying mechanisms. They are stored in a dry, clean and well-ventilated environment to prevent property degradation as a result of exposure to moisture and other undesirable conditions [22].

2.1.2. Mechanical Properties of Sisal Fibers

Mechanical properties of sisal fiber have been investigated by different researchers. For example, the average longitudinal modulus of elasticity ranges from $13-40GPa$, the average tensile strength ranges from $400-675MPa$, and the percent elongation ranges form $1.7-4.3\%$ [28], [32], [47]–[51]. These ranges are attributed to the variation in diameter and gage length of the fibers tested, test methods, plant age and its source. Chand et al. [48] studied the effects of plant age on tensile strength, tensile modulus and toughness by testing sisal fibers extracted from 3,5,7 and 9 years old sisal plants. They also studied the effect of temperature on these properties. It was shown that the fiber tensile strength, tensile modulus and toughness increased with plant age and decreased with increase in temperature. Inacio et al. [49] studied the dependence of tensile strength on diameter of sisal fiber. They showed that diameter of fiber and tensile strength have inverse relation (the smaller the diameter the larger the tensile strength).

2.1.3. Composite Fabrication Methods

In order to fabricate fiber reinforced composites (FRCs), fiber preforms are first prepared and then reinforced with the appropriate matrix material using a variety of methods. Some of the conventional techniques for manufacturing FRCs include the hand lay-up, spray-up, vacuum bagging, resin transfer molding, compression molding, pultrusion process, injection molding and filament winding techniques. These and other advanced composite manufacturing techniques are reviewed in [52]. Each of these manufacturing techniques have their own merits which makes them appropriate to be used in specific applications. Among these techniques the hand lay-up technique (Figure 6) is the most popular. It is a simple and open mold technique used widely in composite manufacturing.

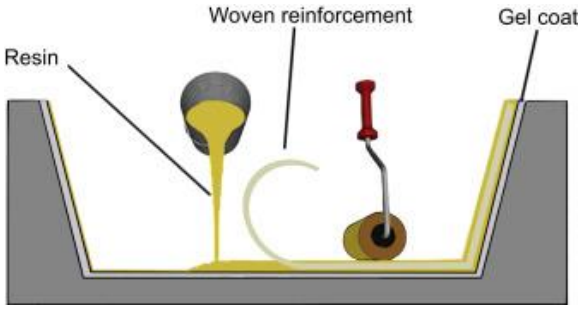

Figure 6 The hand lay-up method

In this technique, first the mold is coated with releasing agent (antiadhesive oil or gel), which allows ease removal of the final part. Then, the required amount of pre-shaped fiber preforms are

placed in the mold as per the desired orientation and sequence. Next, the matrix material is either poured or brushed on. A roller then presses the resin into the fiber preform, ensuring good impregnation of the fiber with the resin.

2.1.4. Mechanical Properties of Sisal/Epoxy Composite

When assessing the applicability of NFCs as engineering load-bearing components, the specific strength and specific stiffness are two of the main engineering properties to be evaluated. These parameters represent how efficient a material is in terms of strength and stiffness relative to its weight. Specifically, they are ratio of effective strength to its density and effective stiffness to its density, respectively. These and other mechanical properties of sisal/epoxy composite have been studied by different researchers.

For unidirectional sisal/epoxy composite, the longitudinal tensile strength and modulus have been evaluated by different researchers. Oksman et al. [28] obtained longitudinal tensile strength of $211\ MPa$, tensile modulus of $19.7\ GPa$ and elongation at break of 1.9 % for fiber volume fraction (V_f) of 46%. Li et al. [29] reported longitudinal tensile strength and modulus of $180.45\ MPa$ and $14.8\ GPa$, respectively for fiber weight percentage of $46\ wt\%$. Whereas, Dagne [30] obtained longitudinal tensile strength and modulus of $102.53\ MPa$ and $4.56\ GPa$, and transverse tensile strength and modulus of $1.387\ MPa$ and $0.17\ GPa$, respectively for fiber volume fraction of 40 %. And, very recently, Zuccarello et al. [32] reported longitudinal tensile strength and modulus of $300\ MPa$, and $15\ GPa$ for fiber volume fraction of 40%.

Dagne [30] also investigated the compressive and in-plane shear properties of unidirectional sisal/epoxy composite and reported a longitudinal and transverse compressive strength of $11.5\ MPa$ and $20.13\ MPa$, and in-plane shear strength and modulus of $0.533\ MPa$ and $0.208\ GPa$, respectively for fiber volume fraction of 40 %. Regarding the flexural strength and modulus of unidirectional sisal/epoxy composite, Bisanda and Ansell [31] obtained $266.5\ MPa$ and $15.93\ GPa$, respectively with fiber volume fraction of 40% and Li et al. [29] obtained $191.37\ MPa$ and $11.86\ GPa$, respectively. Li et al. [29] also evaluated the impact strength of unidirectional sisal/epoxy composite and obtained an impact strength of $46.75\ kJ/m^2$ for fiber weight percentage of $46\ wt\%$.

For randomly oriented chopped sisal/epoxy composite, Betelie et al. [39] studied the tensile, flexural, and impact properties as a function of fiber content. Fiber weight fractions of 15, 25, 30,

35 and 40 $wt\%$ were tested. Fibers were cut to a length of 300 mm and 10% NaOH treatment was applied to improve the interfacial adhesion property of the fiber. A maximum tensile strength of 85.5 MPa and a maximum flexural strength of 85.79 MPa was resulted for fiber weigh fraction of 30 $wt\%$. Whereas, a maximum impact strength of 24.5 kJ/m^2 was found for fiber weight fraction of 40 $wt\%$. For the same material system, Kebede [17] investigated the tensile and compressive properties for fiber weight fraction of 15, 25 and 35 $wt\%$. Fibers were cut to a length of 9 mm and 18% NaOH treatment was applied. Composite samples with untreated fibers were also tested. According to his report, maximum tensile strength of 40.11 MPa was found for the 35 $wt\%$ treated one and higher compressive strength of 10.9 MPa was found for the 25 $wt\%$ untreated one.

For woven sisal/epoxy composite, Dennis [53] investigated the tensile, compressive, impact and flexural properties. Alkaline treatment with 4% NaOH solution for 1 hr was used. For fiber weight fraction of 30 $wt\%$ a tensile strength and modulus of 30.13 MPa and 3.87 GPa; compressive strength and modulus of 22.26 MPa and 2.74 GPa; impact strength of 27.38 kJ/m^2, and flexural strength and modulus of 23.92 MPa and 2.98 GPa was reported, respectively.

A comparative study of tensile and flexural properties between unidirectional and woven fabric form of sisal/epoxy composite was reported by Gupta and Sirvastava [33]. For fiber weight percentage of 30 $wt\%$, a tensile strength of 132.73 MPa and 89.3 MPa, and flexural strength of 288.6 MPa and 152.12 MPa was reported for unidirectional and woven form, respectively. The woven fabric form exhibited less tensile and flexural properties than the unidirectional form. This is quite expected as it is evident that as far as the total fiber content is kept constant there would be less fibers aligned in particular direction for woven fabrics than the unidirectional one. However, it should be noted that the woven form maintains these properties in the transverse direction, whereas the unidirectional form could exhibit transverse properties even lower than the matrix alone [32].

2.1.5. Effect of Fiber Treatment

The chemical composition of sisal fiber depends on its source and plant age. Generally, sisal fiber contains $50-80\%$ cellulose depending on its source and age, the rest being lignin, hemi-cellulose, wax, and ash. Cellulose, which is the largest percentage of the sisal fiber, is a hydrophilic glucan polymer which gives the sisal fiber hydrophilic properties. Owing to their hydrophilic

properties, sisal fibers are known for their weak adhesion to hydrophobic epoxy matrix, which leads to lower mechanical properties and undesired moisture absorption properties [22]. The usual strategy to mitigate this problem is to employ fiber treatments.

Different chemical, physical and radioactive treatments are used to improve the interfacial strength. Chemical treatments such as alkalization, acetylation and salination are observed to improve the interfacial adhesion between sisal fiber and epoxy matrix [23], [24], water resistance [31], [54], [55], porosity [23], tensile [4], [56], compressive [4], [31], interlaminar shear strength (ILSS) [57] and impact [4], [24] properties. But in most cases these treatments were not observed to have significant effect on flexural properties of sisal/epoxy composites [31], [40], [41]. Being less common, physical [24], [58], [59] and radioactive [60] treatments can also be used to improve interfacial adhesion and mechanical properties of sisal/epoxy composites.

Alkaline treatment (also called mercerization) is by far the most widely used chemical treatment method for natural fibers. Alkalization has two effects on the fiber surface, (1) it cleans the surface of the fiber by removing some of the waxy and oily substances, creating more chemically homogeneous fiber surface and exposing cellulose to the surface in a larger extent; (2) it depolymerizes the cellulose and exposes the short length crystallite, creating a rough fiber surface. Both of these effects contribute for enhanced adherence of the fiber with the matrix [61].

Alkalization makes the cellulose more amorphous, which comes at the cost of reducing the amount of crystalline cellulose. The desired condition occurring in the process is the removal of hydrogen bond in the network structure. Addition of alkaline solution to natural fiber facilitates the ionization of the hydroxyl group to the alkoxide. Both the concentration of the alkaline solution and the duration of the treatment have impact on the final fiber properties [61].

$$Fiber\_OH + NaOH \rightarrow Fiber\_ONa^{+} + H_2O$$

If a treatment (chemical, physical or radioactive treatment) could strengthen the sisal fibers themselves and also improve how well they bond with surrounding matrix material, it would significantly enhance the mechanical properties of the resulting composite. An optimized fiber treatment is a way of realizing sisal fiber composites and their hybrids for potential structural application [59].

2.1.6. Other Factors Affecting Mechanical Properties of Sisal/Epoxy Composite

Most of studies in sisal fiber are on the longitudinal properties. Whereas studies on the transverse properties are limited. The anisotropy of sisal fiber has been studied by some researchers. Zuccarello et al. [32], Ntenga et al. [62], and Thomason et al. [63] highlighted that sisal fiber exhibits high degree of anisotropy. These researchers showed that the transverse tensile modulus is about 5%, 12% and 7.3% of the longitudinal one, respectively. Sinitsky et al. [15] showed that this high degree of anisotropy adversely affects the effective transverse modulus of elasticity of SFCs and both the longitudinal and transverse modules must be considered when designing SFC structures.

In addition to the anisotropy of the fiber, properties of sisal/epoxy composite depend on different factors (fiber content, fiber arrangement etc.). Zuccarello et al. [32] also studied the influence of fiber content on mechanical properties of the sisal/epoxy composite. They considered typical range of fiber volume fractions ($0.2 \leq V_f \leq 0.7$) used for structural applications. They showed that while the longitudinal tensile strength and modulus increase with fiber content, transverse tensile strength decreases. Whereas, increasing fiber content (in the range they have considered) seemed to have no significant influence on transverse tensile modulus. Srisuwan et al. [41] have showed that flexural strength and modulus of this composite also tend to increase with fiber contents. Better penetration of epoxy resin into sisal fiber lumens can also improve its tensile, flexural and impact behavior, and enhance its water absorption resistance [29]. It is worth nothing that there is what is called 'optimal fiber volume fraction' beyond which mechanical property starts to decline. For example, Betelie et al. showed that tensile strength [39], flexural strength [39] and intralaminar fracture toughness [12] of sisal/epoxy composite increased with fiber loading and reached its maximum at 30 $wt\%$ and started to decline afterwards.

Considering the sisal fiber arrangement, unidirectional form exhibits better tensile and flexural properties than that of the woven fabric form in the longitudinal direction [33]. Woven fabric composites are getting increasing acceptance in structural applications owing to their excellent packaging of fibers, higher fiber volume fractions for a given volume of composite and superior mechanical performances [11]. Using woven fabric improves the fracture toughness of NFCs [64]. Some of the advantages of woven fabric composites compared to unidirectional composite are enhanced impact resistance, damage tolerance, dimensional stability and ease of manufacturing

[45]. Mahtebu [65] studied the effect of fiber orientation on the fatigue performance of sisal/epoxy composite. Laminates of $[0°, 90°]_2$, $[0°, 45°]_2$, and randomly oriented composite layups were tested under completely reversed stress cycles using three-point bending test system. From his results, all the three laminates manage to reach a fatigue life of $10^6\ cycles$. The $[0°, 45°]_2$ laminate demonstrated a better load carrying capacity with a representative flexural load of $220\ N$. Whereas, the $[0°, 90°]_2$ and the randomly oriented laminates exhibited better fatigue life with a representative flexural load of $150\ N$.

2.2. Hybridization

2.2.1. Hybrid Composites

Hybrid composites are FRCs that are prepared from the systematic combination of two or more reinforcement fibers in a single matrix to achieve desired properties. Generally, hybrid composites are designed to offer synergistic effects of the constituent reinforcements. They could be regarded as the weighted sum of the different constituents, where the disadvantage of one constituent is compensated by the other [21].

Based on fiber distribution, hybridization can be categorized into three, namely, interply, intraply or super hybridization. Interply hybridization involves layers of individual reinforcements stacked one over the other, intraply hybridization involves the mixing of different reinforcements within a ply, whereas, super hybridization comprises layers of metal, composite and matrix combined in a particular sequence [21].

Hybrid composites offer many advantages over monolithic composites, this includes but not limited to, the flexibility of obtaining required properties and possibility of designing cost effective composite. They also offer synergistic effects such as improved tensile and bending strength, and change in fracture propagation behavior as well as compensation of disadvantages such as cost effective and lightweight designs are possible with hybrid composites [21].

2.2.2. Natural/Synthetic Hybrid Composites

As of the inherent hydrophilic nature and variability of properties of natural fibers, NFCs struggle to fulfill the mechanical and thermal property requirements for structural and semi structural applications. Hybridization technique is one of the improvement strategies in this regard [21]. Natural fiber composite has lower strength than that of many of the synthetic fiber composites, however hybridization of natural fiber with synthetic fiber significantly enhances not only its

strength but also has other additional benefits. Hybridization of natural fibers with synthetic fibers in a polymer matrix gives the advantage of obtaining a combination of properties that can overcome the limitations of natural fibers for use in structural components. Hybridization reduces the moisture absorption behavior of NFCs. It is also important to obtain balanced mechanical and thermal properties, and increases the durability of NFCs [3], [7], [21]. In such a hybrid composite a balance of strength, weight and cost can be achieved for specific required application.

2.2.3. Mechanical Properties of Sisal/Glass Hybrid Composite

Addition of glass fiber has shown enhancement in the mechanical properties of SFCs. Arpitha et al. [66] studied the mechanical properties (tensile, flexural and impact) of sisal/glass/epoxy hybrid composite. Both the sisal and E-glass fibers were in plain-woven fabric form. Composite specimens with five layers having different stacking sequence (all-glass, all-sisal, G/S/S/S/G, and G/S/G/S/G) and total weight percentage of fibers ranging from $27 - 37\ wt\%$ were prepared using the hand layup method followed by vacuum bagging. The G/S/G/S/G sequence exhibited better tensile, flexural and impact properties ($168.8\ MPa$, $241.2\ MPa$, and $976.1\ J/m$) following the all-glass specimens ($346.6\ MPa$, $318.7\ MPa$, and $1470.5\ J/m$). The all-sisal specimens exhibited the lowest values ($33.1\ MPa$, $124.6\ MPa$, and $147.1\ J/m$).

Arthanarieswaran et al. [34] evaluated the mechanical properties (tensile, flexural and impact) of sisal/banana/glass fiber reinforced epoxy composite. The natural fibers were in chopped form whereas the E-glass fiber were in woven form. Composite samples having different stacking sequence (B, S, BS, G/B/G, G/S/G, G/BS/G, G/B/G/B/G, G/S/G/S/G and G/BS/G/BS/G) and total fiber volume fraction ranging from $27 - 31\%$ were prepared using the compression molding method. Adding more layers of glass fibers increased its tensile strength. Two layers increased it by a factor of 2.34, and three layers by a factor of 4.13. Better tensile strength ($104\ MPa$) was observed from the G/BS/G/BS/G sequence followed by G/S/G/S/G sequence ($93\ MPa$). Better flexural strength ($192\ MPa$) was observed from the G/BS/G sequence followed by G/S/G/S/G sequence ($184\ MPa$). Better impact strength ($13.3\ J$) was observed from the G/S/G/S/G sequence.

Ramesh et al. [35] evaluated the mechanical properties (tensile, flexural and impact) of sisal/jute/glass fiber reinforced polyester composites. Composite specimens with five layers, the top, middle and bottom layers being unidirectionally woven mat glass fibers and the second and fourth layers being chopped sisal and/or jute fibers were prepared using the hand layup method.

The sisal/glass fiber composite resulted maximum impact strength ($18.67\ J$), jute/glass fiber composite yielded maximum tensile strength ($229.54\ MPa$), and sisal/jute/glass fiber composite displayed maximum flexural strength.

The results of the above researches show that addition of glass improves the mechanical properties of SFCs significantly and the mechanical properties are directly affected by the stacking sequence. Generally, the one with the glass fiber layers being at the top, middle and bottom layers exhibited better properties. This was also evident by the work of Amico [67].

Regarding the fiber orientation, Ram and Raj [36] investigated the influence of fiber orientation ($0/90°$ vs. $\pm 45°$) on mechanical properties of woven sisal/glass/epoxy hybrid composite with a $50:50$ combination of sisal-to-glass ratio. It was shown that the $0/90°$ orientation resulted significantly better tensile strength than the $\pm 45°$ orientation ($172.4\ MPa$ vs. $64.2\ MPa$). Whereas, the impact strength of $\pm 45°$ orientation was shown to be appreciably better than the $0/90°$ orientation ($14.8\ J/cm^2$ vs. $19.2\ J/cm^2$).

Palanikumar et al. [37] investigated the mechanical properties (tensile, flexural and impact) of unidirectionally woven glass and woven sisal fiber reinforced epoxy hybrid composite for different proportion of these two fibers. For all the specimens, ten layers were used by varying the number of sisal-to-glass layers. The volume of the epoxy resin was kept constant and the weight percentage of the two constituent fibers was varied, glass-to-sisal ratio of $100:0$, $90:10$, $80:20$, $70:30$, and $60:40$ were tested. Results showed that the maximum values for the tensile, flexural and impact strength were $181.84\ MPa$, $288.8\ MPa$, and $18.1\ J$ for the pure glass fiber composite and due to the substitution of glass fibers by sisal fibers from 0 to $40\ wt\%$, a decrease in tensile, flexural and impact strength by 21.7%, 27.8%, and 27.1% was observed. They identified the $80:20$ combination as a good combination, which only exhibited 5.8% decrease in tensile strength.

John and Naidu [68] studied the effect of fiber content on impact strength and compressive strength of chopped strand mat sisal/glass fiber reinforced polyester hybrid composite. The study found that increasing glass fiber content as well as total fiber content significantly enhanced the hybrid composite's impact strength. Unlike impact strength, compressive strength of the hybrid composite behaved differently. It decreased as the total fiber content increased, even falling below the compressive strength of the matrix material. However, the compressive strength did actually improve with a higher amount of glass fibers specifically in the hybrid composite.

Arumugam et al. [38] studied the mechanical properties (tensile, flexural and compressive) of plain-woven glass and sisal fibers reinforced epoxy hybrid composite aiming for orthopedic bone plate application. The woven glass fiber and sisal fiber composite layers were arranged as a sandwich structure, single glass fiber layers at the top and bottom, and 3 or 4 sisal fiber layers in the middle. Chitosan particles were used in both type of layers to strength the epoxy matrix. By varying the number of sisal fiber layers and $wt\%$ of chitosan particles used, six composite samples were tested. In their report the tensile strength ranged from $120 - 146\ MPa$, the flexural strength ranged from $201 - 343\ MPa$, and the compressive stress ranged from $237 - 380\ MPa$. Extending the research, in [25] they studied the fatigue properties and biomimetic activity. A fatigue life of more than 1 million cycles ($1.2 \times 10^6\ cycles$) was obtained for the hybrid composite. The requirement for the formation of biological bone apatite layer was confirmed. They concluded that the hybrid composite could be applied for orthopedic bone fracture plate application.

2.3. Fracture Toughness

Fracture toughness is the ability of a material to store energy prior to fracture. It can also be seen as the ability of a material to resist crack propagation [21]. Cracks (defects) originate in a material during manufacturing (inevitable voids during molding, drilling, surface finishing, etc.), transporting (mishandling) and service (impacted foreign objects). Crack initiation and propagation generally cause the release of strain energy. Load bearing materials are expected to absorb some amount of energy before final failure. Final failure is the consequence of unstable propagation of cracks through the material. Fracture toughness is measured in terms of critical stress intensity factor K_C, or critical energy release rate G_C. The fracture toughness of FRCs is evaluated either under quasi-static or cyclic fatigue conditions for the following loading modes: mode I (tensile opening), mode II (in-plane shearing), mode III (out-of-plane twisting) or a combination of them (Figure 7).

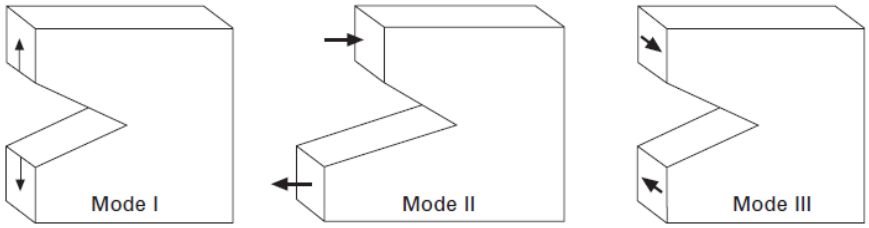

Figure 7 Common modes of fracture [44]

2.3.1. Failure Modes of FRCs

Failure mechanisms of FRCs can be categorized as fiber failure, matrix failure and fiber-matrix debonding. Fiber failure in composites can be of two modes of failure: tensile and compressive fiber failure. Fiber pullout, fiber fracture and debonding are typical tensile fiber failure modes. Fiber pullout failure occurs in composites where both the fiber and matrix are brittle. At the early stage of tensile loading, fracture of local fibers occurs followed by stress redistribution. Then after, fiber matrix debonding occurs which is accompanied by fiber breakage that leads to final failure. However, in compressive loading, fiber failure is more associated with fiber stability like fiber micro buckling and kinking rather than fiber strength. Besides, it is influenced by fiber misalignment. Matrix failure can be categorized as intra-ply matrix failure (inter-fiber fracture) and inter-ply matrix failure (delamination). Intra-ply matrix failure frequently begins at fiber-matrix interface and propagate into the matrix. Delamination is caused by micro cracks in the matrix between plies, which is a result of high interlaminar stresses [45]. Yet the most prevalent failure mode in laminated FRCs is delamination [21].

2.3.2. Types and Modes of Fracture.

Prior to the final failure of FRC structures, various damage mechanisms occur which involve crack initiation and propagation. For the effective, safe and long-lasting design of FRC structures, the assessment of damage onset, crack propagation mechanisms, and the corresponding fracture toughness values are fundamental factors to be considered. In FRC laminates, fracture can occur either between two adjacent laminas (interlaminar fracture or delamination) or within lamina (intralaminar or translaminar fracture) (Figure 8) [43].

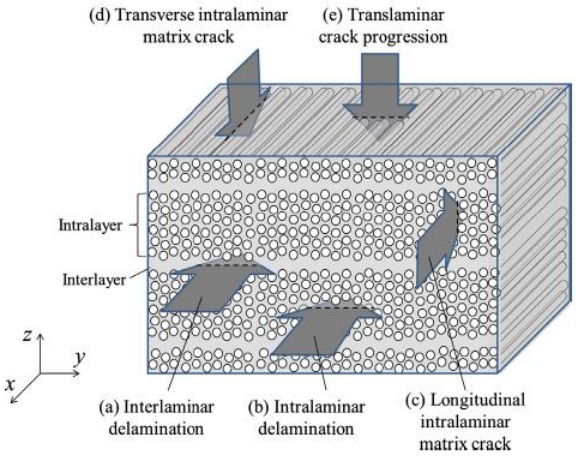

Figure 8 Fracture modes in laminated composites [69]

The first results in debonding of consecutive layers and crack growth is majorly through matrix failure or matrix-to-fiber debonding. Besides, some fibers bridging the crack may break as well. In the second case, cracks inside a layer (intralaminar cracks) can propagate in two ways: either along the fibers (propagation by matrix crack) or at an angle to them (propagation by both matrix and fiber fracture). When these cracks take an angled path, the fibers that bridge the cracks either arrest it or reduce the propagation rate until they themselves break [43].

Though the energy associated with fiber fracture is almost always higher than the others, for the accurate numerical modeling of composite laminates all the three failure types (matrix fracture, matrix-to-fiber debonding and fiber fracture) should be experimentally characterized [43]. Damage propagation can be numerically modelled and analyzed employing cohesive elements, smeared crack models, or X-FEM. For a successful modelling of a particular failure mode using these numerical models, an experimentally determined fracture toughness value of the respective failure mode is necessary [44].

The fracture toughness associated with interlaminar fracture has been given so much attention in the literature for several years. As a result, different test specimens, testing methods and standards have been developed for different modes of fracture [70]–[72]. However, the characterization of intralaminar fracture toughness has not been studied in a greater extent as the occurrence of large-scale fiber bridging poses some difficulties during the experimental process [46].

2.3.3. Fracture Toughness Test Standards

As can be referred in the ASTM E399-12 standard [73], the compact tension (CT) test specimen was originally developed for studying crack propagation in metallic materials. It has also been commonly used to evaluate intralaminar fracture toughness parameters in fiber reinforced polymer composite (FRPC) laminates. A similar standard to that of the above standard which uses CT test specimen for evaluating fracture toughness parameters of plastic materials is the ASTM D5045-14 standard [74]. This standard has also been commonly employed to characterize intralaminar fracture toughness in FRPCs [75].

The extended compact tension (ECT) specimen is another ASTM standardized specimen (ASTM E1922-04 [76]) for characterizing translaminar fracture toughness in laminated polymer matrix composites. The design of the ECT specimen is similar to the CT specimen, but taller in height. There are also other varieties of the CT specimen such as widened compact tension (WCT) and

tapered compact tension (TCT). The WCT and TCT specimens were proposed as alternative versions of the CT specimen which can reduce the induced vertical compressive stresses generated in the right edge of the CT specimen. Induced vertical compression stress in these specimens might cause failure of the composite as a result of vertical compressive fiber breaking or kinking [75].

The use of the above standards for FRPCs should guarantee that the dominating damage mechanism be crack propagation in the expected crack plane. To confirm that the expected crack propagates without any other damage mechanism, Blanco et al. [75] studied the different varieties of the CT specimen to determine the most suitable geometry for the characterization of tensile intralaminar fracture toughness in woven composite materials. Using the finite element analysis in combination with virtual crack closure technique, they examined the effect of various geometrical parameters for the initiation and propagation of several failure mechanisms on different versions of the CT specimens (CT, ECT, WCT, TCT) and a newly proposed doubly-tapered compact tension (2TCT) specimen.

Examining the results of the considered specimens, they deduced that the 2TCT specimen offers better assurance for crack propagation in the expected crack plane for intralaminar fracture toughness characterization of woven laminated composites. They also noted that while this specimen geometry could not guarantee the occurrence of other failure mechanisms during an experimental test, it results in lower probability of failure by other failure mechanisms. Particularly a 60% reduction in failure index was attained by the 2TCT specimen in failure due to vertical compression stress at the right edge, which is the most undesired failure mechanism in CT specimen. Particularly this is achieved when the specimen has sufficient thickness to avoid failure due to global instability [75]. The proposed geometry of the 2TCT specimen is shown in Figure 9 where the initial crack length is $a_0 = 20mm$.

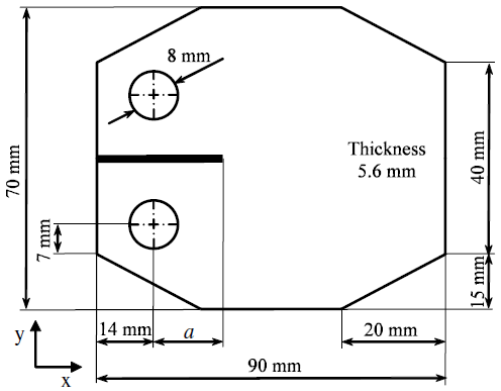

Figure 9 Doubly-tapered compact tension (2TCT) specimen geometry [43]

In the second part of the research by Blanco et al. [43] they experimentally examined the usefulness of the 2TCT specimen for tensile intralaminar fracture toughness characterization of woven composite laminates using carbon/epoxy composite. To determine the existence of other damage mechanisms affecting the experiment by dissipating energy, they examined images captured using digital image correlation (DIC), X-Ray and ultrasounds (C-Scan), during and after the test. They concluded that the presence and effect of damage mechanisms other than intralaminar crack advancement along the expected crack plane was insignificant and the experimental results were reliable.

2.3.4. Factors Affecting Fracture Toughness of Natural Fiber Composites

There are number of research papers that focus on fracture characterization of NFCs in which some of these were recently reviewed by Chittimenu et al. [8]. From their review they concluded that since most of the NFCs incorporate a brittle matrix and a high elastic modulus fiber, their fracture toughness could be determined using the linear elastic fracture mechanics (LEFMs) approach, which considers materials behave elastically at the vicinity of the crack tip, with stress intensity factor and energy release rate being the primary parameters. They also pointed that fracture toughness of NFCs depend on fiber parameters like fiber type, fiber architecture, fiber treatment, fiber orientation and fiber hybridization, and are affected by hydrothermal aging.

Silva et al. [77] studied the effect of fiber type, fiber architecture, fiber treatment and displacement rate on fracture toughness (G_{IC}) of sisal and coconut fibers reinforced castor oil polyurethane composites employing the compact tension (CT) method. Short fibers and woven fabric were used with and without 10% NaOH treatment. Their result shows that woven sisal fabric possessed the highest G_{IC} and short sisal fibers displayed better G_{IC} than the coconut fiber composite. The alkaline treatment reduced the G_{IC} of sisal fiber/castor oil polyurethane composite. Whereas, for the coconut fiber/castor oil polyurethane composite the alkaline treatment improved the fracture toughness. They pointed that the fracture toughness was not significantly influenced by strain rate.

Ismail et al. [78] investigated the role of fiber orientation on fracture toughness (K_{IC}) of woven kenaf/polyester composite with the single-edge notch bend (SENB) test. They used fiber orientations such as $0/15/0/-15/0$, $0/30/0/-30/0$, $0/45/0/-45/0$, and $0/90/0/-90/0$. In addition, they tested unidirectional type. From their result it was shown that there was no strong relationship between fiber orientation and fracture toughness and unidirectional type composites

showed better K_{IC} compared to woven one since fibers are mostly aligned in the stress direction. Whereas, Pinto et al. [79] studied the effects of fiber architecture on the fracture toughness of jute/epoxy composite using the double cantilever beam (DCB) method. They showed that woven form had better fracture toughness than the unidirectional form.

Liu and Hughes [80] studied the influence of linear density, weave configuration and stacking sequence on fracture toughness (K_{IC}) of woven flax fiber reinforced epoxy composite using the CT method. They found that addition of woven fabric reinforcement enhanced the K_{IC} value by a factor of $2-4$ times when compared with that of the pure epoxy. The K_{IC} value was highly influenced by the linear density of the weft tows and orientation of the stacking sequence; however, the weave configuration had no significant effect. They concluded that fracture toughness is appreciably affected by the fiber volume fraction rather than the fiber architecture.

Regarding effects of fiber treatment on fracture toughness, Abdullah et al. [81] examined the effect of alkaline and silane treatments, and their combination on fracture toughness (K_{IC}) of coconut spathe fibers reinforced in epoxy resin. Composites with treated fibers showed decreased K_{IC} values as compared to their untreated counterparts. Specifically alkaline treatment showed 60% drop and the other treatments displayed a slight drop. The sharp drop with the alkaline treatment was due to the enhanced interfacial adhesion, which weakened the major energy absorption mechanisms namely, debonding and fiber pullout. Pickering et al. [82] also reported the decreasing trend of fracture toughness with alkaline treatment in random short hemp fiber/polylactide (PLA) composite. Whereas, Li et al. [83] reported an improvement in fracture toughness of woven sisal/vinyl ester composite when the fiber is treated with chemical coupling with silane and oxidization with permanganate ($KMnO_4$) and dicumyl peroxide. Pinto et al. [79] also reported an improvement in fracture toughness of jute/epoxy composite with alkaline treatment.

Zhang et al. [84] studied the interply hybridization effect on fracture toughness (G_{IC}) of composites made by synthetic and natural fibers. Unidirectional flax/glass fibers reinforced in phenolic resin was tested using DCB method. They found that the fracture toughness of the hybrid composites was even higher than pure glass fiber composite which was due to the improved performance of the hybrid interface. Pereira et al. [85] examined the effect of intraply hybridization on fracture toughness (G_{IC}) of sisal+curauá/epoxy and jute+curauá/epoxy composites using DCB method.

They also found that the hybrid composites have higher G_{IC} value than pure sisal and jute composites. They pointed that the intraply hybridization suppressed the crack propagation.

Alomayri et al. [86] investigated the influence of water absorption on fracture toughness of cotton fabric reinforced geopolymer composites. They exposed the composite to water aging for 133 days. The results showed that, magnitude of water uptake and diffusion coefficient increased with an increase in fiber content and fracture toughness (K_{IC}) value is decreased as a result of water absorption. Islam et al. [87] examined the influence of hygrothermal aging on fracture toughness (K_{IC}) of hemp/polylactic acid (PLA) composites using SENB test. The hygrothermal aging was introduced by immersing composite samples in distilled water at 25℃ and 50℃ for 3 months. K_{IC} value of the composite was found to decrease in both the water and hygrothermal aging cases. The effect was more pronounced in the latter case. Islam et al. [88] further expanded their research to study the influence of accelerated weathering. The hemp/PLA composite was exposed to ultra violate (UV) irradiation and sprayed water at a temperature of 50℃ for time intervals of 250, 500, 750, and 1000 hours). Their results showed a decrease in K_{IC} value of the composite with increasing weathering time. Despite the decline in K_{IC} value, the composite was found to perform better that neat PLA.

2.3.5. Intralaminar Fracture Toughness of Natural Fiber Composites

Fracture toughness of the intralaminar failure mode is one of the fundamental mechanical properties of FRCs. It is designated by G_{IC} when articulated in terms of fracture energy, or K_{IC} when described in terms of stress intensity factor. With growing application of NFCs, the measurement of their intralaminar fracture toughness plays essential role in designing damage tolerant structural and semi-structural components. In the literature, studies investigating the intralaminar fracture toughness of NFCs are limited.

Hughes et al. [89] studied the intralaminar fracture toughness of chopped hemp and jute fiber reinforced polyester composites using SENB test and compared with that of laminate reinforced with chopped strand mat glass fiber. K_{IC} value of the NFCs was found to be three times lower than the volume equivalent ($V_f = 0.2$) of glass fiber mat composite. They explained that this is because various micro-structural toughening mechanisms are not being stimulated to the same extent in the NFCs as they are in GFRP composite.

Silva et al. [77] reported $G_{IC} = 11.5\ kJ/m^2$ of woven sisal/castor oil polyurethane composites with $V_f \approx 30\%$ using the CT method according to ASTM D5045 standard. Using the same method and standard, Li et al. [83] obtained $K_{IC} = 4.2\ MPam^{1/2}$ for untreated woven sisal/vinyl ester composites which improved to 5.5 and $6.0\ MPam^{1/2}$ with silane and $KMnO_4$ treatments, respectively with $V_f \approx 32\%$. Ismail et al. [78] used the SENB test according to ASTM D5045 standard to evaluate the intralaminar fracture toughness of woven kenaf/polyester composite and obtained $K_{IC} = 4.0\ MPam^{1/2}$. For the unidirectional kenaf/polyester composite K_{IC} was as high as $8.0\ MPam^{1/2}$. Using the same method and standard, Ashik et al. [90] reported $K_{IC} = 7.7\ MPam^{1/2}$ for woven jute/epoxy composite with $50\ wt\%$ of fibers. Liu and Hughes [80] obtained $K_{IC} = 9.0\ MPam^{1/2}$ of woven flax/epoxy composite with $V_f \approx 39\%$ using the CT method according to BS 7448 standard. Recently, Saadati et al. [91] studied translaminar fracture toughness of unidirectional flax/epoxy composite using the compact tension (CT) method according to ASTM E1922 standard. They reported $G_{IC} = 7.37\ kJ/m^2$ for $V_f = 41\%$.

Gudeta [92] investigated the intralaminar fracture toughness and the effect of water aging on the intralaminar fracture toughness of sisal/glass/polyester hybrid composite. The 2TCT specimens according to ASTM D5045 and rectangular specimens according to ASTM 5229 were used for the mode-I intralaminar fracture toughness and water absorption tests, respectively, which were manufactured by the hand lay-up method. A $2\ mm$ and $5\ mm$ thickness specimens were prepared from 5% NaOH treated woven sisal fibers and randomly oriented E-glass fibers with total $V_f \approx 50\%$ and relative Sisal-to-Glass fiber volume ratio of $45{:}55$ with a stacking sequence of G/4S/G and G/10S/G were used. The rectangular specimens were immersed in rain water for one week period. He reported fracture toughness value of $K_{IC} = 10.2\ MPam^{1/2}$ and $K_{IC} = 16.68\ MPam^{1/2}$, and maximum water absorption value of 0.063% and 0.034% for $2\ mm$ and $5\ mm$ thickness specimens, respectively. Also, due to 7 days of rain water aging, the fracture toughness value of the $5\ mm$ thickness specimen was reported to decrease to $K_{IC} = 12.27\ MPam^{1/2}$.

In the literature, very few studies are available regarding the intralaminar fracture toughness of sisal/epoxy composite. Betelie et al. [12] investigated the intralaminar fracture toughness of chopped sisal/epoxy composite with fiber weight percentage ranging from $15 - 40\ wt\%$ using the CT method according to ASTM D5045 standard. Composites were manufactured using the hand

lay-up and compression molding techniques. Fracture toughness tests were conducted at crosshead speed of $0.5\ mm/min$ using universal testing machine (UTM). Results showed that K_{IC} value increased as fiber content increased and reached a maximum value of $K_{IC} = 5.54\ MPam^{1/2}$ (or $G_{IC} = 13.72\ kJ/m^2$) at fiber weight percentage of 30 $wt\%$, and decreased afterwards.

Using the same method and standard, Kim and Seo [42] studied the influence of water absorption on intralaminar fracture toughness of woven sisal/epoxy and sisal/vinyl ester. Two layers of plain-woven sisal fibers which are twisted 3 times per inch were used with $V_f \approx 32\%$. Composite samples, fabricated using resin transfer mold (RTM) method, were subjected to cycles of wetting with distilled water for 9 days until it was fully saturated and dried for one day at a temperature of $50℃$. Fracture toughness tests were conducted before and after 5 cycles of subsequent wetting and drying. In both of the considered composites, water absorption by the composite was found to increase and K_{IC} value was found to decrease with increasing cycle times of wetting and drying. The K_{IC} value for the sisal/epoxy and sisal/vinyl ester composites reached a maximum of $2.20\ MPam^{1/2}$ and $1.41\ MPam^{1/2}$, respectively.

On the other hand, using the SENB test method along with ASTM D5045 standard, Sahoo et al. [11] investigated the effect of the addition of woven sisal fiber on intralaminar fracture toughness of unmodified epoxy and bioresin modified epoxy matrix. In order to effectively toughen the epoxy matrix, two different bioresins, epoxidized soybean oil (ESO) and epoxy methyl soyate (EMS), were employed. Two woven sisal fabric layers were reinforced in epoxy resin with maximum of $V_f \approx 17\%$. Composites were manufactured using the hand lay-up and compression molding techniques. SENB tests were carried out using UTM at crosshead speed of $1\ mm/min$. The K_{IC} value was found to be 4.3, 4.8 and $5.8\ MPam^{1/2}$, respectively, for woven sisal fiber reinforced with unmodified epoxy, modified with ESO and modified with EMS. They explained that the enhancement in K_{IC} value was due to the enhanced fiber-to-bioresin matrix interfacial bond.

2.4. Concluding Points and Research Gaps

For structural and semi-structural engineering applications, in addition to strength and stiffness, the characterization of fracture toughness of NFCs and their hybrids is very essential. The desire for an optimized, economical, damage tolerant and eco-friendly product along with ever growing application of NFCs and their hybrids necessitates characterizing their fracture toughness. The problem of lacking specific standardized procedure for characterizing the intralaminar fracture

toughness of NFCs, enforced researchers to rely on different related standards originally prepared for isotropic materials. This posed a challenge to researchers in providing reliable data about fracture behavior of these composites. From the literature survey so far, it is quite evident that very limited data is available about the intralaminar fracture characterization of sisal fiber reinforced epoxy composite and the effect of glass fiber hybridization has not been adequately addressed yet. In this research, the intralaminar fracture toughness of woven sisal/epoxy composite and the effect of glass fiber hybridization on its intralaminar fracture toughness will be studied using the 2TCT specimen as recommended in [43] for woven composite laminates.

Chapter 3

Materials and Methods

3.1. Materials

3.1.1. Fiber

For this experimental investigation, plain-woven sisal fiber (Figure 10(a)) and plain-woven E-glass fiber (Figure 10(b)) were used as a reinforcement. Sisal fiber was first extracted from sisal plant and plain-woven sisal fiber was prepared using the hand weaving process (see Section 3.2.1). Plain-woven E-glass fiber was purchased from World Fiber Glass and Water Proofing Engineering, Addis Ababa, Ethiopia.

Sisal fiber is among the strongest natural fibers. Its abundance, inexpensiveness, economical processing, less density, higher specific strength, and good interfacial interaction makes it suitable for using as a reinforcement in thermoset polymers [16]. E-glass fiber is the most widely used of all reinforcement fibers as it offers good balance between performance and cost, high strength and stiffness, good insulating properties and excellent resistance to chemical, moisture and heat [93], [94].

(a) (b)

Figure 10 Fibers used for the study (a) Plain-woven sisal fiber (b) Plain-woven E-glass fiber

3.1.2. Matrix

For this study, epoxy resin (LY556) was used as matrix material and hardener (HY951) was used for curing the epoxy resin, both imported from India. Epoxy resin is the most common type of polymer matrix material as of its high strength, low viscosity, low flow rates, low volatility during cure, low shrinkage rates, excellent resistance to chemicals and excellent adhesion to wide range of fibers and fillers [93]. Typical properties of cured epoxy are presented in Table 1.

Table 1 Typical properties of cured epoxy [95]

Density	1.2 g/cm^3
Tensile strength	72 MPa
Tensile modulus	3.4 GPa
Poisson's ratio	0.3
Shear strength	34 MPa
Shear modulus	1.308 GPa

3.1.3. Other Chemicals

Distilled water and sodium hydroxide (NaOH) were used for processing and treating the sisal fiber. Wax (Honey Wax 250) was applied as a mold releasing agent on the surface of the mold to prevent the fabricated part form sticking into the mold surface. All the aforementioned chemicals (Figure 11) were purchased from local market (Addis Ababa, Ethiopia).

(a) (b) (c)

Figure 11 (a) Distilled Water (b) Sodium Hydroxide (NaOH) Pellet (c) Mold Releasing Agent

3.2. Experimental Methods

3.2.1. Fiber Processing

- ***Fiber extraction***

Sisal leaves were collected from local sources (Butajira, Ethiopia). They were harvested from matured non-flowered sisal plant having dark green leaves. Sisal fibers were extracted from the collected sisal leaves using manual decortication method as this method results in high quality fibers [22]. First a separate leaf was sliced longitudinally in two mutually orthogonal directions to give four pieces. This increases the quality and amount of fiber that can be extracted from a single leaf by reducing fiber loss during the decortication process. The extracted fibers were then washed and rinsed using plenty of pure water to remove wastes such as leaf juices, chlorophyll and adhesive solids. The fibers were then dried in the sun and stored in room atmosphere. The fiber extraction process is shown in Figure 12.

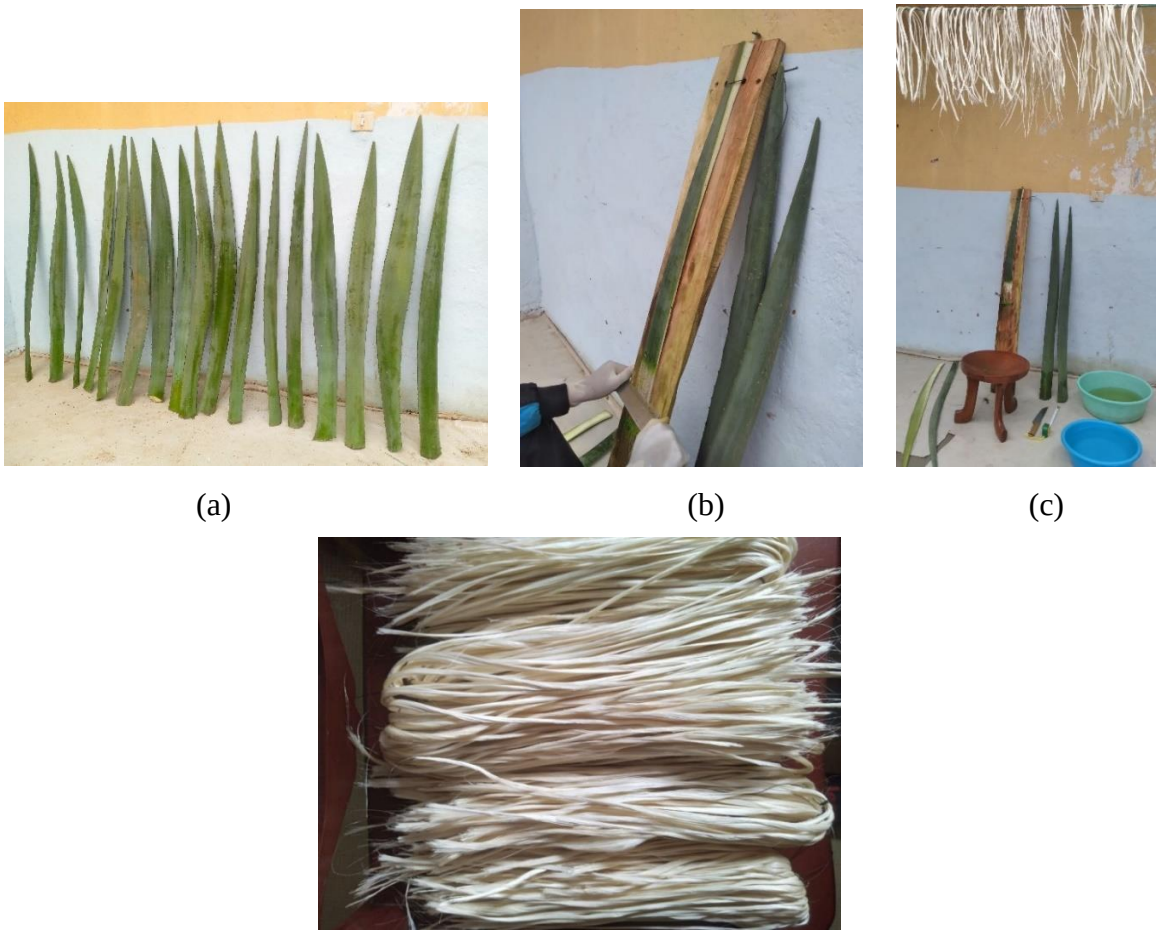

(a) (b) (c)

(d)

Figure 12 The fiber extraction process (a) Sisal leaves (b) Extracting sisal fibers (c) Washing and drying in the sun (d) Dried sisal fibers

- ***Fiber fabric preparation***

Plain-woven sisal fabric (warp and weft preform) was prepared using the hand weaving process (Figure 13). First $230\,mm$ by $550\,mm$ wooden frame was prepared and pattern of nail was created with $5\,mm$ gap between successive nails around the wooden frame to represent grid of mesh $5\,mm$ by $5\,mm$. The total amount of fiber required for two layers of the composite laminate was determined and measured. 35% extra fiber was used to compensate for the lost fibers in the weaving process – this percentage loss was determined in a pilot fabric preparation and treatment test. The measured fiber was then distributed evenly into the warp and weft tows by first aligning the warp tows and interlacing the weft tows into the aligned warp tows as shown in Figure 13.

Figure 13 The hand weaving process

- ***Fiber treatment***

After extraction and fabric preparation process, the fibers were treated with $0.5\ N$ solution of NaOH (i.e, 2% NaOH solution – $20\ g$ of solid NaOH pallets in 1 liter of distilled water) for $4\ hrs$ at room temperature in an airtight plastic container. This enhances its strength and surface adhesion property as this concentration and soaking time resulted in optimal fiber properties [61] and surface adhesion with epoxy resin [23] (Figure 14). The fibers were then washed thoroughly with plenty of pure water to remove excess NaOH on the fibers. Finally, the fibers were rinsed with distilled water and dried in the sun.

Figure 14 The fiber treatment (with 2% NaOH solution for 4hrs)

3.2.2. Specimen Preparation

- ***Fabrication of laminate composite panels***

Four $200mm \times 250mm \times 5.6mm$ composite laminate panels (pure sisal, two hybrids of sisal and glass, and pure glass fiber) were fabricated using the hand layup method followed by compression molding technique. In the hybrid laminate design, the outer layers were glass fiber layers to enhance the composite's moisture absorption resistance property as glass fibers have better moisture absorption resistance capacity. For all the tests total fiber volume fraction of 30% and number of layers (seven) were kept constant. Table 2 shows the relative percentage of constituents in the composite laminate panels. The detail analysis of the composite constituent was determined

using standard composite micromechanics analysis procedure and can be referred from Appendix A. The schematic representation of the four laminate designs is shown in Figure 15.

Table 2 Relative percentage of constituents in the composite laminates

Laminate Designation	**Constituents** (all 7 layers)	**Fiber (V_f)**		**Fiber ($wt\%$)**[1]	
		Sisal	**Glass**	**Sisal**	**Glass**
S	S/S/S/S/S/S/S	30	0	34.12	0
H1	G/G/S/S/S/G/G	13	17	12.91	29.57
H2	G/G/S/G/S/G/G	8.5	21.5	8.17	36.18
G	G/G/G/G/G/G/G	0	30	0	47.57

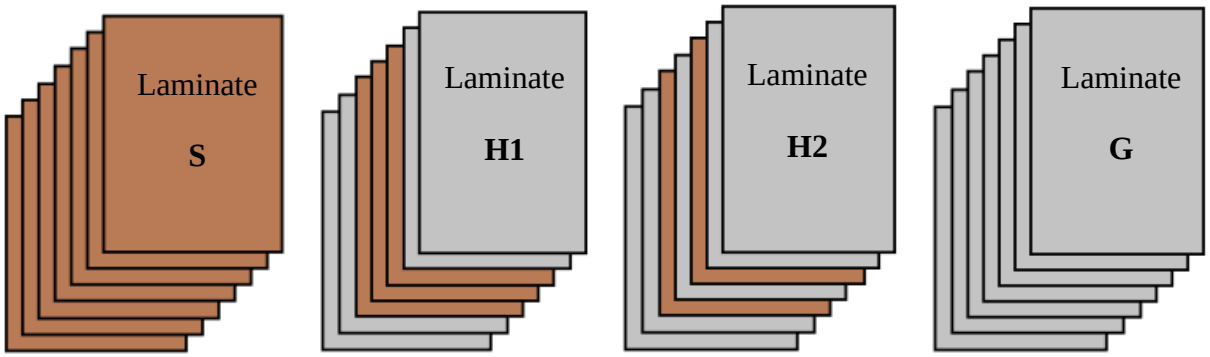

Figure 15 Schematic representation of the four laminate designs (Brown: Sisal fabric layers and Grey: Glass fabric layers)

The required quantity of fabric and matrix for each composite laminate panels were precisely measured using precision balance (to the nearest $0.1g$). Epoxy resin (LY556) was then thoroughly mixed with hardener (HY951) in stochiometric ratio of $100:10$ by weight as recommended by the manufacturer. A rectangular steel mold of dimension $200mm \times 250mm \times 5.6mm$ (Figure 16) was used to fabricate composite laminates by the hand lay-up method followed by compression molding process (Figure 18). A thin layer of mold release agent (Honey Wax 250) was applied on the surface of the steel mold for hindering adherence of epoxy into the steel mold and ease removal of the fabricated composite panels. After wetting the bottom surface of the mold with sufficient resin, the reinforcement fabric layers were successively placed along with the required quantity of the resin, applied uniformly using a brush. A spike roller (Figure 17) was used during the hand

[1] Calculated values taking density of sisal fiber $1.45\ g/cm^3$ [22], [50], E-glass fibers $2.54\ g/cm^3$ [94], and cured epoxy resin $1.2\ g/cm^3$ [93].

lay-up process to distribute the epoxy resin evenly into the reinforcement fabrics and remove trapped air.

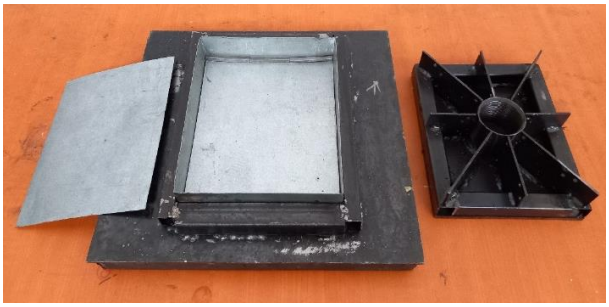

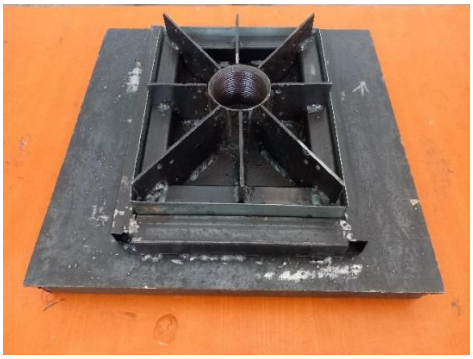

Figure 16 Steel mold

Figure 17 Spike roller

After impregnating the reinforcement fabrics with epoxy resin in the steel mold, the mold was closed and allowed to cure under a compressive load in a press machine at room temperature for $24hrs$. A $5.6\,mm$ thickness steel inserts (Figure 16) were used as a spacer between the bottom and upper mold part periphery to limit the thickness of the resulting composite panels. The fabricated four composite panels are shown in Figure 19.

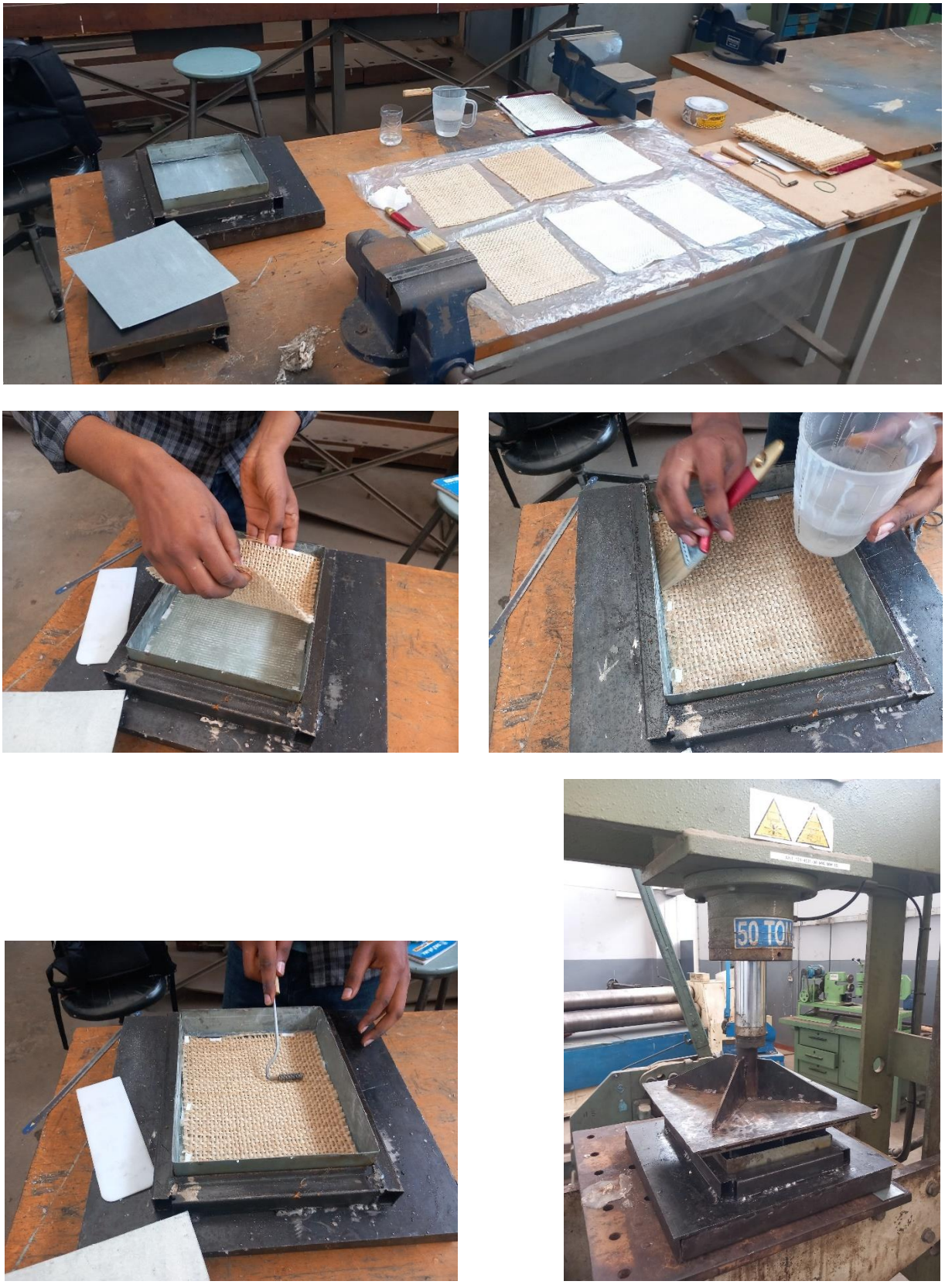

Figure 18 The hand layup and compression molding process

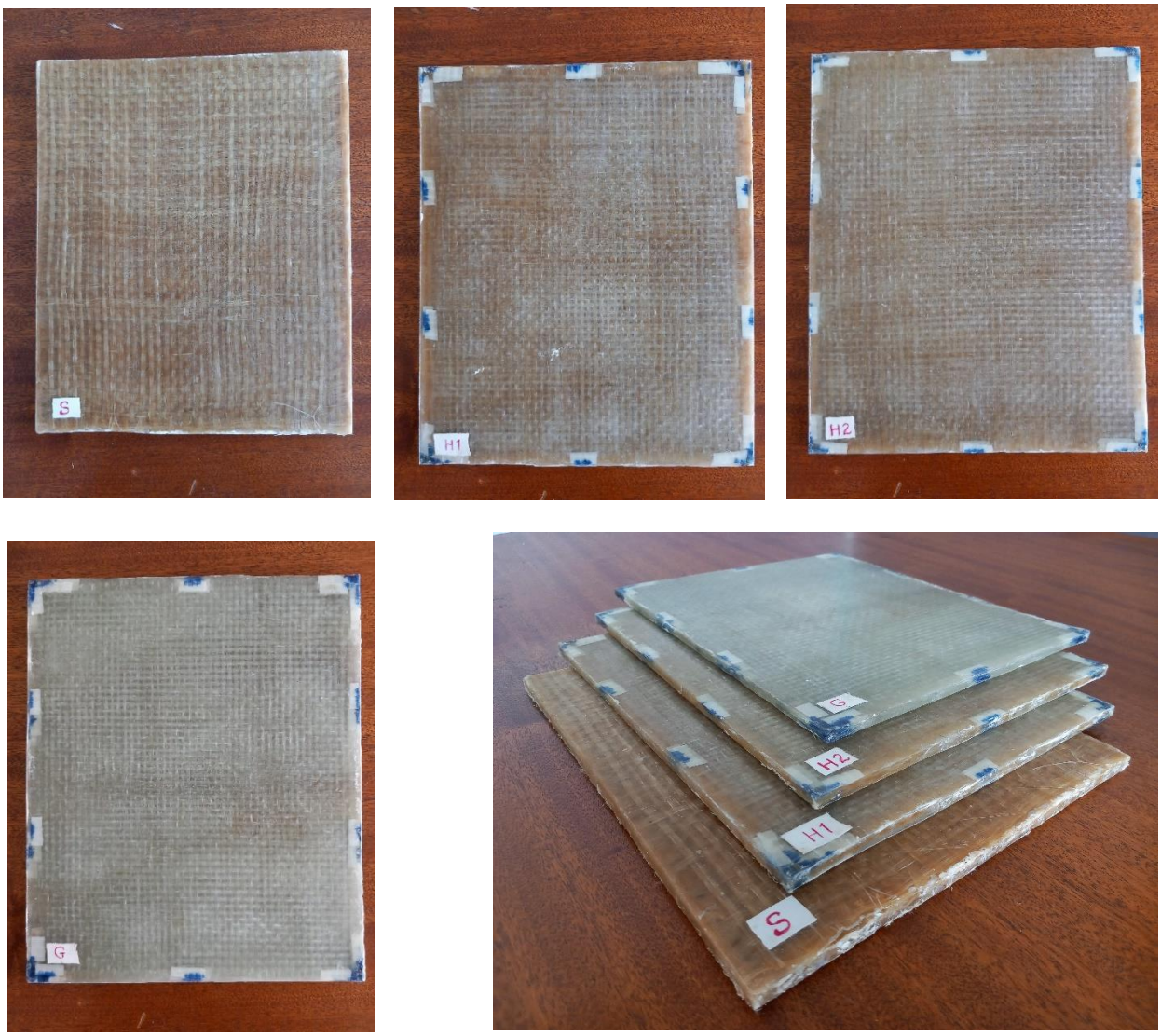

Figure 19 The fabricated four composite panels

- ***Specimen cutting***

To evaluate the intralaminar fracture toughness parameters, critical energy release rate G_{IC}, specimens were prepared by cutting parts from the fabricated composite laminate panels using hack saw. Doubly-tapered compact tension (2TCT) specimens were used as suggested for woven composite laminates in [75]. The specimen was cut so that the warp direction of the woven fabrics is oriented parallel to the direction of loading for better tracking of the crack propagation along the expected crack plane [43]. The geometry and dimensions of the 2TCT specimen are shown in Figure 9 and the configuration of six 2TCT specimens in the composite panels is shown in Figure 20. A 1 mm increment scale was drawn on the front face of the specimen to monitor the crack

propagation length during test. The dimensions of each specimen were finally measured (Figure 21).

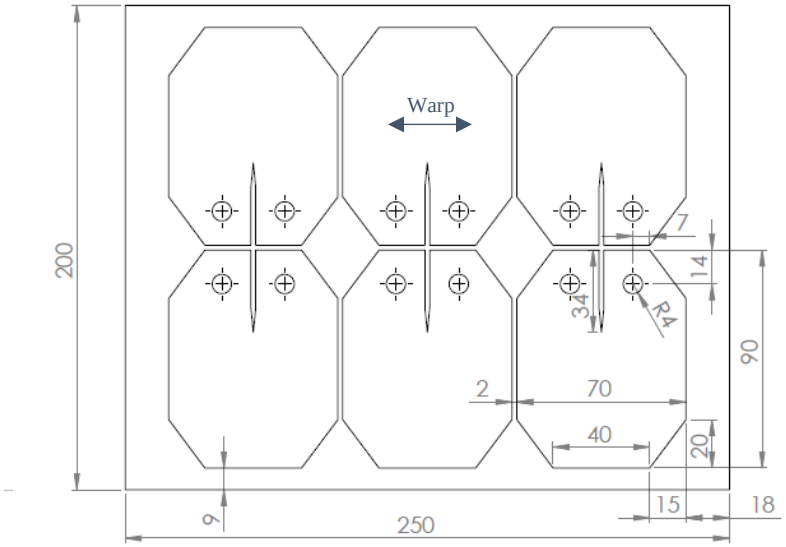

Figure 20 2TCT specimen configuration (all dimensions in mm)

Figure 21 Specimen marking, drilling, cutting and measuring process

To establish a sharp crack tip for the initial crack (pre-crack), first 33 mm V-notch was created (having 4 mm gap at its mouse) using 0.6 mm thick hack saw blade. Then, the final 1 mm sharp tip was introduced using 0.4 mm thick surgical blade and 0.1 mm thick razor blade successively by sawing action. The morphology of the initial crack and the magnified view of the crack tip is shown in Figure 22. Figure 23 shows five 2TCT specimens from each four groups of composite laminate panels ready for conducting intralaminar fracture toughness test.

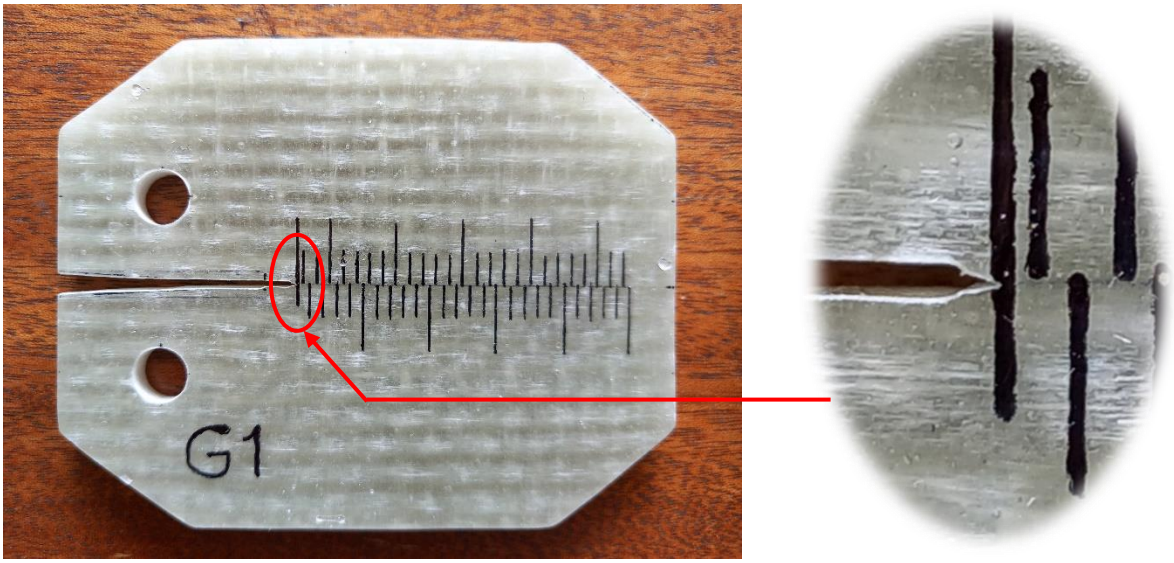

Figure 22 Morphology of the initial crack and magnified view of the crack tip

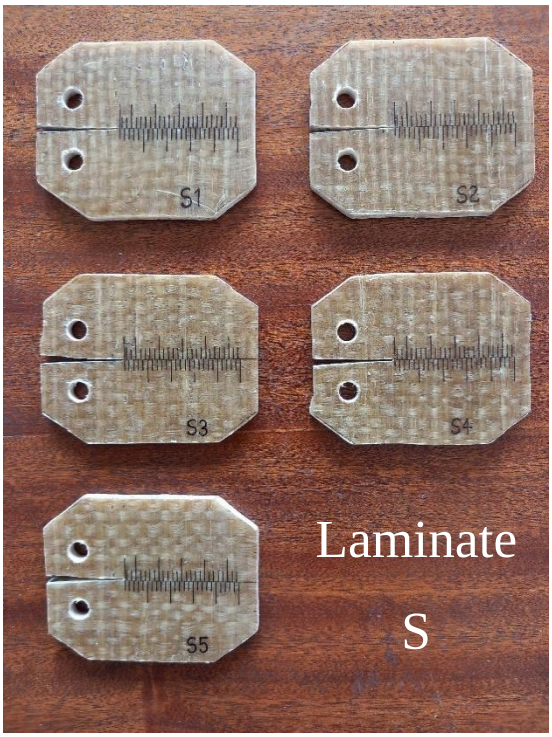

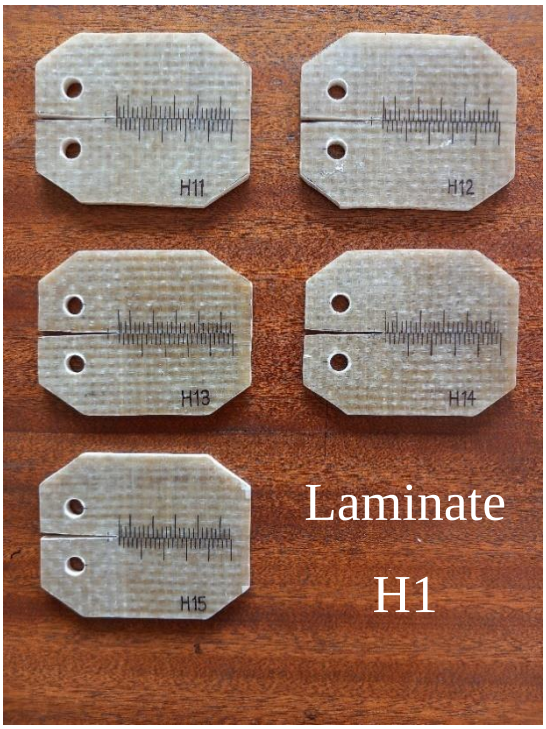

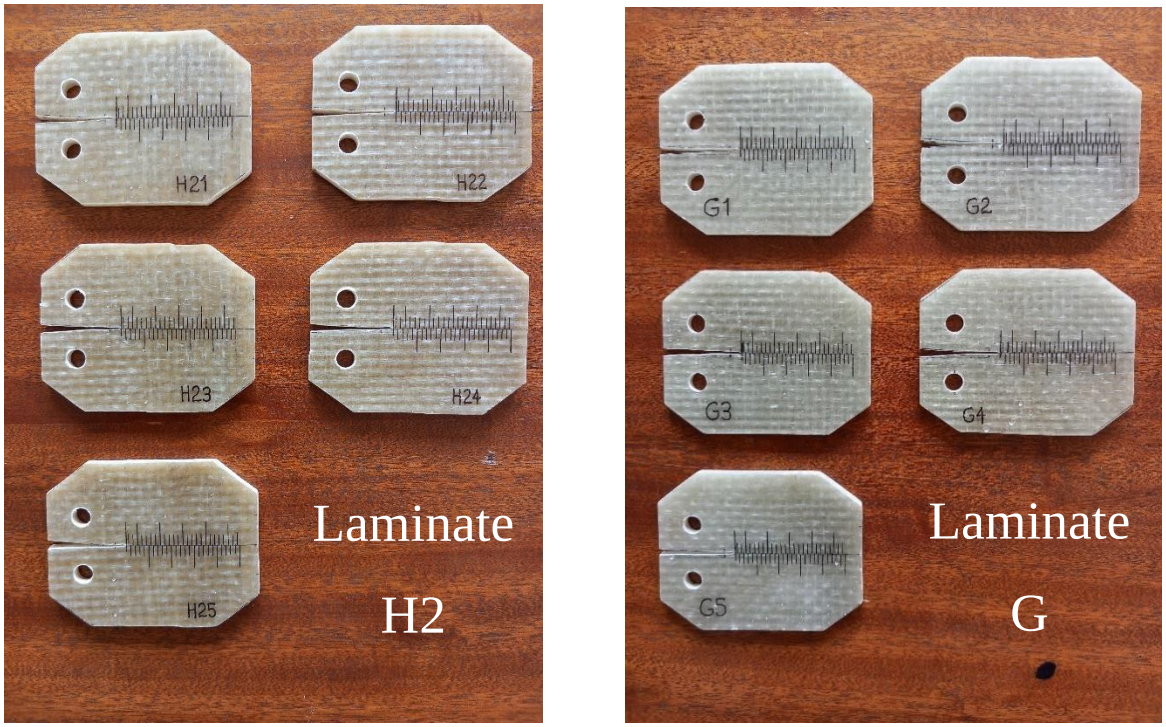

Figure 23 Specimens ready for testing (five specimens for each group)

3.2.3. Test Procedure and Setups

To experimentally evaluate the intralaminar fracture toughness parameters, mode-I tensile tests were performed on 2TCT specimens using Universal Testing Machine (Model: WDW-100S with $100kN$ load capacity) (Figure 25(a)) under displacement control at room temperature and crosshead speed of $0.5\ mm/min$. A fixture (Figure 24) was used to load the 2TCT specimen. The test procedures and setups were adopted from the ASTM D5045-14 standard [74]. The propagation of the initial crack (pre-crack) was recorded using digital camera during the test (Figure 25(b)). The load, displacement and time data were recorded in the computer system and the length of the propagated crack was measured with millimeter scale drawn on surface of the specimens.

Figure 24 Loading fixture

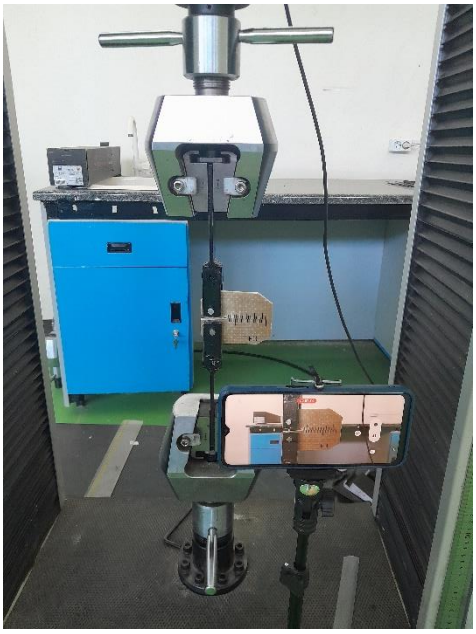

(a) (b)

Figure 25 (a) Universal testing machine (b) Loading and camera set up

3.3. Computational Methods

3.3.1. Data Reduction Technique

The determination of fracture toughness parameters for orthotropic materials needs special attention. The majority of the researchers have used the stress intensity approach as per the ASTM D5045 standard [74] which is developed for plastic materials or its metal counterpart ASTM E399 standard [73]. Both of these standards assume the materials being isotropic in nature. Due to this isotropy assumption, a difference in result has been observed when comparing fracture toughness values of composite laminates obtained from FEA and the stress intensity factor equations of the above standards [96].

Observing this difference noticed in [96], Pinho et al. [97] developed a more accurate data reduction formula for determining the fracture toughness of composite laminates based on energy release rate using the FEA. Blanco et al. [43] also recommend this method for woven composite laminates. The data reduction formula for calculating the critical energy release rate G_{IC} is expressed as a function of the applied load, specimen thickness, and crack length as [43], [97]:

$$G_{IC} = \left(\frac{P_c}{t}\right)^2 (c_3 a^3 + c_2 a^2 + c_1 a + c_0) \quad (1)$$

Where P_c is the experimental load associated with crack propagation at specific crack length a, t is the specimen thickness, and c_i's are polynomial coefficients determined from the FEA. The FEA procedure for evaluating the polynomial coefficients is briefly described in [97].

In Eq. (1) the polynomial function expresses the normalized energy release rate $f(a)$ obtained from the J-integral (J) around the crack tip of the composite specimen of unit thickness subjected to unit load which is defined as:

$$f(a) = J.\left(\frac{1mm}{1N}\right)^2 \tag{2}$$

Once finding the values of the normalized energy release rate for different crack length, the polynomial coefficients c_i's were determined for ranges of crack length along with the associated interpolation error.

To find the critical value of the experimental load P_c for crack initiation, as recommended in ASTM D5045-14 standard [74], first a straight line AB (Figure 26) was drawn on the linear portion of the load-displacement curve to determine the initial compliance (C) which is the reciprocal of the slope of line AB. Then a second straight line AB' was drawn with a compliance 5% greater than that of line AB. If the maximum load P_{max} which the material is able to withstand falls between line AB and AB', then P_{max} is used as a critical value P_c for crack initiation. If the P_{max} is outside the line AB and AB', then the intersection point P_Q of line AB' and the load-displacement curve is used as a critical value P_c for crack initiation.

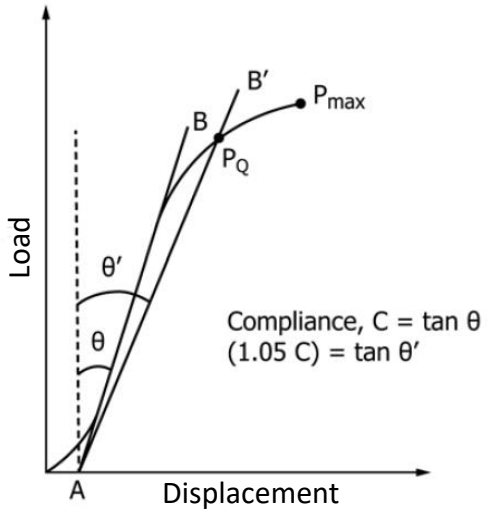

Figure 26 Determination of critical load P_c for crack initiation

3.3.2. The FEA Procedure

Taking advantage of the symmetry of the 2TCT specimen, a half crack model was developed using 3D deformable shell planar model in Abaqus/CAE 2017. Uniform square 8-noded (S8R5) elements were used to mesh the model adopting finer mesh around the crack tip and load application points. Elastic properties of the composite laminates (Table 4) were employed which were obtained from the laminae values (Table 3) using the lamination theory. Symmetry boundary condition was applied at the symmetric plane and the displacement of bottom right node was constrained in the x-direction (Figure 27). The 2TCT specimen model was developed using unit thickness and a tensile unit load was applied at top of the pin hole which tries to open the initial crack. Defining the position of the crack front at the crack tip and setting the direction of propagation of the crack along the expected crack plane, the FEA was run to evaluate J-integrals of 5 contours around the crack tip.

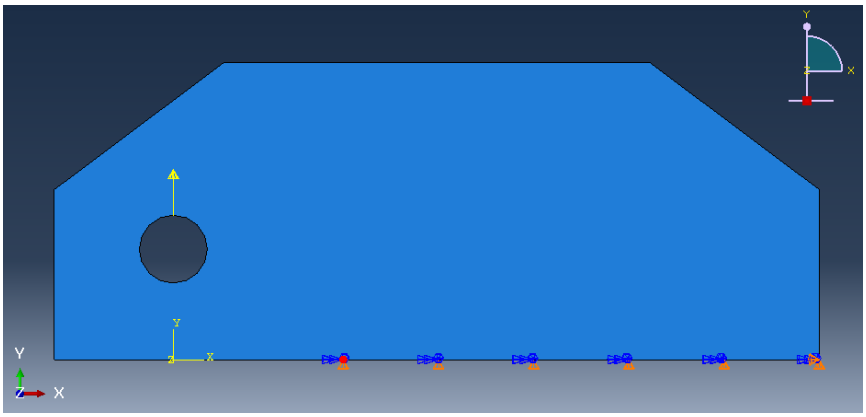

Figure 27 2TCT FE half crack model in Abaqus (the red spot represents the crack tip position)

As these FEA was to be repeated several times starting from the crack length $a = 20\ mm$ with an increment of $1\ mm$ up to $a = 64\ mm$ for all the material models under consideration, to facilitate readjustment of the crack length (position of the crack tip), material properties and mesh refinements, a Python code was written (Appendix B) which performs the aforementioned FEA procedure. Editing the crack length, material properties and mesh size factors, the Python code was run in Abaqus to obtain J-integral values of the specific composite laminate at specific crack lengths.

The laminae elastic properties of sisal fabric and glass fabric composite are presented in Table 3. For the sisal/epoxy lamina, the tensile modulus values were taken from [53] and the in-plane shear modulus and major Poisson's ratio values were taken as that of the matrix [95], as these properties

are matrix dominated properties (since experimental values of these properties are not available). For the glass/epoxy lamina, the elastic properties were taken from [98]. Elastic properties of the composite laminates (Table 4) that were required as an input in the FEA were calculated from the respective laminae properties (Table 3) using lamination theory.

Table 3 Elastic properties of the composite laminae [53], [95], [98]

Lamina	**Elastic Modulus (GPa)**			**Major Poisson's ratio, ν_{12}**
	E_1	E_2	G_{12}	
Sisal/Epoxy	3.870	3.870	1.308	0.30
Glass/Epoxy	14.352	14.352	4.728	0.24

Table 4 Elastic properties of the composite laminates

Laminate	**Elastic Modulus (GPa)**			**Major Poisson's ratio, ν_{12}**
	E_1	E_2	$G_{12} = G_{13} = G_{23}$	
S	3.870	3.870	1.308	0.30
H1	9.86514	9.86514	3.26229	0.2504
H2	11.3611	11.3611	3.75086	0.2460
G	14.352	14.352	4.728	0.24

3.3.3. Convergence Test

The mesh convergence test was performed considering different levels of mesh refinements. Two mesh size factors (maximum and minimum size factors) were employed to control the mesh refinement. The minimum size factor controls element sizes around the crack tip and load application points, and the maximum size factor controls element sizes far from these locations. Figure 28 shows 2TCT FE models representing coarse, intermediate and refined mesh refinements.

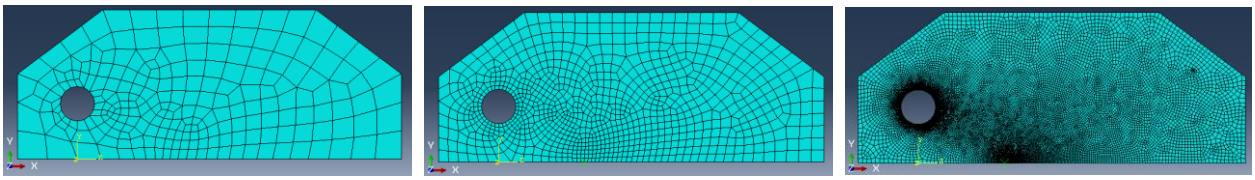

(a) Coarse mesh	(b) Intermediate mesh	(c) Refined mesh
Maximum size factor = 6 mm Minimum size factor = 1.7 mm Number of elements = 236	Maximum size factor = 3 mm Minimum size factor = 0.8 mm Number of elements = 964	Maximum size factor = 1 mm Minimum size factor = 0.1 mm Number of elements = 17,788

Figure 28 2TCT FE model mesh refinements

Editing the two mesh size factors in the Python code (Appendix B), the mesh convergence analysis was performed and mesh convergence analysis plot and data are shown in Figure 29 and Table 5, respectively.

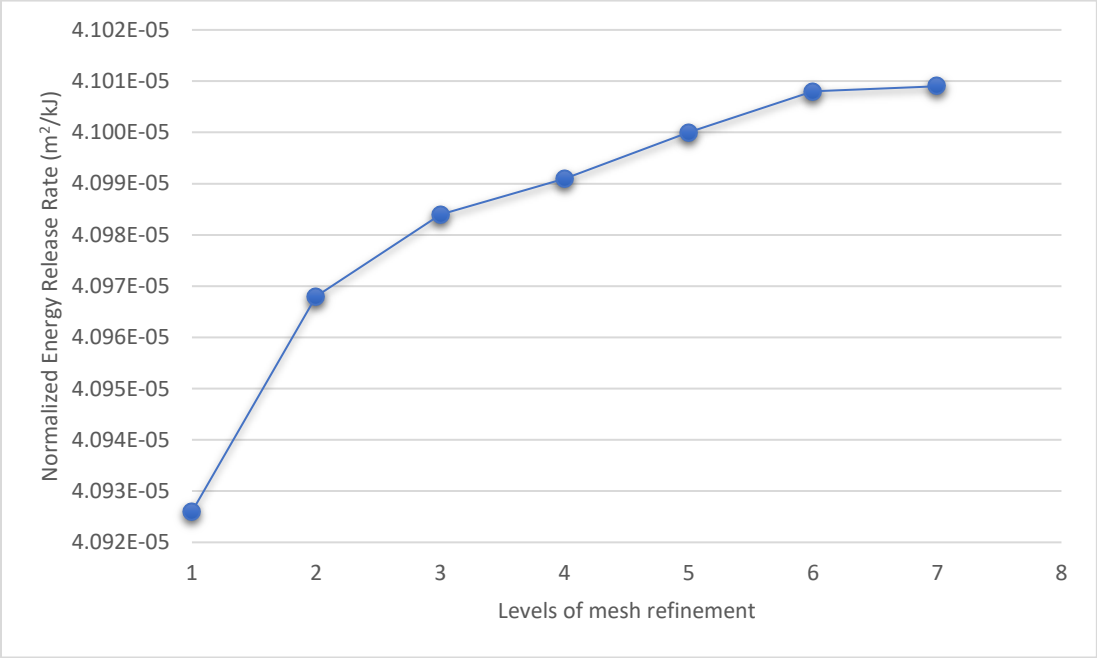

Figure 29 Mesh convergence plot

Table 5 Mesh convergence analysis data

Mesh Refinement Level	**Maximum Size Factor** (mm)	**Minimum Size Factor** (mm)	**Number of Elements**	**Total CPU Time** (Sec)	**Normalized Energy Release Rate** (m^2/kJ)	**Percentage Error** (%)
1	6	1.7	236	0.6	4.0926E-05	0.2024
2	5	1.4	333	0.7	4.0968E-05	0.1000
3	4	1.1	558	1.3	4.0984E-05	0.0610
4	3	0.8	964	1.9	4.0991E-05	0.0439
5	2	0.5	2185	3.4	4.1000E-05	0.0219
6	1	0.2	10235	19.1	4.1008E-05	0.0024
7	1	0.1	17788	24.4	4.1009E-05	Reference

Figure 29 shows that the analysis result converges to a certain value as the mesh of the model is refined. Taking the refined mesh (level 7) as a reference, the normalized energy release rate value for the intermediate mesh (level 4) differs in 0.0439% and for the coarse mesh (level 1) differs in

0.2024%. Considering the percentage error and total CPU time, mesh refinement level 6 was chosen for the analysis (Figure 30).

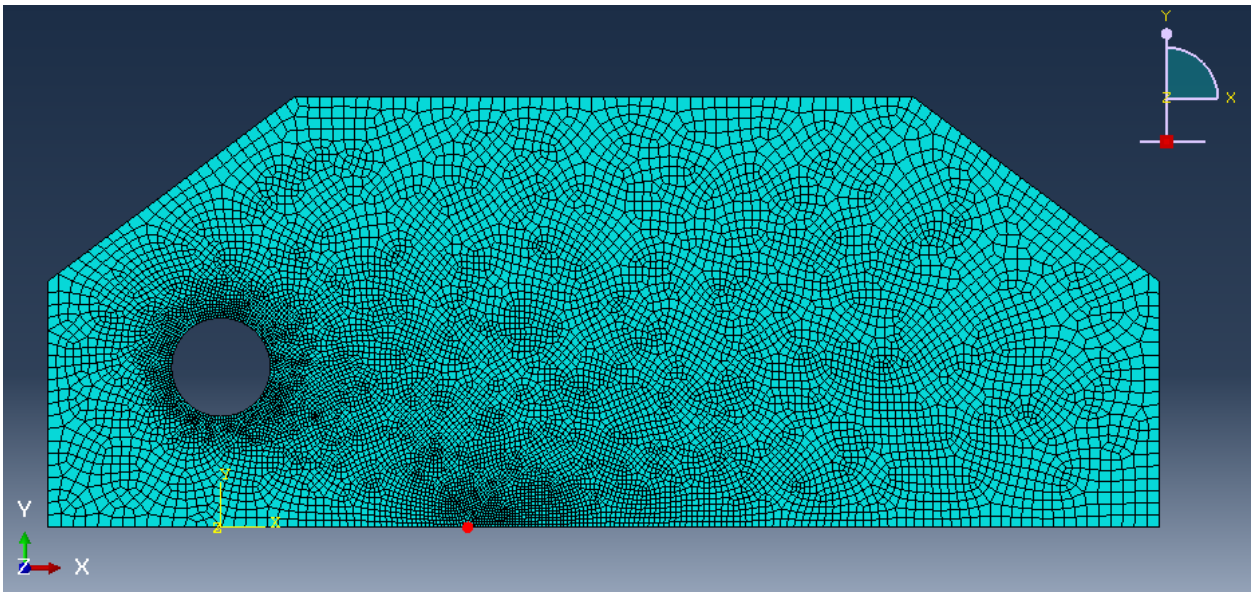

Figure 30 Chosen mesh refinement (Level 6) (the red spot represents the crack tip position)

Chapter 4

Results and Discussion

4.1. Polynomial Coefficients

The stress distribution in the 2TCT specimen is shown in Figure 31 (von Mises) and Figure 32 (maximum in-plane principal). It can be seen that the stress is confined around the crack tip position, which favors the extension of the crack along the expected crack plane. As in this analysis only a unit load (1 N) is applied, the stress magnitudes are very small.

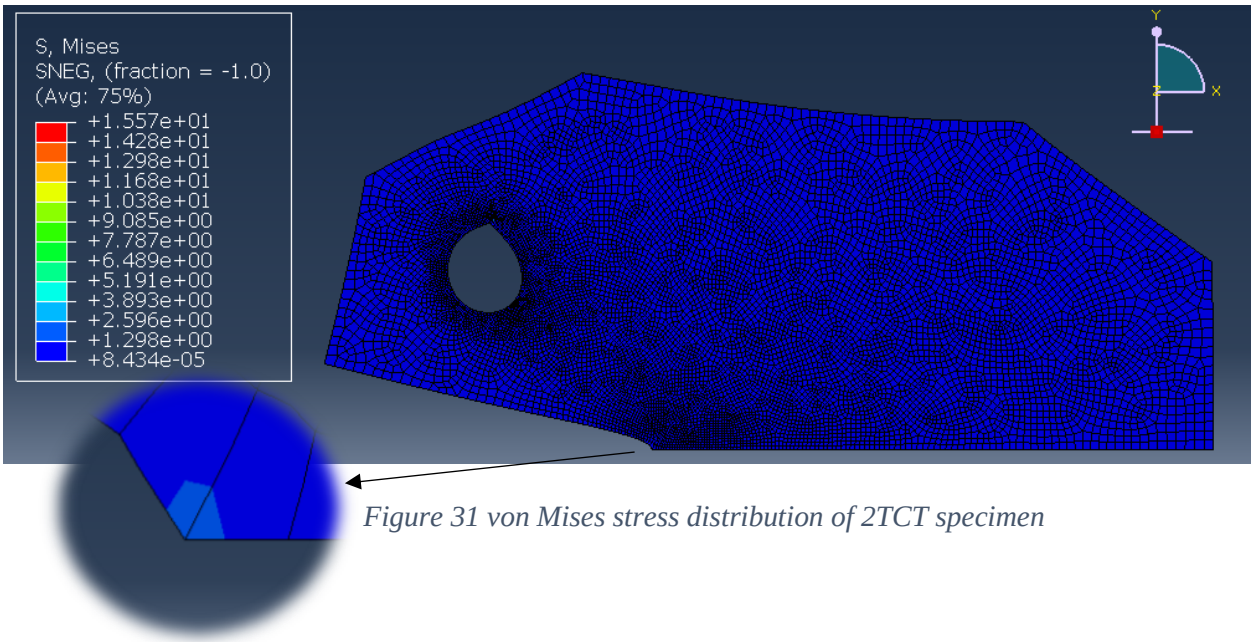

Figure 31 von Mises stress distribution of 2TCT specimen

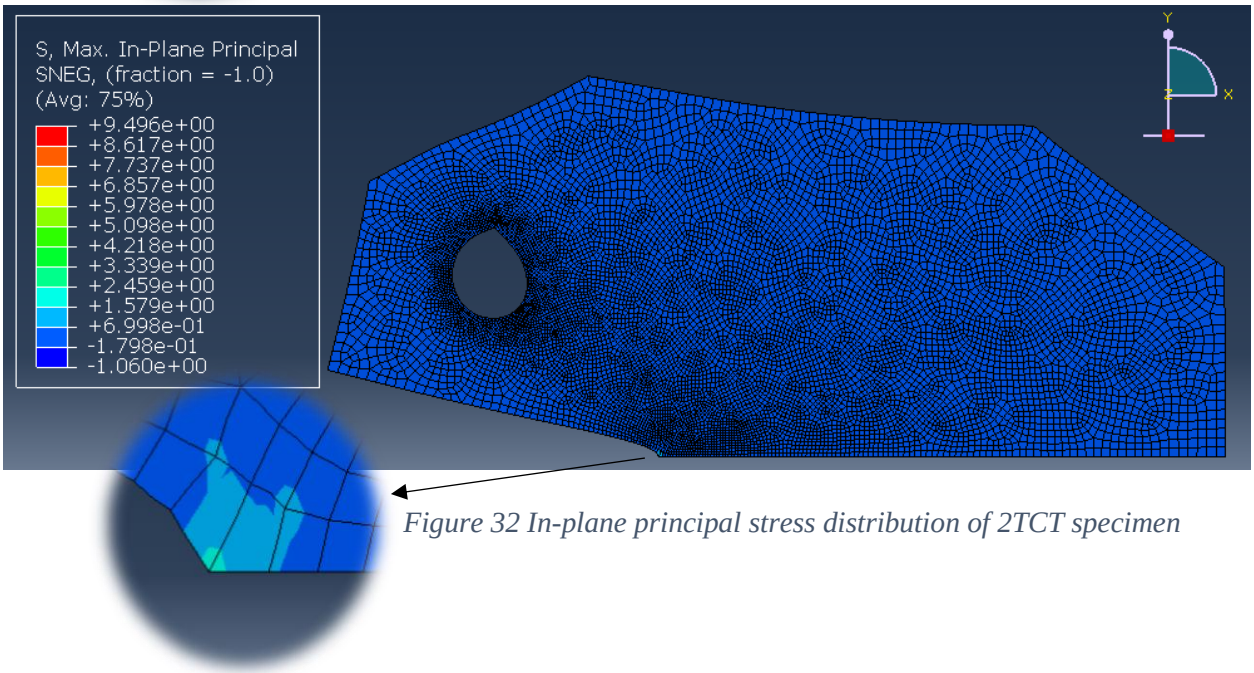

Figure 32 In-plane principal stress distribution of 2TCT specimen

Readjusting the elastic property parameters and crack length in the Python code (Appendix B) for the four composite laminates under consideration and running in Abaqus/CAE 2017, the values of normalized energy release rate $f(a)$ for crack length a ranging from $19 - 64\ mm$ were computed and are presented in Appendix C. The values of the polynomial coefficients c_i's for the interpolation of $f(a)$ for ranges of crack length a were computed using MATLAB R2013a and are presented in Table 6 along with associated maximum error.

Table 6 Values of polynomial coefficients for the four composite laminates

Crack Length Range	c_3	c_2	c_1	c_0	**Error** (%)
For Laminate 'S'					
$19 \le a < 30\ mm$	1.049×10^{-8}	-5.908×10^{-7}	1.599×10^{-5}	-5.144×10^{-5}	< 0.02
$30 \le a < 40\ mm$	4.174×10^{-8}	-3.383×10^{-6}	1.045×10^{-4}	-9.633×10^{-4}	< 0.03
$40 \le a < 50\ mm$	2.274×10^{-7}	-2.622×10^{-5}	1.043×10^{-3}	-1.385×10^{-2}	< 0.07
$50 \le a < 60\ mm$	2.532×10^{-6}	-3.825×10^{-4}	1.942×10^{-2}	-3.300×10^{-1}	< 0.33
$60 \le a < 65\ mm$	3.198×10^{-5}	-5.681×10^{-3}	3.374×10^{-1}	-6.693	< 0.09
For Laminate 'H1'					
$19 \le a < 30\ mm$	4.155×10^{-9}	-2.008×10^{-7}	6.300×10^{-6}	-1.951×10^{-5}	< 0.02
$30 \le a < 40\ mm$	1.674×10^{-8}	-1.358×10^{-6}	4.195×10^{-5}	-3.870×10^{-4}	< 0.03
$40 \le a < 50\ mm$	9.054×10^{-8}	-1.044×10^{-5}	4.152×10^{-4}	-5.510×10^{-3}	< 0.07
$50 \le a < 60\ mm$	1.006×10^{-6}	-1.520×10^{-4}	7.717×10^{-3}	-1.311×10^{-1}	< 0.32
$60 \le a < 65\ mm$	1.274×10^{-5}	-2.264×10^{-3}	1.344×10^{-1}	-2.667	< 0.09
For Laminate 'H2'					
$19 \le a < 30\ mm$	3.616×10^{-9}	-1.748×10^{-7}	5.482×10^{-6}	-1.696×10^{-5}	< 0.02
$30 \le a < 40\ mm$	1.448×10^{-8}	-1.173×10^{-6}	3.622×10^{-5}	-3.338×10^{-4}	< 0.03
$40 \le a < 50\ mm$	7.856×10^{-8}	-9.055×10^{-6}	3.600×10^{-4}	-4.777×10^{-3}	< 0.07
$50 \le a < 60\ mm$	8.744×10^{-7}	-1.321×10^{-4}	6.704×10^{-3}	-1.139×10^{-1}	< 0.33
$60 \le a < 65\ mm$	1.106×10^{-5}	-1.964×10^{-3}	1.167×10^{-1}	-2.314	< 0.09
For Laminate 'G'					
$19 \le a < 30\ mm$	2.874×10^{-9}	-1.391×10^{-7}	4.359×10^{-6}	-1.352×10^{-5}	< 0.02
$30 \le a < 40\ mm$	1.149×10^{-8}	-9.315×10^{-7}	2.876×10^{-5}	-2.650×10^{-4}	< 0.03
$40 \le a < 50\ mm$	6.237×10^{-8}	-7.190×10^{-6}	2.859×10^{-4}	-3.794×10^{-3}	< 0.07
$50 \le a < 60\ mm$	6.937×10^{-7}	-1.048×10^{-4}	5.319×10^{-3}	-9.040×10^{-2}	< 0.33
$60 \le a < 65\ mm$	8.775×10^{-6}	-1.559×10^{-3}	9.257×10^{-2}	-1.837	< 0.09

4.2. Load-Displacement Curves

The intralaminar fracture toughness test was conducted as per the conditions described in Section 3.2.3. The resulting load-displacement (load versus load-point displacement) curves for each specimen of the four laminates are presented in Figure 33 (a) to (d). The general shape of the load-displacement curves of the four laminates showed similar trend.

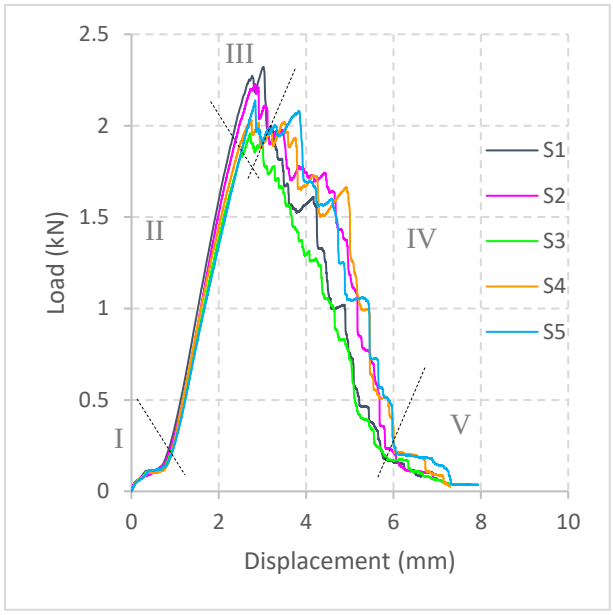

(a) Laminate 'S'

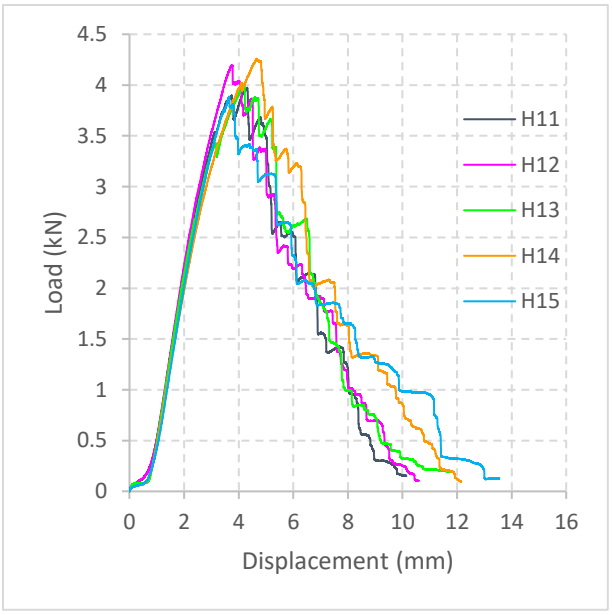

(b) Laminate 'H1'

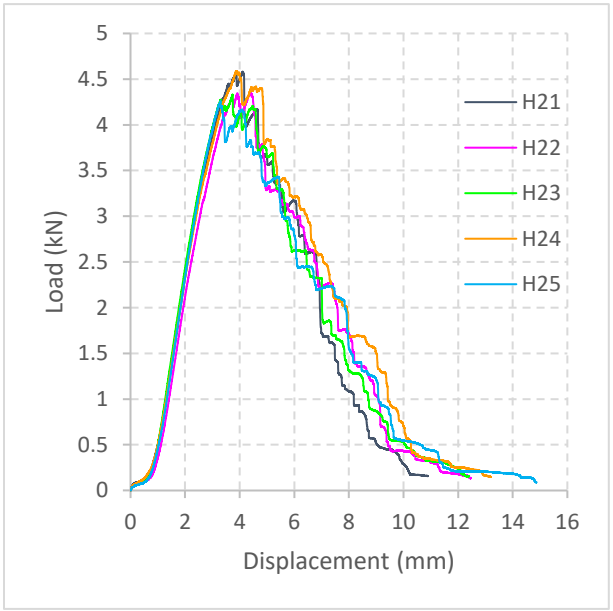

(c) Laminate 'H2'

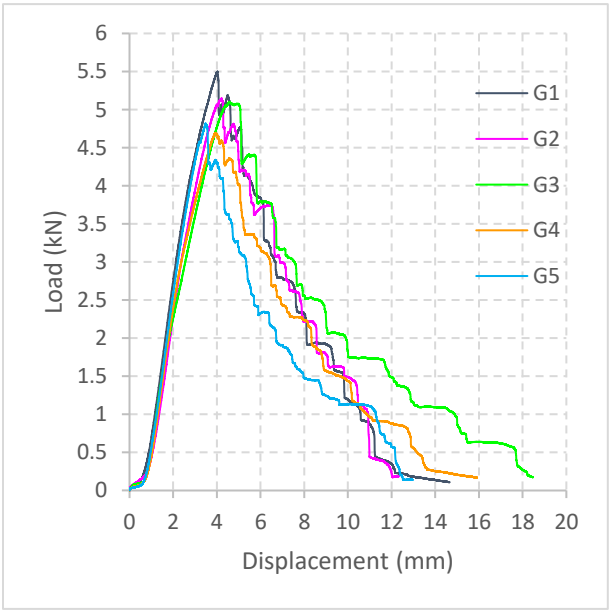

(d) Laminate 'G'

Figure 33 Load-displacement curves for the four laminates (S: Sisal, H: Hybrid, and G: Glass)

Five major phases can be discussed from the curves (Figure 33 (a)): Phase I (Preloading), Phase II (Elastic), Phase III (Damage initiation), Phase IV (Damage propagation), and Phase V (Final failure). At Phase I or preloading phase, the loading pins (upper and lower pins) depress and micro-penetrate the specimen holes to bring about system compliance. At Phase II or elastic phase, the load is nearly proportional to the displacement and deformations are almost reversible. At Phase III or damage initiation phase (or transition phase), the curves start to slightly shift from linearity and form an abrupt changes around the peak load. At this phase, some of the fibers around the crack tip start to break and debond from the matrix, which was identified by the clicking sounds they made. No visible crack propagation was observed at this phase.

At Phase IV or damage propagation phase, a continual sudden falling and stablization of load is observed and the curves reseble a falling steps.The sudden falling of the load is a result of unstable crack propagation through the matrix rich zones where as the stablization of load is associated with a stable crack propagation through fiber dominated zones. Crack propagation is continually retarded whenever the crack tip faces bundles of fibers, and when the local fiber bundles are all broken and the crack tip arrives at matrix rich zone, the crack propagates abruptly. The fact that damage is progressive (not catastrophic) is one of the desirable properties of such FRC materials.

At Phase V or final failure phase, in addition to tensile failure around the crack tip, vertical compressive failure modes such as fiber kinking, matrix crushing and delamination were observed at the right side of the specimen for crack lengths greater than about $50\ mm$. The test results showed good repeatablity. The average stiffness in the elastic phase for each laminates from (a) to (d) are 1.17, 1.43, 1.72, and $1.76\ kN/mm$, respectively, and the average peak load each laminates from (a) to (d) were able to sustain are 2.14, 4.07, 4.42, and $5.05\ kN$, respectively.

4.3. Critical Energy Release Rate Values

Using the load-displacement data along with the data reduction technique described in Section 3.3.1, fracture toughness values based on critical energy release rate (G_{IC}) were computed for the four laminates and presented in Table 7 and Figure 34 along with their respective standard deviation (SD). The G_{IC} value of hybrid laminate 'H2' was found to be higher than that of hybrid laminate 'H1' as the middle glass fabric layer in laminate 'H2' offered better resistance against the propagating crack through the middle layer. The G_{IC} values of the hybrid laminates 'H1' and 'H2' lied between the G_{IC} values of the monolithic laminates 'S' and 'G' (Figure 34).

Table 7 Results of critical energy release rate (G_{IC}) values

Parameters	Laminate S	Laminate H1	Laminate H2	Laminate G
$\boldsymbol{G_{IC}}$ (kJ/m^2)	16.32	25.06	27.64	39.62
SD (kJ/m^2)	1.65	2.45	1.59	2.79

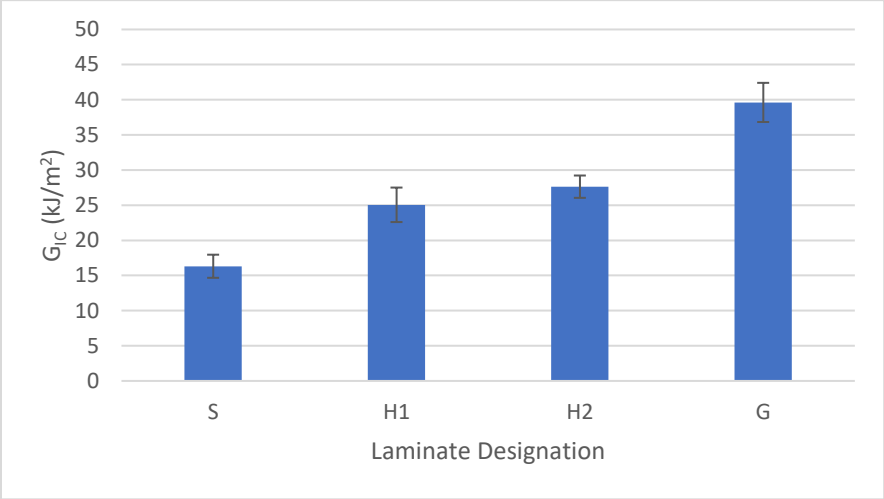

Figure 34 Results of critical energy release rate values (S: Sisal, H: Hybrid, and G: Glass)

An introduction of 56.7% of glass fibers from the constant total fiber volume fraction into the pure sisal fiber laminate (to give laminate 'H1') increased the critical energy release rate value of pure sisal fiber laminate by 53.6%. And, an introduction of that of 71.7% glass fibers into the pure sisal fiber laminate (to give laminate 'H2') increased the critical energy release rate value of pure sisal fiber laminate by 69.4%. On the other hand, with reference to the pure glass fiber laminate, an introduction of 28.3% of sisal fibers from the constant total fiber volume fraction into the pure glass fiber laminate (to give laminate 'H2') lowered the critical energy release rate value of pure glass fiber laminate by 30.2%. In addition, an introduction of that of 43.3% of sisal fibers into the pure glass fiber laminate (to give laminate 'H1') lowered the critical energy release rate value of pure glass fiber laminate by 36.7%.

For comparison purpose, the critical energy release rate (G_{IC}) and critical stress intensity factor (K_{IC}) values were also computed according to the data reduction formula suggested in ASTM D5045-14 standard [74] for plastic materials (isotropic materials). The difference in critical energy release rate (G_{IC}) values computed according to the data reduction formula Eq. (1) and the one suggested in ASTM D5045-14 standard was found to be significant (Table 8).

Table 8 Comparison of critical energy release rate values obtained using data reduction formula of Eq. (1) and ASTM D5045 standard

Laminates	Fracture Toughness Values			
	Using Eq. (1) $G_{IC}\ (kJ/m^2)$	Using ASTM D5045 Standard		Percentage Difference
		$G_{IC}\ (kJ/m^2)$	$K_{IC}\ (MPa\ m^{1/2})$	
Laminate S	16.32	9.88	6.05	39.46 %
Laminate H1	25.06	15.14	11.84	39.58 %
Laminate H2	27.64	16.69	13.34	39.61 %
Laminate G	39.62	23.92	17.93	39.63 %

As can be referred from Table 8, the data reduction formula suggested in ASTM D5045-14 standard for plastic materials resulted values that are about 40% lower than that of the one computed using Eq. (1). This shows that the use of data reduction formula of ASTM D5045-14 standard for orthotropic composite materials is not recommended since this approach underestimates their fracture toughness values. Such difference was also observed in [97]. Table 9 presents available literature data for intralaminar fracture toughness of related polymer matrix composites.

Table 9 Intralaminar fracture toughness of related polymer matrix composites in the literature

Material System	Fiber Content	Data Reduction Method	G_{IC} (kJ/m^2)	K_{IC} $(MPa\ m^{1/2})$	Ref.
Woven Sisal/Epoxy	$\approx 32\%\ V_f$	ASTM D5045	-	2.20	[42]
Chopped Sisal/Epoxy	$30\%\ wt\%$	ASTM D5045	13.72	5.54	[12]
Woven Sisal/Vinyl ester	$\approx 32\%\ V_f$	ASTM D5045	-	$4.2 - 6$	[83]
Woven Sisal/Polyurethane	$\approx 30\%\ V_f$	ASTM D5045	11.5	-	[77]
Woven Sisal/Polyester	$50 - 55\%\ V_f$	ASTM E1922	-	6.5	[99]
Woven Flax/Epoxy	$\approx 33\%\ V_f$	BS 7448	-	7.2	[80]
Woven Jute/Epoxy	$50\ wt\%$	ASTM D5045	-	7.71	[90]
Woven/chopped hybrid Glass/Polypropylene	$39\ wt\%$	ASTM E399	78.2	-	[100]
Unidirectional Flax/Epoxy	$41\%\ V_f$	ASTM E1922	14.27	15.71	[91]

4.4. Resistance Curves (R-Curves)

Using the video data for monitoring the crack length 'a' and load-displacement data along with the data reduction technique described in Section 3.3.1, the R-curves (G_{IC} vs. a) were plotted for the four laminates and presented in Figure 35 (a) to (d).

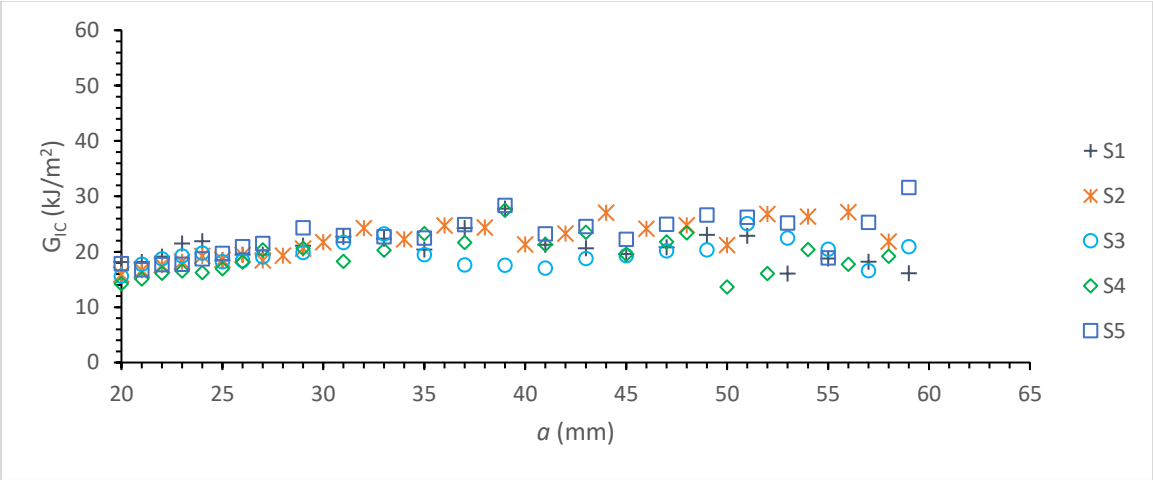

(a) Laminate 'S'

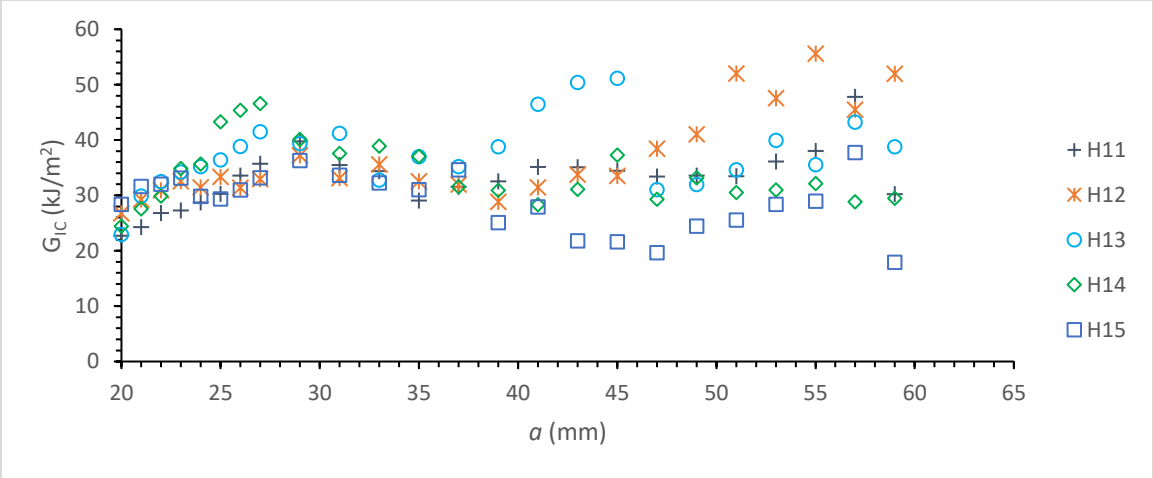

(b) Laminate 'H1'

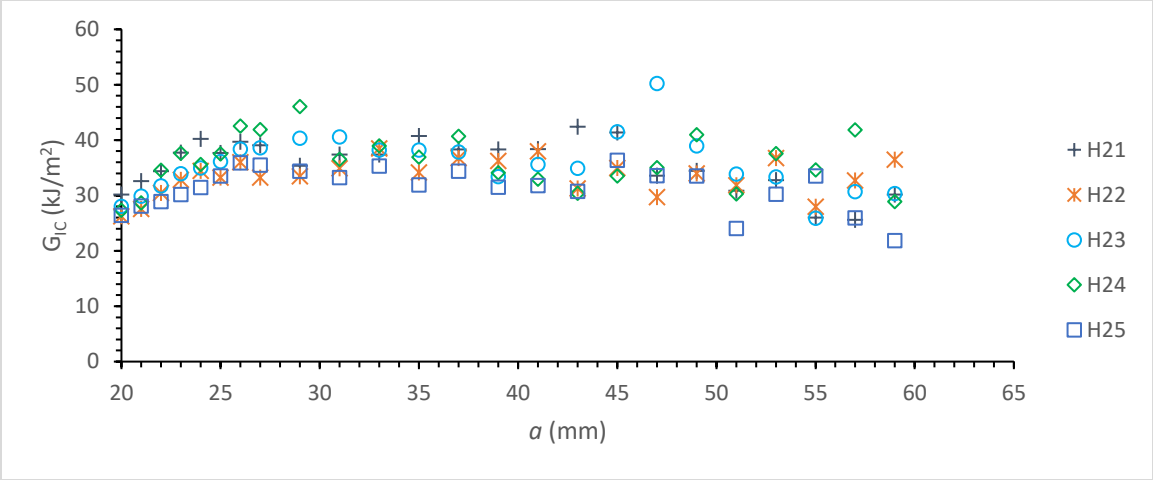

(c) Laminate 'H2'

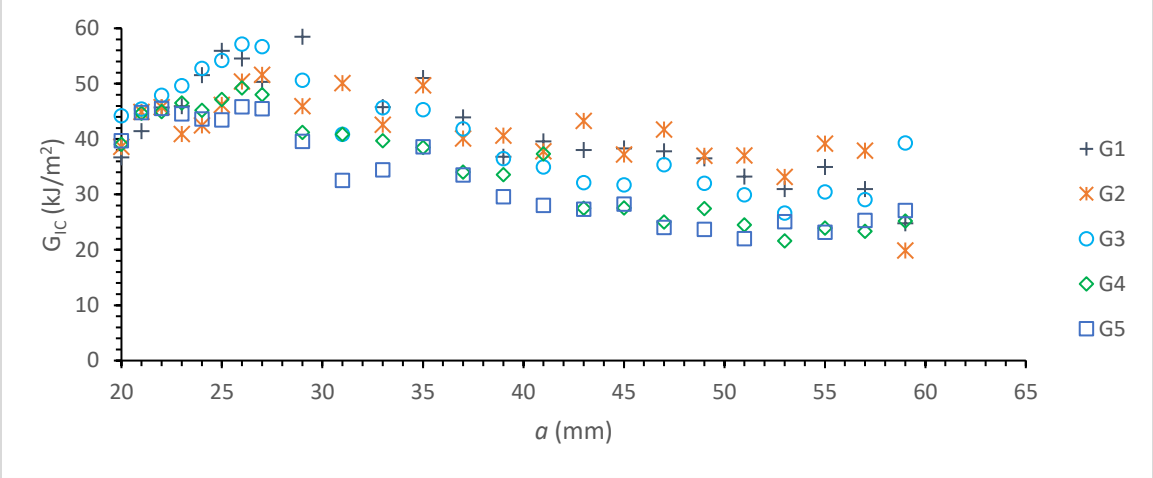

(d) Laminate 'G'

Figure 35 R-curves for the four laminates (S: Sisal, H: Hybrid, and G: Glass)

The R-curves of the five specimens of each laminates showed good agreement with each other except at higher crack lengths (typically for $a > 50\ mm$). The general trend of the R-curves obtained for the four laminates can be discussed by dividing the curves into three sections: Section I ($a < 30\ mm$), Secion II ($30 \leq a \leq 50\ mm$), and Section III ($a > 50\ mm$).

In Section I of the R-curves or for crack length $a < 30\ mm$, the G_{IC} values are less scattered and show general positive trend for all the four laminates. Good agreement is also found for the initiation values of G_{IC}. In Section II of the R-curves or for crack length $30 \leq a \leq 50\ mm$, G_{IC} values showed nearly constant trend for Laminate 'S' and 'H2', a slight negative trend for Laminate 'G', and for Laminate 'H1', G_{IC} values showed a negative trend for almost half the range

and positive trend for the rest half. In Section III of the R-curves or for crack length $a > 50\ mm$, as described when discussing Phase V of the load-displacement curves in Section 4.2, due to the considerable vertical compressive stress in the right side of the specimen, compressive failure modes such as fiber kinking, matrix crushing and delamination were also observed in addition to tensile failures around the crack tip. The G_{IC} values in this section are influenced by compressive failure modes. The statistics for the G_{IC} values are highly scattered and no specific trend could be captured for the five specimens of each laminate in this section. The crack propagation in all the four laminates was very progressive, and no unexpected damage was observed during the test.

From the R-curves (Figure 35), the values of the average critical energy release rate for crack propagation ($G_{IC,Pro}$) were evaluated for the four laminates. When computing the $G_{IC,Pro}$ values, data points in Section III (crack length $a > 50\ mm$) of the R-curves were not included as these values are also influenced by the effect of the vertical compression stress at the right side of the specimen. The $G_{IC,Pro}$ values of the four laminates are presented in Table 10 and Figure 36 along with their respective standard deviation (SD).

Table 10 Results of average critical energy release rate for crack propagation ($G_{IC,\,Pro}$) values

Parameters	Laminate S	Laminate H1	Laminate H2	Laminate G
$\boldsymbol{G_{IC,Pro}}$ (kJ/m^2)	20.80	33.68	35.74	41.83
SD (kJ/m^2)	3.27	5.63	4.06	8.38

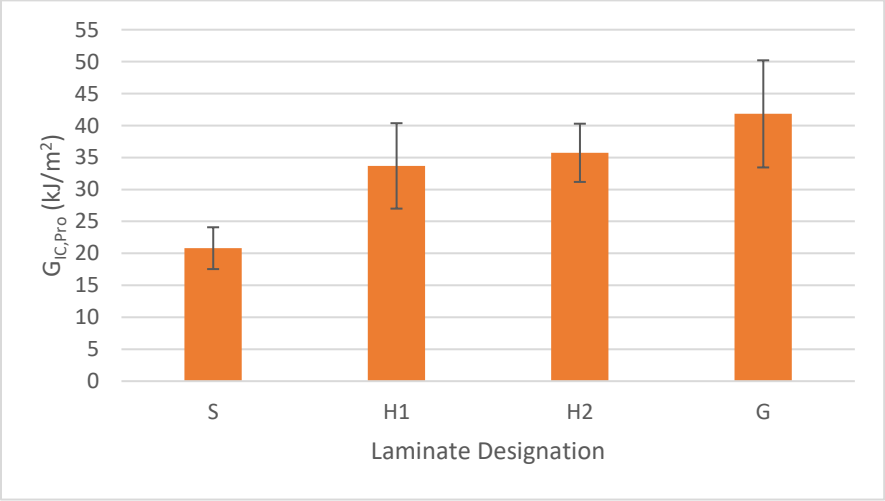

Figure 36 Results of average critical energy release rate for crack propagation values (S: Sisal, H: Hybrid, and G: Glass)

For all the four laminates, the G_{IC} values in Table 9 are lower than the average propagation $G_{IC,Pro}$ values in Table 10. This is because the initial fracture from the pre-crack plane was almost planar and involved insignificant fiber pullouts, whereas, crack propagation along the crack plane involved extensive fiber fracture and to some degree fiber pullouts, since woven fabrics were used as reinforcement. Fiber-dominated failure modes (such as fiber pullout and fiber fracture) are high-energy processes.

The trend of the R-curves and G_{IC} values obtained in this research are comparable with the one obtained by Blanco et al. [43] for woven carbon fiber reinforced polymer composite using the same 2TCT specimen and data reduction method based on FE approach. They obtained critical energy release rate (G_{IC}) value of $59.9\ kJ/m^2$ and average critical energy release rate for crack propagation ($G_{IC,Pro}$) of $63.7\ kJ/m^2$. Using the same data reduction method based on FE approach along with CT specimen for unidirectional carbon fiber reinforced polymer composite, Pinho et al. [97] obtained critical energy release rate (G_{IC}) value of $91.6\ kJ/m^2$ and average critical energy release rate for crack propagation ($G_{IC,Pro}$) of $133\ kJ/m^2$.

4.5. Fractography

A representative close-up view of the front faces of the fractured specimens for the four laminates is shown in Figure 37. For all the specimens of the four laminates, the results showed brittle fracture behavior, where extensive plastic deformation has not been observed before final failure of the composites. However, crack propagation was progressive (not catastrophic) in all the four laminates. Crack propagation direction was confined to the area around the expected crack plane (the crack propagated just above the centerline). No visible damage was observed other than crack propagation along the expected crack plane in the crack propagation zone. Crack propagation was not totally on a straight line, rather it followed a direction between two adjacent weft tows within a ply. Tow splitting in composite laminates is one of fiber failure modes where breakage of fiber bundles from external layers occurs at a certain distance from the crack plane. Laminates H1, H2 and G showed similar trend of slight tow splitting in the outer layers of the specimens as these laminates all have woven glass fiber outer layers, whereas, in Laminate S no tow splitting was observed. On Laminates H1, H2 and G, visible compressive failures such as matrix crushing, fiber kinking and delamination of layers was observed on the right side of the specimen. On the hybrid laminates, delamination of layers was observed around the crack propagation plane, which can be

identified by the white spotted areas. This shows that interlayer bond in these hybrid laminates was not as strong as that of their monoletic counterparts.

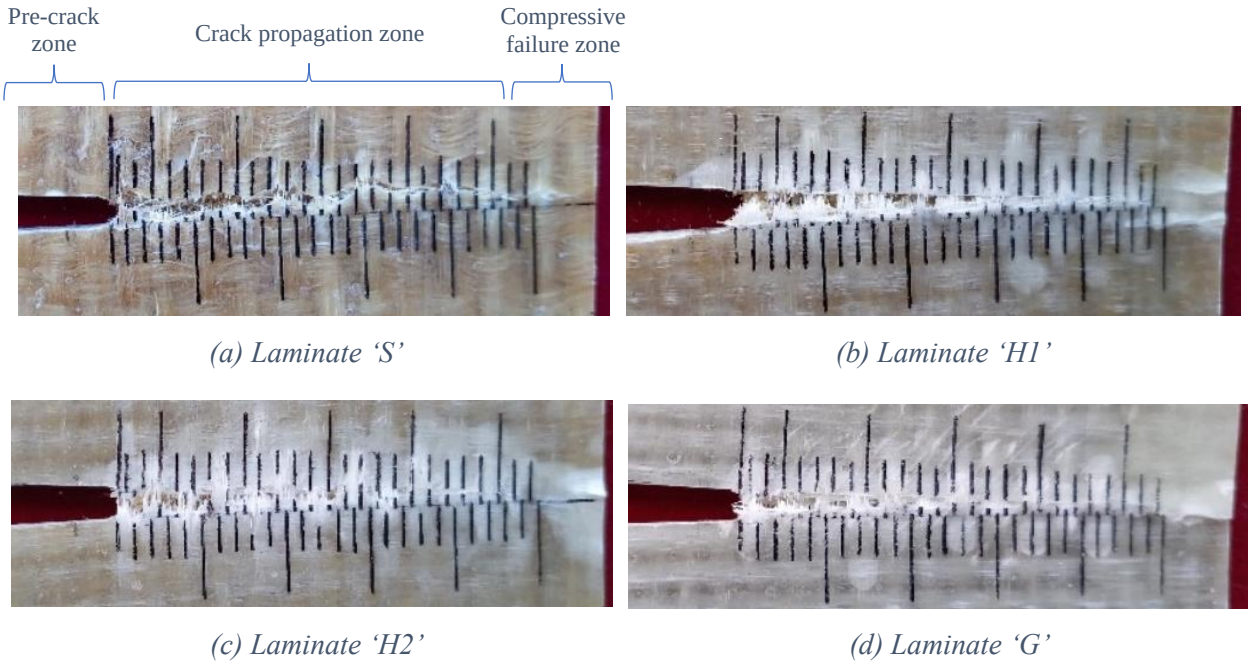

(a) Laminate 'S'

(b) Laminate 'H1'

(c) Laminate 'H2'

(d) Laminate 'G'

Figure 37 Close-up view of the front faces of the fractured specimens

After the test has been conducted representative specimens of the four laminates were opened completely to investigate the fracture surface. Figure 38 shows the fracture surfaces (Upper and lower surfaces, respectively) for the four laminates.

The fracture surface was not planar, rather it displayed fiber pullout in the warp tows of woven glass fiber layers. Fiber pullout is one of fiber failure modes which involves pulling out of certain length of fiber bundles from their pockets in the matrix as crack propagates. It is a high energy process as it involves both debonding of fiber interface from its matrix and fiber fracture. The fiber pullouts in the laminates H1, H2 and G are confined to the crack propagation zone with a slight irregularity in distribution and length across the thickness of the specimen.

In the compressive failure zone of these laminates, no fiber pullouts are observed, rather compressive failure modes such as fiber kinking, matrix crushing and delamination of layers are observed widening the thickness of the specimen at this zone. The fracture behavior of laminate S is different than the rest. The fibers fractured without pullout in the crack propagation zone. No visible compressive damage is observed in the compressive failure zone.

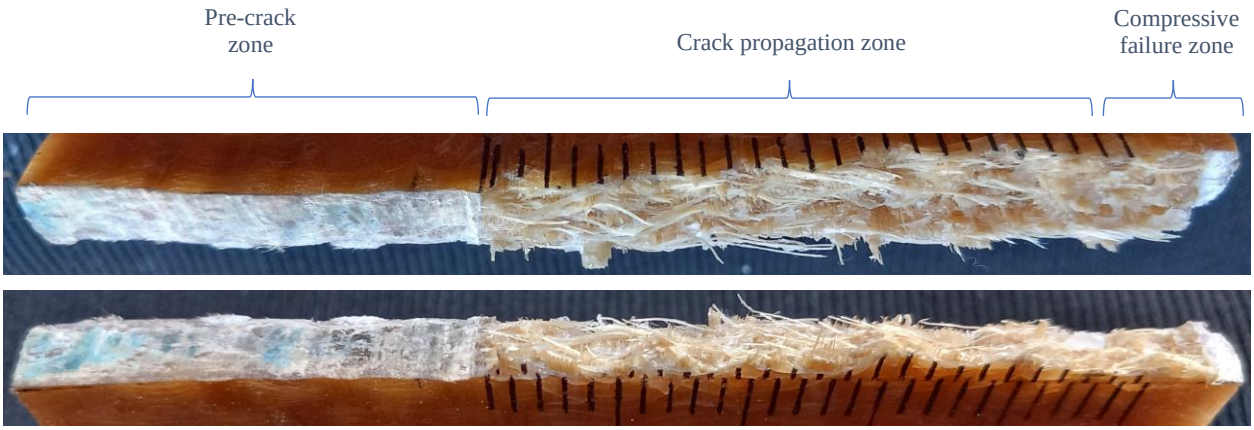

(a) Laminate 'S'

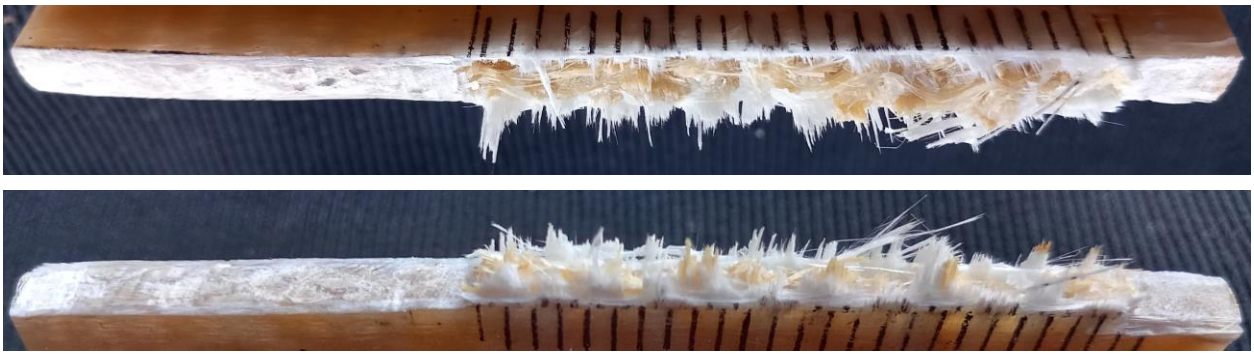

(b) Laminate 'H1'

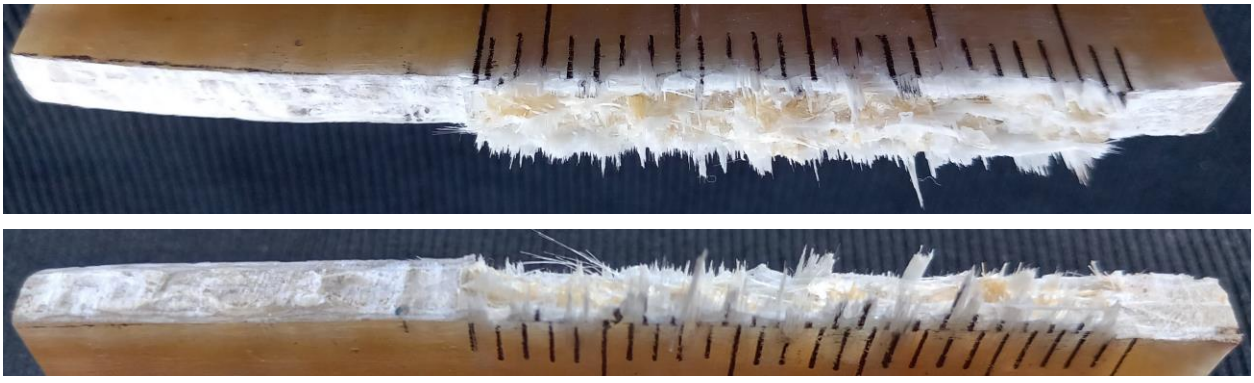

(c) Laminate 'H2'

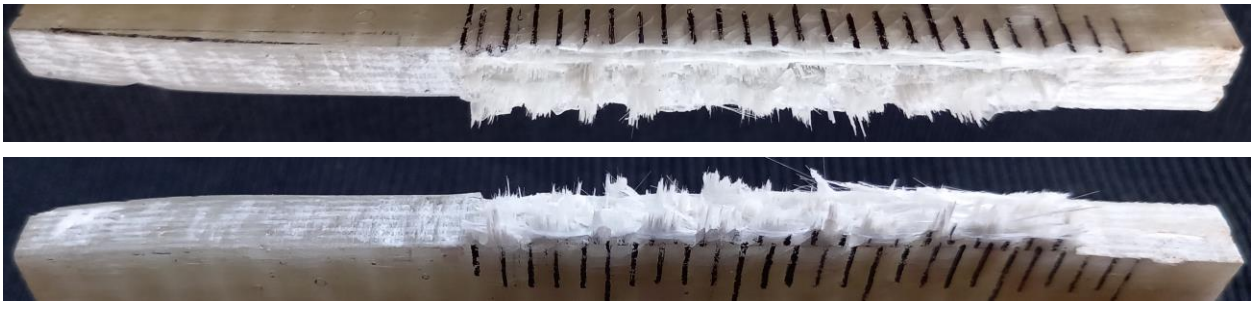

(d) Laminate 'G'

Figure 38 Image of fracture surface (top image: upper surface; bottom image: lower surface)

Chapter 5

Conclusion and Recommendation

5.1. Conclusion

In this research, an experimental investigation has been carried out to characterize the intralaminar fracture toughness of woven sisal fiber reinforced epoxy composite material and study the effect of woven glass fiber hybridization using doubly-tapered compact tension (2TCT) specimen. Four different laminates (pure sisal, two hybrids of sisal and glass, and pure glass fiber reinforced epoxy composite laminates) have been tested with five specimens for each group. A data reduction technique recommended for composite materials based on the FE approach has been used. No other damages have been encountered during the tests other than the expected crack propagation in the expected crack plane up to crack length $a = 50mm$. For crack length $a > 50mm$, compressive damages have been observed on the right side of the specimens for the hybrids and pure glass fiber laminates. No visible compressive damage has been observed for the pure sisal laminate. From the results it is possible to conclude that the 2TCT specimen ensure crack propagation without other damage mechanisms for the considered materials at least for up to crack length $a = 50mm$.

Load-displacement responses were obtained, fracture toughness values based on critical energy release rate (G_{IC}) were evaluated, and resistance curves (R-curves) were plotted. Results of load-displacement response showed good repeatability. The critical energy release rate (G_{IC}) values of the pure sisal, two hybrids of sisal and glass, and pure glass fiber reinforced epoxy composites were found to be 16.32, 25.06, 27.64, and 39.62 kJ/m^2, respectively. The general shape of the R-curves was found to be in agreement with previous literature on related composite materials. The hybridization of woven sisal fibers with woven glass fibers in epoxy matrix displayed synergetic effect. The G_{IC} values of the woven sisal/epoxy composite laminate were improved by an amount nearly equal to that of the volume percentage of the added glass fibers. The intralaminar fracture toughness of the hybrid laminates (Laminates H1 and H2) lied between that of their monolithic counterparts (Laminates S and G). The results obtained have been found to be comparable with available literature data of related composite materials. The fracture behavior of the four laminates has also been discussed after completely opening the fractured specimen to

expose the fracture surface. All the four laminates showed a brittle fracture behavior. A slight fiber pullouts and tow splitting was observed in the hybrid and pure glass fiber laminates.

5.2. Recommendation

The study carried out on the four composite laminates showed that woven sisal fiber reinforced epoxy composite and its glass fiber hybrids have demonstrated comparable intralaminar fracture toughness values with pure glass fiber reinforced epoxy composite material. Depending on the toughness requirements of a specific application, woven sisal fiber reinforced epoxy composite and its glass fiber hybrids can be considered as a suitable alternative of pure glass fiber reinforced epoxy composite material, which can considerably reduce the cost and weight of the structure.

From the results, it is possible to recommend the 2TCT specimen geometry along with data reduction technique based on FE approach as a suitable method for computing intralaminar fracture toughness values of other similar natural fiber composite laminates and their glass fiber interply hybrids.

5.3. Future Works

In the present study, the mode-I tensile intralaminar fracture toughness of woven sisal/epoxy composite and the effect of glass fiber hybridization is studied experimentally by considering four different laminates (pure sisal, two hybrids of sisal and glass, and pure glass fiber reinforced epoxy composite laminates). To extend the research under this topic area, the following study directions could be suggested:

- ☞ The characterization of the intralaminar fracture toughness under loading modes mode-II, mode-III and mixed modes.
- ☞ The study of the effect of intraply hybridization.
- ☞ The investigation of the effect of fiber orientation and fiber loading, and the effect of hybridization with other synthetic fibers.
- ☞ The characterization of the compressive intralaminar fracture toughness.
- ☞ The study of the effect of addition of nanoparticles for toughening the matrix.

References

[1] W. Zhang and J. Xu, “Advanced lightweight materials for Automobiles: A review,” *Materials and Design*, vol. 221. 2022.

[2] J. Spasenović and I. Blagojević, “Composite materials in automotive industry: A review,” *Industrija*, vol. 49, no. 2, 2021.

[3] B. Ravishankar, S. K. Nayak, and M. A. Kader, “Hybrid composites for automotive applications – A review,” *Journal of Reinforced Plastics and Composites*, vol. 38, no. 18, pp. 835–845, 2019.

[4] T. Padmavathi, S. V. Naidu, and R. Rao, “Studies on Mechanical Behavior of Surface Modified Sisal Fibre – Epoxy Composites,” *Journal of Reinforced Plastics and Composites*, vol. 31, no. 8, pp. 519–532, 2012.

[5] W. G. Roeseler, B. Sarh, and M. U. Kismarton, “Composite structures: The first 100 years,” in *ICCM International Conferences on Composite Materials*, 2007.

[6] J. Bachmann, C. Hidalgo, and S. Bricout, “Environmental analysis of innovative sustainable composites with potential use in aviation sector—A life cycle assessment review,” *Science China Technological Sciences*, vol. 60, no. 9. 2017.

[7] K. Senthilkumar *et al.*, “Mechanical properties evaluation of sisal fibre reinforced polymer composites: A review,” *Constr Build Mater*, vol. 174, pp. 713–729, 2018.

[8] H. Chittimenu, M. Pasupureddy, C. Muthukumar, S. Krishnasamy, S. M. K. Thiagamani, and S. Siengchin, “Fracture Toughness of the Natural Fiber-Reinforced Composites: A Review,” in *Mechanical and Dynamic Properties of Biocomposites*, 2021, pp. 293–304.

[9] H. Kim and D. Seo, “Influence of water saturation on fracture toughness in woven natural fiber reinforced composites,” *Advanced Composite Materials*, vol. 16, no. 2, pp. 83–94, 2007.

[10] J. M. L. Reis, “Sisal fiber polymer mortar composites: Introductory fracture mechanics approach,” *Constr Build Mater*, vol. 37, pp. 177–180, 2012.

[11] S. K. Sahoo, S. Mohanty, and S. K. Nayak, “Study on the effect of woven sisal fiber mat on mechanical and viscoelastic properties of petroleum based epoxy and bioresin modified toughened epoxy network,” *J Appl Polym Sci*, vol. 132, no. 43, 2015.

[12] A. A. Betelie, Y. T. Megera, D. T. Redda, and A. Sinclair, “Experimental investigation of fracture toughness for treated sisal epoxy composite,” *AIMS Mater Sci*, vol. 5, no. 1, pp. 93–104, 2018.

[13] M. Boopalan, M. Niranjanaa, and M. J. Umapathy, “Study on the mechanical properties and thermal properties of jute and banana fiber reinforced epoxy hybrid composites,” *Compos B Eng*, vol. 51, pp. 54–57, 2013.

[14] Z. Zhang *et al.*, “High performances of plant fiber reinforced composites—A new insight from hierarchical microstructures,” *Compos Sci Technol*, vol. 194, 2020.

[15] O. Sinitsky, N. Trabelsi, and E. Priel, “The Mechanical Response of Epoxy-Sisal Composites Considering Fiber Anisotropy: A Computational and Experimental Study,” *Fibers*, vol. 10, no. 5, pp. 43–60, 2022.

[16] A. K. Mohanty, M. Misra, and L. T. Drzal, *Natural Fibers, Bio- polymers, and Biocomposites*, 1st ed. Boca Raton: CRC Press, 2005.

[17] M. Kebede, “Fabrication and Mechanical Property Characterization of Sisal fiber Reinforced Epoxy Resin Composite Material for Automotive body Application,” MSc Thesis, Addis Ababa University, Addis Ababa, 2015.

[18] A. kumre, R. S. Rana, and R. Purohit, “A Review on mechanical property of sisal glass fiber reinforced polymer composites,” *Mater Today Proc*, vol. 4, no. 2, Part A, pp. 3466–3476, 2017.

[19] A. Y. Al-Maharma and P. Sendur, “Review of the main factors controlling the fracture toughness and impact strength properties of natural composites,” *Mater Res Express*, vol. 6, no. 2, 2019.

[20] M. S. Fogorasi and I. Barbu, “The potential of natural fibres for automotive sector - review,” *IOP Conf Ser Mater Sci Eng*, vol. 252, no. 1, 2017.

[21] S. O. Ismail, E. Akpan, and H. N. Dhakal, “Review on natural plant fibres and their hybrid composites for structural applications: Recent trends and future perspectives,” *Composites Part C: Open Access*, vol. 9, 2022.

[22] Y. Li, Y. W. Mai, and L. Ye, “Sisal fibre and its composites: a review of recent developments,” *Compos Sci Technol*, vol. 60, no. 11, pp. 2037–2055, 2000.

[23] E. T. N. Bisanda, “The Effect of Alkali Treatment on the Adhesion Characteristics of Sisal Fibres,” *Applied Composite Materials*, vol. 7, no. 5, pp. 331–339, 2000.

[24] M. Z. Rong, M. Q. Zhang, Y. Liu, H. M. Yan, G. C. Yang, and H. M. Zeng, “Interfacial interaction in sisal/epoxy composites and its influence on impact performance,” *Polym Compos*, vol. 23, no. 2, pp. 182–192, 2002.

[25] S. Arumugam, J. Kandasamy, M. T. H. Sultan, A. U. M. Shah, and S. N. A. Safri, “Investigations on fatigue analysis and biomimetic mineralization of glass fiber/sisal fiber/chitosan reinforced hybrid polymer sandwich composites,” *Journal of Materials Research and Technology*, vol. 10, pp. 512–525, 2021.

[26] K. Palani Kumar, A. Shadrach Jeya Sekaran, L. Dinesh, D. Hari Prasad, and K. Deepak kumar, “Natural sisal fiber-based woven glass hybrid polymer composites for mono leaf spring: Experimental and numerical analysis,” *Progress in Rubber, Plastics and Recycling Technology*, vol. 37, no. 1, pp. 32–48, 2020.

[27] P. Kumar Bajpai, K. Ram, L. Kumar Gahlot, and V. Kumar Jha, “Fabrication of Glass/Jute/Epoxy Composite Based Industrial Safety Helmet,” *Mater Today Proc*, vol. 5, no. 2, pp. 8699–8706, 2018.

[28] K. Oksman, L. Wallström, L. A. Berglund, and R. D. T. Filho, “Morphology and mechanical properties of unidirectional sisal– epoxy composites,” *J Appl Polym Sci*, vol. 84, no. 13, pp. 2358–2365, 2002.

[29] Y. Li, H. Ma, Y. Shen, Q. Li, and Z. Zheng, “Effects of resin inside fiber lumen on the mechanical properties of sisal fiber reinforced composites,” *Compos Sci Technol*, vol. 108, pp. 32–40, 2015.

[30] H. Dagne, “Impact analysis of sisal fiber reinforced epoxy resin composite material for Automotive applications,” MSc Thesis, Addis Ababa University, Addis Ababa, 2017.

[31] E. T. N. Bisanda and M. P. Ansell, “The effect of silane treatment on the mechanical and physical properties of sisal-epoxy composites,” *Compos Sci Technol*, vol. 41, no. 2, pp. 165–178, 1991.

[32] B. Zuccarello, C. Militello, and F. Bongiorno, “Influence of the anisotropy of sisal fibers on the mechanical properties of high performance unidirectional biocomposite lamina and micromechanical models,” *Compos Part A Appl Sci Manuf*, vol. 143, 2021.

[33] M. K. Gupta and R. K. Srivastava, “Tensile and Flexural Properties of Sisal Fibre Reinforced Epoxy Composite: A Comparison between Unidirectional and Mat form of Fibres,” *Procedia Materials Science*, vol. 5, pp. 2434–2439, 2014.

[34] V. P. Arthanarieswaran, A. Kumaravel, and M. Kathirselvam, “Evaluation of mechanical properties of banana and sisal fiber reinforced epoxy composites: Influence of glass fiber hybridization,” *Mater Des*, vol. 64, 2014.

[35] M. Ramesh, K. Palanikumar, and K. H. Reddy, “Mechanical property evaluation of sisal–jute–glass fiber reinforced polyester composites,” *Compos B Eng*, vol. 48, pp. 1–9, 2013.

[36] K. Hari Ram and R. Edwin Raj, “Synthesis and mechanical characterization of sisal-epoxy and hybrid- epoxy composites in comparison with conventional fiber glass-epoxy composite,” in *Advanced Materials Research*, 2014, pp. 285–290.

[37] K. Palanikumar, M. Ramesh, and K. Hemachandra Reddy, “Experimental Investigation on the Mechanical Properties of Green Hybrid Sisal and Glass Fiber Reinforced Polymer Composites,” *Journal of Natural Fibers*, vol. 13, no. 3, pp. 321–331, 2016.

[38] S. Arumugam *et al.*, “Investigations on the Mechanical Properties of Glass Fiber/Sisal Fiber/Chitosan Reinforced Hybrid Polymer Sandwich Composite Scaffolds for Bone Fracture Fixation Applications,” *Polymers (Basel)*, vol. 12, no. 7, 2020.

[39] A. A. Betelie, A. N. Sinclair, M. Kortschot, Y. Li, and D. T. Redda, “Mechanical properties of sisal-epoxy composites as functions of fiber-to-epoxy ratio,” *AIMS Mater Sci*, vol. 6, no. 6, pp. 985–996, 2019.

[40] V. Fiore, T. Scalici, F. Nicoletti, G. Vitale, M. Prestipino, and A. Valenza, “A new eco-friendly chemical treatment of natural fibres: Effect of sodium bicarbonate on properties of sisal fibre and its epoxy composites,” *Compos B Eng*, vol. 85, pp. 150–160, 2016.

[41] S. Srisuwan and P. Chumsamrong, “Effects of Weave Type and Fiber Content on Physical Properties of Sisal Fiber/Epoxy Composites,” *Adv Mat Res*, vol. 123–125, pp. 1139–1142, 2010.

[42] H. J. Kim and D. W. Seo, “Effect of water absorption fatigue on mechanical properties of sisal textile-reinforced composites,” *Int J Fatigue*, vol. 28, no. 10, pp. 1307–1314, 2006.

[43] N. Blanco, D. Trias, S. T. Pinho, and P. Robinson, “Intralaminar fracture toughness characterisation of woven composite laminates. Part II: Experimental characterisation,” *Eng Fract Mech*, vol. 131, pp. 361–370, 2014.

[44] M. J. Laffan, S. T. Pinho, P. Robinson, and A. J. McMillan, “Translaminar fracture toughness testing of composites: A review,” *Polym Test*, vol. 31, no. 3, pp. 481–489, 2012.

[45] S. Wicaksono and G. B. Chai, “A review of advances in fatigue and life prediction of fiber-reinforced composites,” *Proceedings of the Institution of Mechanical Engineers, Part L: Journal of Materials: Design and Applications*, vol. 227, no. 3, pp. 179–195, 2012.

[46] M. F. S. F. de Moura, R. D. S. G. Campilho, A. M. Amaro, and P. N. B. Reis, “Interlaminar and intralaminar fracture characterization of composites under mode I loading,” *Compos Struct*, vol. 92, no. 1, 2010.

[47] F. de A. Silva, N. Chawla, and R. D. de T. Filho, “Tensile behavior of high performance natural (sisal) fibers,” *Compos Sci Technol*, vol. 68, no. 15, pp. 3438–3443, 2008.

[48] N. Chand and S. A. R. Hashmi, “Mechanical properties of sisal fibre at elevated temperatures,” *J Mater Sci*, vol. 28, no. 24, pp. 6724–6728, 1993.

[49] W. P. Inacio, F. P. D. Lopes, and S. N. Monteiro, “Diameter dependence of tensile strength by Weibull analysis: Part III sisal fiber,” *Matéria (Rio de Janeiro)*, vol. 15, no. 2, pp. 124–130, 2010.

[50] P. S. Mukherjee and K. G. Satyanarayana, “Structure and properties of some vegetable fibres: Part 1 Sisal Fibre,” *J Mater Sci*, vol. 19, no. 12, pp. 3925–3934, 1984.

[51] M. E. Alves Fidelis, T. V. C. Pereira, O. da F. M. Gomes, F. de Andrade Silva, and R. D. Toledo Filho, “The effect of fiber morphology on the tensile strength of natural fibers,” *Journal of Materials Research and Technology*, vol. 2, no. 2, pp. 149–157, 2013.

[52] D. K. Rajak, D. D. Pagar, P. L. Menezes, and E. Linul, “Fiber-Reinforced Polymer Composites: Manufacturing, Properties, and Applications,” *Polymers (Basel)*, vol. 11, no. 10, 2019.

[53] B. Dennis, “Fabrication and Determination of Mechanical Properties of Woven Sisal Fabric Reinforced Epoxy Composite,” MSc Thesis, MOI University, Eldoret, 2017.

[54] N. Chand, S. Verma, and A. C. Khazanchi, “SEM and strength characteristics of acetylated sisal fibre,” *J Mater Sci Lett*, vol. 8, no. 11, pp. 1307–1309, 1989.

[55] P. Sahu and M. K. Gupta, “Lowering in water absorption capacity and mechanical degradation of sisal/epoxy composite by sodium bicarbonate treatment and PLA coating,” *Polym Compos*, vol. 41, no. 2, pp. 668–681, 2020.

[56] M. M. Mughal, M. W. Akhtar, M. M. Baloch, M. A. Memon, J. A. Syed, and J. S. Kim, “Effect of silanized sisal fiber on thermo-mechanical properties of reinforced epoxy composites,” *J Compos Mater*, vol. 54, no. 15, pp. 2037–2050, 2019.

[57] Y. Li and Y. W. Mai, “Interfacial Characteristics of Sisal Fiber and Polymeric Matrices,” *J Adhes*, vol. 82, no. 5, pp. 527–554, 2006.

[58] S. Kalia and S. Vashistha, “Surface Modification of Sisal Fibers (Agave sisalana) Using Bacterial Cellulase and Methyl Methacrylate,” *J Polym Environ*, vol. 20, no. 1, pp. 142–151, 2012.

[59] M. Z. Rong, M. Q. Zhang, Y. Liu, G. C. Yang, and H. M. Zeng, “The effect of fiber treatment on the mechanical properties of unidirectional sisal-reinforced epoxy composites,” *Compos Sci Technol*, vol. 61, no. 10, pp. 1437–1447, 2001.

[60] B. Dorneles de Castro, K. M. Machado Neves Silva, R. Maziero, P. E. de Faria, P. Pereira Silva-Caldeira, and J. C. Campos Rubio, “Influence of Gamma Radiation Treatment on the Mechanical Properties of Sisal Fibers to Use into Composite Materials,” *Fibers and Polymers*, vol. 21, no. 8, pp. 1816–1823, 2020.

[61] M. Akram Khan, S. Guru, P. Padmakaran, D. Mishra, M. Mudgal, and S. Dhakad, “Characterisation studies and impact of chemical treatment on mechanical properties of sisal fiber,” *Compos Interfaces*, vol. 18, no. 6, 2011.

[62] R. Ntenga, A. Béakou, J. Atangana Atéba, and L. Ayina Ohandja, “Estimation of the elastic anisotropy of sisal fibres by an inverse method,” *J Mater Sci*, vol. 43, no. 18, pp. 6206–6213, 2008.

[63] J. Thomason, L. Yang, and F. Gentles, “Characterisation of the Anisotropic Thermoelastic Properties of Natural Fibres for Composite Reinforcement,” *Fibers*, vol. 5, no. 4, pp. 36–47, 2017.

[64] J. Kandasamy, A. Soundhar, M. Rajesh, D. Mallikarjuna Reddy, and V. R. Kar, “Natural Fiber Composite for Structural Applications,” in *Structural Health Monitoring System for Synthetic, Hybrid and Natural Fiber Composites*, M. Jawaid, A. Hamdan, and M. T. Hameed Sultan, Eds., Singapore: Springer Singapore, 2021, pp. 23–35.

[65] S. M. Mahtebu, “Experimental Fatigue Behavior Investigation of Sisal Reinforced Epoxy Composite,” MSc Thesis, Addis Ababa University, Addis Ababa, 2019.

[66] G. R. Arpitha, M. R. Sanjay, P. Senthamaraikannan, C. Barile, and B. Yogesha, “Hybridization effect of sisal/glass/epoxy/filler based woven fabric reinforced composites,” *Exp Tech*, vol. 41, no. 6, 2017.

[67] S. C. Amico, C. C. Angrizani, and M. L. Drummond, “Influence of the stacking sequence on the mechanical properties of glass/sisal hybrid composites,” *Journal of Reinforced Plastics and Composites*, vol. 29, no. 2, pp. 179–189, 2010.

[68] K. John and S. Venkata Naidu, “Sisal fiber/glass fiber hybrid composites: The impact and compressive properties,” *Journal of Reinforced Plastics and Composites*, vol. 23, no. 12, pp. 1253–1258, 2004.

[69] N. Sato, M. Hojo, and M. Nishikawa, “Intralaminar fatigue crack growth properties of conventional and interlayer toughened CFRP laminate under mode i loading,” *Compos Part A Appl Sci Manuf*, vol. 68, 2015.

[70] ASTM D5528/D5528M-21, “Standard Test Method for Mode I Interlaminar Fracture Toughness of Unidirectional Fiber-reinforced Polymer Matrix Composites.” ASTM International, 2007.

[71] ISO 15024:2001, “Determination of Mode I Interlaminar Fracture Toughness, GIC, for Unidirectionally Reinforced Materials.” International Organization for Standardization, 2001.

[72] ASTM D 6671/D 6671M-06, “ Mixed Mode I-Mode II Interlaminar Fracture Toughness of Unidirectional Fiber Reinforced Polymer Matrix Composites.” ASTM International, 2006.

[73] ASTM E399-12, “Standard Test Method for Linear-Elastic Plane-Strain Fracture Toughness KIc of Metallic Materials.” ASTM International, 2012.

[74] ASTM D5045-14, “Standard Test Methods for Plane-Strain Fracture Toughness and Strain Energy Release Rate of Plastic Materials.” ASTM International, 2014.

[75] N. Blanco, D. Trias, S. T. Pinho, and P. Robinson, “Intralaminar fracture toughness characterisation of woven composite laminates. Part I: Design and analysis of a compact tension (CT) specimen,” *Eng Fract Mech*, vol. 131, pp. 349–360, 2014.

[76] ASTM E1922-04, “Standard Test Method for Translaminar Fracture Toughness of Laminated and Pultruded Polymer Matrix Composite Materials.” ASTM International, 2004.

[77] R. V Silva, D. Spinelli, W. W. Bose Filho, S. Claro Neto, G. O. Chierice, and J. R. Tarpani, “Fracture toughness of natural fibers/castor oil polyurethane composites,” *Compos Sci Technol*, vol. 66, no. 10, pp. 1328–1335, 2006.

[78] A. E. Ismail *et al.*, “Fracture toughness of woven kenaf fibre reinforced composites,” *IOP Conf Ser Mater Sci Eng*, vol. 160, no. 1, 2016.

[79] M. A. Pinto, V. B. Chalivendra, Y. K. Kim, and A. F. Lewis, “Effect of surface treatment and Z-axis reinforcement on the interlaminar fracture of jute/epoxy laminated composites,” *Eng Fract Mech*, vol. 114, 2013.

[80] Q. Liu and M. Hughes, “The fracture behaviour and toughness of woven flax fibre reinforced epoxy composites,” *Compos Part A Appl Sci Manuf*, vol. 39, no. 10, 2008.

[81] A. H. Abdullah, F. F. Abdul Mutalib, and M. F. Mat, “Tensile and Fracture Toughness Properties of Coconut Spathe Fibre Reinforced Epoxy Composites: Effect of Chemical Treatments,” *Adv Mat Res*, vol. 1133, pp. 603–607, 2016.

[82] K. L. Pickering, M. A. Sawpan, J. Jayaraman, and A. Fernyhough, “Influence of loading rate, alkali fibre treatment and crystallinity on fracture toughness of random short hemp fibre reinforced polylactide bio-composites,” *Compos Part A Appl Sci Manuf*, vol. 42, no. 9, pp. 1148–1156, 2011.

[83] Y. Li, Y. W. Mai, and L. Ye, “Effects of fibre surface treatment on fracture-mechanical properties of sisal-fibre composites,” *Compos Interfaces*, vol. 12, no. 1–2, pp. 141–163, 2005.

[84] Y. Zhang, Y. Li, H. Ma, and T. Yu, “Tensile and interfacial properties of unidirectional flax/glass fiber reinforced hybrid composites,” *Compos Sci Technol*, vol. 88, pp. 172–177, 2013.

[85] A. L. Pereira, M. D. Banea, and A. B. Pereira, “Effect of intralaminar hybridization on mode I fracture toughness of natural fiber-reinforced composites,” *Journal of the Brazilian Society of Mechanical Sciences and Engineering*, vol. 42, no. 9, pp. 451–458, 2020.

[86] T. Alomayri, H. Assaedi, F. U. A. Shaikh, and I. M. Low, “Effect of water absorption on the mechanical properties of cotton fabric-reinforced geopolymer composites,” *Journal of Asian Ceramic Societies*, vol. 2, no. 3, pp. 223–230, 2014.

[87] M. S. Islam, K. L. Pickering, and N. J. Foreman, “Influence of Hygrothermal Ageing on the Physico-Mechanical Properties of Alkali Treated Industrial Hemp Fibre Reinforced Polylactic Acid Composites,” *J Polym Environ*, vol. 18, no. 4, pp. 696–704, 2010.

[88] M. S. Islam, K. L. Pickering, and N. J. Foreman, “Influence of accelerated ageing on the physico-mechanical properties of alkali-treated industrial hemp fibre reinforced poly(lactic acid) (PLA) composites,” *Polym Degrad Stab*, vol. 95, no. 1, pp. 59–65, 2010.

[89] M. Hughes, C. A. S. Hill, and J. R. B. Hague, “The fracture toughness of bast fibre reinforced polyester composites: Part 1 Evaluation and analysis,” *J Mater Sci*, vol. 37, no. 21, pp. 4669–4676, 2002.

[90] K. P. Ashik, R. S. Sharma, and N. Raghavendra, “Evaluation of Tensile, Modal and Fracture Properties of Jute/Epoxy Natural Composites with addition of Silicon di Oxide as Filler Material,” in *Materials Today: Proceedings*, 2017, pp. 9586–9591.

[91] Y. Saadati, G. Lebrun, C. Bouvet, J. F. Chatelain, and Y. Beauchamp, “Study of translaminar fracture toughness of unidirectional flax/epoxy composite,” *Composites Part C: Open Access*, vol. 1, 2020.

[92] O. K. Gudeta, “Experimental Evaluation of Fracture Toughness and Water Absorption Behavior of Woven Sisal and E-Glass Fibers Reinforced Hybrid Composite Material,” MSc Thesis, Addis Ababa University, Addis Ababa, 2021.

[93] P. K. Mallick, *Fiber-reinforced composites: Materials, manufacturing, and design, third edition*. Boca Raton: CRC Press, 2007.

[94] “E-Glass and S-Glass,” JPS Composite Materials. Accessed: Jun. 25, 2023. [Online]. Available: https://jpscm.com/products/e-glass-s-glass/

[95] A. K. Kaw, *Mechanics of composite materials, second edition*. Boca Raton: CRC Press, 2005.

[96] S. Jose, R. Ramesh Kumar, M. K. Jana, and G. Venkateswara Rao, “Intralaminar fracture toughness of a cross-ply laminate and its constituent sub-laminates,” *Compos Sci Technol*, vol. 61, no. 8, 2001.

[97] S. T. Pinho, P. Robinson, and L. Iannucci, “Fracture toughness of the tensile and compressive fibre failure modes in laminated composites,” *Compos Sci Technol*, vol. 66, no. 13, pp. 2069–2079, 2006.

[98] S. Ekşi and L. Genel, “Comparison of mechanical properties of unidirectional and woven carbon, glass and aramid fiber reinforced epoxy composites,” *Acta Phys Pol A*, vol. 132, no. 3, pp. 879–882, 2017.

[99] C. Chizyuka and K. Shamitiba, “Effects of Hydrothermal Ageing on the Fracture Damage of Sisal Fibre Reinforced Polyester Composites,” University of Zambia, Lusaka, 2013.

[100] A. O. Ozdemir and C. Karatas, “Experimental Determination of Fracture Toughness of Woven/Chopped Glass Fiber Hybrid Reinforced Thermoplastic Composite Laminates,” *Scientia Iranica*, vol. 0, no. 0, 2020.

Appendix

A. Data of Composite Constituents

Laminate S - S/S/S/S/S/S/S			
Constants	**Values**	**Parameters**	**Values**
Total fiber volume fraction V_f	0.3	Density of composite, ρ (g/cm^3)	1.275
Required sisal fiber V_f	0.3	Mass of composite, m (g)	357
Required glass fiber V_f	0	Volume of sisal fiber (cm^3)	84
Required relative Sisal:Glass V_f	1	Volume of glass fiber (cm^3)	0
Density of sisal fiber, ρ_s (g/cm^3)	1.45	Volume of epoxy (cm^3)	196
Density of glass fiber, ρ_f (g/cm^3)	2.54	Mass of sisal fiber, m_s (g)	121.8
Density of epoxy, ρ_e (g/cm^3)	1.2	Mass of glass fiber, m_g (g)	0
Volume of composite, V (cm^3)	280	Mass of epoxy, m_e (g)	235.2
		Sisal fiber wt%	0.3412
		Glass fiber wt%	0
		Relative Sisal:Glass wt%	1
Laminate H1 - G/G/S/S/S/G/G			
Constants	**Values**	**Parameters**	**Values**
Total fiber volume fraction V_f	0.3	Density of composite, ρ (g/cm^3)	1.4603
Required sisal fiber V_f	0.13	Mass of composite, m (g)	408.884
Required glass fiber V_f	0.17	Volume of sisal fiber (cm^3)	36.4
Required relative Sisal:Glass V_f	0.4333	Volume of glass fiber (cm^3)	47.6
Density of sisal fiber, ρ_s (g/cm^3)	1.45	Volume of epoxy (cm^3)	196
Density of glass fiber, ρ_f (g/cm^3)	2.54	Mass of sisal fiber, m_s (g)	52.78
Density of epoxy, ρ_e (g/cm^3)	1.2	Mass of glass fiber, m_g (g)	120.904
Volume of composite, V (cm^3)	280	Mass of epoxy, m_e (g)	235.2
		Sisal fiber wt%	0.1291
		Glass fiber wt%	0.2957
		Relative Sisal:Glass wt%	0.3039
Laminate H2 - G/G/S/G/S/G/G			
Constants	**Values**	**Parameters**	**Values**
Total fiber volume fraction V_f	0.3	Density of composite, ρ (g/cm^3)	1.5094
Required sisal fiber V_f	0.085	Mass of composite, m (g)	422.618
Required glass fiber V_f	0.215	Volume of sisal fiber (cm^3)	23.8
Required relative Sisal:Glass V_f	0.2833	Volume of glass fiber (cm^3)	60.2
Density of sisal fiber, ρ_s (g/cm^3)	1.45	Volume of epoxy (cm^3)	196
Density of glass fiber, ρ_f (g/cm^3)	2.54	Mass of sisal fiber, m_s (g)	34.51
Density of epoxy, ρ_e (g/cm^3)	1.2	Mass of glass fiber, m_g (g)	152.908

Volume of composite, V (cm^3)	280	Mass of epoxy, m_e (g)	235.2
		Sisal fiber wt%	0.0817
		Glass fiber wt%	0.3618
		Relative Sisal:Glass wt%	0.1841
Laminate G - G/G/G/G/G/G/G			
Constants	**Values**	**Parameters**	**Values**
Total fiber volume fraction V_f	0.3	Density of composite, ρ (g/cm^3)	1.602
Required sisal fiber V_f	0	Mass of composite, m (g)	448.56
Required glass fiber V_f	0.3	Volume of sisal fiber (cm^3)	0
Required relative Sisal:Glass V_f	0	Volume of glass fiber (cm^3)	84
Density of sisal fiber, ρ_s (g/cm^3)	1.45	Volume of epoxy (cm^3)	196
Density of glass fiber, ρ_f (g/cm^3)	2.54	Mass of sisal fiber, m_s (g)	0
Density of epoxy, ρ_e (g/cm^3)	1.2	Mass of glass fiber, m_g (g)	213.36
Volume of composite, V (cm^3)	280	Mass of epoxy, m_e (g)	235.2
		Sisal fiber wt%	0
		Glass fiber wt%	0.4757
		Relative Sisal:Glass wt%	0

B. Python Code for Normalized Energy Release Rate Analysis of 2TCT Specimen

```
#**************************************************************************#
#Normalized Energy Release Rate Analysis of 2TCT Specimen                  #
#**************************************************************************#
#==========================================================================#
#Preparation
#==========================================================================#
from abaqus import *
from abaqusConstants import *
session.viewports['Viewport: 1'].makeCurrent()
session.viewports['Viewport: 1'].maximize()
from caeModules import *
from driverUtils import executeOnCaeStartup
executeOnCaeStartup()
Mdb ()
import os
os.chdir(r"S:\Programs\ABAQUSTemp")
s = mdb.models['Model-1'].ConstrainedSketch(name='__profile__',
    sheetSize=200.0)
g, v, d, c = s.geometry, s.vertices, s.dimensions, s.constraints
s.setPrimaryObject(option=STANDALONE)
#==========================================================================#
#Parameters                                                                #
#==========================================================================#
#Crack Length
Csize = 20.0
#Material Properties
E1 = 14352.0
E2 = 14352.0
Nu = 0.24
G12 = 4728.0
G13 = 4728.0
G23 = 4728.0
#Mesh Size Factors
MAXsize = 1.0
MINsize = 0.2
#==========================================================================#
#Part Module                                                               #
#==========================================================================#
#Sketch the Geometry
s.Line(point1=(0.0, 0.0), point2=(Csize, 0.0))
s.HorizontalConstraint(entity=g[2], addUndoState=False)
s.Line(point1=(Csize, 0.0), point2=(76.0, 0.0))
s.HorizontalConstraint(entity=g[3], addUndoState=False)
s.ParallelConstraint(entity1=g[2], entity2=g[3], addUndoState=False)
s.Line(point1=(76.0, 0.0), point2=(76.0, 20.0))
s.VerticalConstraint(entity=g[4], addUndoState=False)
s.PerpendicularConstraint(entity1=g[3], entity2=g[4], addUndoState=False)
s.Line(point1=(76.0, 20.0), point2=(56.0, 35.0))
s.Line(point1=(56.0, 35.0), point2=(6.0, 35.0))
s.HorizontalConstraint(entity=g[6], addUndoState=False)
s.Line(point1=(6.0, 35.0), point2=(-14.0, 20.0))
```

```
s.Line(point1=(-14.0, 20.0), point2=(-14.0, 0.0))
s.VerticalConstraint(entity=g[8], addUndoState=False)
s.Line(point1=(-14.0, 0.0), point2=(0.0, 0.0))
s.HorizontalConstraint(entity=g[9], addUndoState=False)
s.PerpendicularConstraint(entity1=g[8], entity2=g[9], addUndoState=False)
s.CircleByCenterPerimeter(center=(0.0, 13.0), point1=(0.0, 17.0))
#Create 3D, Deformable, Shell Planar Part
p = mdb.models['Model-1'].Part(name='Part-1', dimensionality=THREE_D,
    type=DEFORMABLE_BODY)
p = mdb.models['Model-1'].parts['Part-1']
p.BaseShell(sketch=s)
s.unsetPrimaryObject()
p = mdb.models['Model-1'].parts['Part-1']
session.viewports['Viewport: 1'].setValues(displayedObject=p)
del mdb.models['Model-1'].sketches['__profile__']
#Create Set 'CrackTip', 'SymmetricLine', and 'EndConstraintPoint'
session.viewports['Viewport: 1'].setValues(displayedObject=None)
p = mdb.models['Model-1'].parts['Part-1']
v = p.vertices
verts = v.getSequenceFromMask(mask=('[#8 ]', ), )
p.Set(vertices=verts, name='CrackTip')
p = mdb.models['Model-1'].parts['Part-1']
e = p.edges
edges = e.getSequenceFromMask(mask=('[#8 ]', ), )
p.Set(edges=edges, name='SymmetricLine')
p = mdb.models['Model-1'].parts['Part-1']
v = p.vertices
verts = v.getSequenceFromMask(mask=('[#10 ]', ), )
p.Set(vertices=verts, name='EndConstraintPoint')
#Create the Set 'LoadingPoint'
p = mdb.models['Model-1'].parts['Part-1']
session.viewports['Viewport: 1'].setValues(displayedObject=p)
p = mdb.models['Model-1'].parts['Part-1']
v = p.vertices
verts = v.getSequenceFromMask(mask=('[#1 ]', ), )
p.Set(vertices=verts, name='LoadingPoint')
#==============================================================================#
#Property Module                                                               #
#==============================================================================#
#Set Material Property
mdb.models['Model-1'].Material(name='Material-1')
mdb.models['Model-1'].materials['Material-1'].Elastic(type=LAMINA, table=((
    E1, E2, Nu, G12, G13, G23), ))
#Section Creation and Assignment
mdb.models['Model-1'].HomogeneousShellSection(name='Section-1',
    preIntegrate=OFF, material='Material-1', thicknessType=UNIFORM,
    thickness=1.0, thicknessField='', nodalThicknessField='',
    idealization=NO_IDEALIZATION, poissonDefinition=DEFAULT,
    thicknessModulus=None, temperature=GRADIENT, useDensity=OFF,
    integrationRule=SIMPSON, numIntPts=3)
p = mdb.models['Model-1'].parts['Part-1']
f = p.faces
```

```
faces = f.getSequenceFromMask(mask=('[#1 ]', ), )
region = regionToolset.Region(faces=faces)
p = mdb.models['Model-1'].parts['Part-1']
p.SectionAssignment(region=region, sectionName='Section-1', offset=0.0,
    offsetType=MIDDLE_SURFACE, offsetField='',
    thicknessAssignment=FROM_SECTION)
#==========================================================================#
#Assembly Module                                                           #
#==========================================================================#
a = mdb.models['Model-1'].rootAssembly
a.DatumCsysByDefault(CARTESIAN)
p = mdb.models['Model-1'].parts['Part-1']
a.Instance(name='Part-1-1', part=p, dependent=OFF)
#==========================================================================#
#Interaction Module                                                        #
#==========================================================================#
a = mdb.models['Model-1'].rootAssembly
session.viewports['Viewport: 1'].setValues(displayedObject=a)
session.viewports['Viewport: 1'].assemblyDisplay.setValues(interactions=ON,
    constraints=ON, connectors=ON, engineeringFeatures=ON)
a = mdb.models['Model-1'].rootAssembly
crackFront = a.instances['Part-1-1'].sets['CrackTip']
a = mdb.models['Model-1'].rootAssembly
crackTip = a.instances['Part-1-1'].sets['CrackTip']
v11 = a.instances['Part-1-1'].vertices
v21 = a.instances['Part-1-1'].vertices
a.engineeringFeatures.ContourIntegral(name='Crack-1', symmetric=ON,
    crackFront=crackFront, crackTip=crackTip,
    extensionDirectionMethod=Q_VECTORS, qVectors=((v11[3], v21[4]), ),
    midNodePosition=0.5, collapsedElementAtTip=NONE)
#==========================================================================#
#Step Module                                                               #
#==========================================================================#
#Create 'LoadingStep'
mdb.models['Model-1'].StaticStep(name='Loading', previous='Initial')
session.viewports['Viewport: 1'].assemblyDisplay.setValues(step='Loading')
#Create 'History Output-1'
mdb.models['Model-1'].historyOutputRequests['H-Output-1'].setValues(
    frequency=LAST_INCREMENT, contourIntegral='Crack-1', sectionPoints=DEFAULT,
    rebar=EXCLUDE, numberOfContours=5)
#==========================================================================#
#Load Module                                                               #
#==========================================================================#
#Create 'BC-1' and 'BC-2'
a = mdb.models['Model-1'].rootAssembly
session.viewports['Viewport: 1'].setValues(displayedObject=a)
session.viewports['Viewport: 1'].assemblyDisplay.setValues(step='Initial')
a = mdb.models['Model-1'].rootAssembly
region = a.instances['Part-1-1'].sets['SymmetricLine']
mdb.models['Model-1'].YsymmBC(name='BC-1', createStepName='Initial',
    region=region, localCsys=None)
a = mdb.models['Model-1'].rootAssembly
```

```
region = a.instances['Part-1-1'].sets['EndConstraintPoint']
mdb.models['Model-1'].DisplacementBC(name='BC-2', createStepName='Initial',
    region=region, u1=SET, u2=UNSET, u3=UNSET, ur1=UNSET, ur2=UNSET, ur3=UNSET,
    amplitude=UNSET, distributionType=UNIFORM, fieldName='', localCsys=None)
session.viewports['Viewport: 1'].assemblyDisplay.setValues(step='Loading')
#Create 'Load-1' (concentrated load of 1N)
a = mdb.models['Model-1'].rootAssembly
region = a.instances['Part-1-1'].sets['LoadingPoint']
mdb.models['Model-1'].ConcentratedForce(name='Load-1',
    createStepName='Loading', region=region, cf2=1.0, distributionType=UNIFORM,
    field='', localCsys=None)
#============================================================================#
#Mesh Module                                                                 #
#============================================================================#
a = mdb.models['Model-1'].rootAssembly
session.viewports['Viewport: 1'].setValues(displayedObject=a)
a = mdb.models['Model-1'].rootAssembly
f1 = a.instances['Part-1-1'].faces
pickedRegions = f1.getSequenceFromMask(mask=('[#1 ]', ), )
a.setMeshControls(regions=pickedRegions, elemShape=QUAD)
elemType1 = mesh.ElemType(elemCode=S8R5, elemLibrary=STANDARD)
elemType2 = mesh.ElemType(elemCode=STRI65, elemLibrary=STANDARD)
a = mdb.models['Model-1'].rootAssembly
f1 = a.instances['Part-1-1'].faces
faces1 = f1.getSequenceFromMask(mask=('[#1 ]', ), )
pickedRegions =(faces1, )
a.setElementType(regions=pickedRegions, elemTypes=(elemType1, elemType2))
a = mdb.models['Model-1'].rootAssembly
e1 = a.instances['Part-1-1'].edges
pickedEdges = e1.getSequenceFromMask(mask=('[#1f2 ]', ), )
a.seedEdgeBySize(edges=pickedEdges, size=MAXsize, deviationFactor=0.1,
    constraint=FINER)
a = mdb.models['Model-1'].rootAssembly
e1 = a.instances['Part-1-1'].edges
pickedEdges = e1.getSequenceFromMask(mask=('[#1 ]', ), )
a.seedEdgeBySize(edges=pickedEdges, size=MINsize, deviationFactor=0.1,
    constraint=FINER)
a = mdb.models['Model-1'].rootAssembly
e1 = a.instances['Part-1-1'].edges
pickedEdges2 = e1.getSequenceFromMask(mask=('[#4 ]', ), )
a.seedEdgeByBias(biasMethod=SINGLE, end2Edges=pickedEdges2, minSize=MINsize,
    maxSize=MAXsize, constraint=FINER)
a = mdb.models['Model-1'].rootAssembly
e1 = a.instances['Part-1-1'].edges
pickedEdges1 = e1.getSequenceFromMask(mask=('[#8 ]', ), )
a.seedEdgeByBias(biasMethod=SINGLE, end1Edges=pickedEdges1, minSize=MINsize,
    maxSize=MAXsize, constraint=FINER)
a = mdb.models['Model-1'].rootAssembly
partInstances =(a.instances['Part-1-1'], )
a.generateMesh(regions=partInstances)
```

```
#==========================================================================#
#Job Module                                                                #
#==========================================================================#
#Create Job Named 'J_study_G_a20' and Submit for Analysis
mdb.Job(name='J_study_G_a20', model='Model-1', description='', type=ANALYSIS,
    atTime=None, waitMinutes=0, waitHours=0, queue=None, memory=90,
    memoryUnits=PERCENTAGE, getMemoryFromAnalysis=True,
    explicitPrecision=SINGLE, nodalOutputPrecision=SINGLE, echoPrint=OFF,
    modelPrint=OFF, contactPrint=OFF, historyPrint=OFF, userSubroutine='',
    scratch='', resultsFormat=ODB, multiprocessingMode=DEFAULT, numCpus=1,
    numGPUs=0)
mdb.jobs['J_study_G_a20'].submit(consistencyChecking=OFF)
session.viewports['Viewport: 1'].view.fitView()
```

C. Normalized Energy Release Rate Values $f(a)$ (m^2/kJ) for values of the crack length a ranging from 19 – 64 mm

Laminate S - S/S/S/S/S/S/S							
a	19	20	21	22	23	24	25
f(a)	1.4033E-04	1.4838E-04	1.5669E-04	1.6533E-04	1.7434E-04	1.8376E-04	1.9366E-04
a	26	27	28	29	30	31	32
f(a)	2.0410E-04	2.1516E-04	2.2694E-04	2.3946E-04	2.5289E-04	2.6737E-04	2.8294E-04
a	33	34	35	36	37	38	39
f(a)	2.9986E-04	3.1825E-04	3.3835E-04	3.6044E-04	3.8462E-04	4.1144E-04	4.4122E-04
a	40	41	42	43	44	45	46
f(a)	4.7432E-04	5.1135E-04	5.5293E-04	5.9985E-04	6.5279E-04	7.1299E-04	7.8178E-04
a	47	48	49	50	51	52	53
f(a)	8.6061E-04	9.5154E-04	1.0568E-03	1.1794E-03	1.3232E-03	1.4928E-03	1.6941E-03
a	54	55	56	57	58	59	60
f(a)	1.9352E-03	2.2262E-03	2.5807E-03	3.0169E-03	3.5596E-03	4.2429E-03	5.1146E-03
a	61	62	63	64			
f(a)	8.3208E-02	6.2446E-03	7.7335E-03	9.7359E-03			
Laminate H1 - G/G/S/S/S/G/G							
a	19	20	21	22	23	24	25
f(a)	5.6221E-05	5.9422E-05	6.2723E-05	6.6160E-05	6.9745E-05	7.3495E-05	7.7438E-05
a	26	27	28	29	30	31	32
f(a)	8.1595E-05	8.6002E-05	9.0693E-05	9.5683E-05	1.0104E-04	1.0681E-04	1.1302E-04
a	33	34	35	36	37	38	39
f(a)	1.1977E-04	1.2710E-04	1.3511E-04	1.4392E-04	1.5357E-04	1.6427E-04	1.7615E-04
a	40	41	42	43	44	45	46
f(a)	1.8935E-04	2.0412E-04	2.2072E-04	2.3943E-04	2.6056E-04	2.8458E-04	3.1202E-04
a	47	48	49	50	51	52	53
f(a)	3.4347E-04	3.7974E-04	4.2172E-04	4.7061E-04	5.2796E-04	5.9552E-04	6.7575E-04
a	54	55	56	57	58	59	60
f(a)	7.7181E-04	8.8767E-04	1.0288E-03	1.2024E-03	1.4184E-03	1.6902E-03	2.0370E-03
a	61	62	63	64			
f(a)	2.4864E-03	3.0785E-03	3.8748E-03	4.9667E-03			
Laminate H2 - G/G/S/G/S/G/G							
a	19	20	21	22	23	24	25
f(a)	4.8903E-05	5.1685E-05	5.4555E-05	5.7543E-05	6.0660E-05	6.3920E-05	6.7348E-05
a	26	27	28	29	30	31	32
f(a)	7.0962E-05	7.4793E-05	7.8872E-05	8.3211E-05	8.7867E-05	9.2885E-05	9.8283E-05
a	33	34	35	36	37	38	39

f(a)	1.0415E-04	1.1053E-04	1.1749E-04	1.2516E-04	1.3354E-04	1.4284E-04	1.5317E-04
a	40	41	42	43	44	45	46
f(a)	1.6466E-04	1.7750E-04	1.9193E-04	2.0820E-04	2.2657E-04	2.4746E-04	2.7132E-04
a	47	48	49	50	51	52	53
f(a)	2.9867E-04	3.3021E-04	3.6670E-04	4.0921E-04	4.5908E-04	5.1783E-04	5.8758E-04
a	54	55	56	57	58	59	60
f(a)	6.7109E-04	7.7182E-04	8.9455E-04	1.0455E-03	1.2332E-03	1.4695E-03	1.7710E-03
a	61	62	63	64			
f(a)	2.1616E-03	2.6764E-03	3.3686E-03	4.3177E-03			
Laminate G - G/G/G/G/G/G/G							
a	19	20	21	22	23	24	25
f(a)	3.8802E-05	4.1008E-05	4.3284E-05	4.5653E-05	4.8124E-05	5.0709E-05	5.3427E-05
a	26	27	28	29	30	31	32
f(a)	5.6292E-05	5.9330E-05	6.2565E-05	6.6005E-05	6.9698E-05	7.3677E-05	7.7958E-05
a	33	34	35	36	37	38	39
f(a)	8.2612E-05	8.7668E-05	9.3194E-05	9.9270E-05	1.0592E-04	1.1330E-04	1.2149E-04
a	40	41	42	43	44	45	46
f(a)	1.3060E-04	1.4078E-04	1.5223E-04	1.6513E-04	1.7970E-04	1.9627E-04	2.1519E-04
a	47	48	49	50	51	52	53
f(a)	2.3688E-04	2.6189E-04	2.9084E-04	3.2455E-04	3.6410E-04	4.1068E-04	4.6599E-04
a	54	55	56	57	58	59	60
f(a)	5.3222E-04	6.1209E-04	7.0940E-04	8.2905E-04	9.7791E-04	1.1653E-03	1.4043E-03
a	61	62	63	64			
f(a)	1.7140E-03	2.1221E-03	2.6709E-03	3.4234E-03			